#2

DECISION-FEEDBACK EQUALIZATION
FOR DIGITAL COMMUNICATION OVER DISPERSIVE CHANNELS

M. E. AUSTIN

loan copy only

TECHNICAL REPORT 461

AUGUST 11, 1967

MASSACHUSETTS INSTITUTE OF TECHNOLOGY
RESEARCH LABORATORY OF ELECTRONICS
CAMBRIDGE, MASSACHUSETTS 02139

MASSACHUSETTS INSTITUTE OF TECHNOLOGY

RESEARCH LABORATORY OF ELECTRONICS

Technical Report 461

LINCOLN LABORATORY

Technical Report 437

August 11, 1967

DECISION-FEEDBACK EQUALIZATION
FOR DIGITAL COMMUNICATION OVER DISPERSIVE CHANNELS

M. E. Austin

Abstract

In this report, a decision-theory approach to the problem of digital communication
over known dispersive channels is adopted to arrive at the structures of the optimal
and two sub-optimal receivers: the "conventional" and "decision-feedback" equal-
izers, both employing matched and transversal filters. The conventional equalizer
is similar to some equalization modems finding current application, while the new
decision-feedback equalizer (as its name implies) utilizes its previous decisions in
making a decision on the present baud.

The parameters of these two equalizers are optimized under a criterion which min-
imizes the sum of the intersymbol interference and additive noise distortions appearing
at their outputs. Algorithms for evaluating the performances of the conventional and
decision-feedback equalizers are developed, proving especially useful at high SNR
where simulation techniques become ineffective.

To determine the dependence of their performance and sidelobe-suppression prop-
erties upon SNR and transversal filter length, the new algorithms were used to study
the conventional and decision-feedback equalizers when they are applied in equalization
of the class of channels exhibiting the maximum realizable intersymbol interference.
In addition, error-propagation effects found to arise in the decision-feedback equal-
izer operation are studied. High overall error rates (as found at low SNR) lead to a
threshold effect as the decision-feedback equalizer performance becomes poorer than
that of the conventional equalizer.

Despite such error-propagation behavior, however, the decision-feedback equalizer
is found to be considerably better than the conventional equalizer at all SNR and error
rates of practical importance, due to its sidelobe-suppression behavior; moreover,
its advantages become more pronounced, the higher the SNR and the greater the chan-
nel dispersion.

TABLE OF CONTENTS

DECISION-FEEDBACK EQUALIZATION
FOR DIGITAL COMMUNICATION OVER DISPERSIVE CHANNELS

I. INTRODUCTION – INTERSYMBOL INTERFERENCE AND EQUALIZATION

Commercial and military demands for higher data rates in the transmission of digital information over dispersive media, such as telephone links and the HF ionospheric channel, are continually increasing. This has led to a widespread interest in the development of receivers capable of mitigating the familiar intersymbol interference effects which inevitably accompany such increased data rates. Receiver filters designed to partially compensate for the dispersive characteristics of channels, or for the intersymbol interference distortion occurring when passing signals through dispersive channels, are referred to as "equalization" filters, or "equalizers."

The two principal objectives of this report are (a) to present a receiver structure which uses its previous decisions to reduce intersymbol interference in high-speed data transmission over dispersive channels – the decision-feedback equalizer, and (b) to compare the performance of this new equalizer structure with that of the conventional equalizer structure currently being employed.

In Sec. II, we first derive the optimal receiver for the problem of interest: synchronous transmission of binary data over fixed, known dispersive channels. The main innovation here is in the approach to receiver design in the presence of intersymbol interference – equalization is attacked not as a problem in linear filtering theory as it has been previously, but rather from a decision-theory viewpoint. This leads to the equations which specify the operations the receiver must perform on its input to minimize its probability of error. Our interpretation of these equations results in the optimal equalizer structure, a nonlinear receiver which unfortunately is too complex and impractical to construct, but which is nonetheless of interest for the insight it affords us in considering sub-optimal equalization. By modifying the assumptions used in arriving at the optimal equalizer, we next derive a sub-optimal equalizer structure which we refer to as the "conventional" equalizer. We then determine the equations specifying those parameter settings of the conventional equalizer which minimize the distortion energy appearing at its output, and we prove the existence and uniqueness of their solution. Section II concludes with a discussion relating this present work to that of earlier authors.

Adding to the assumptions used in deriving the conventional equalizer structure, we further assume in Sec. III that the receiver has made no decision errors on previous bauds, leading to our derivation of the decision-feedback equalizer. After interpreting the operation of this new equalizer structure and the nature of its decision feedback, we optimize its parameters under a minimum total output distortion energy criterion. Next, we consider conventional and decision-feedback equalization with regard to the degrees of freedom associated with their respective structures, and their manner of treating the intersymbol interference arising from both past and future bauds. We conclude Sec. III with heuristic arguments for the error-propagation effects anticipated in the operation of the decision-feedback equalizer.

With a view to obtaining a quantitative comparison of the performances of the conventional and decision-feedback equalizers, in Sec. IV we begin by deriving the channels we wish to study — the maximal distortion channels. For channels with a given overall channel dispersion length, the maximal distortion channels exhibit the largest possible distortion under a sum of the side-lobe magnitudes distortion measure. We then seek a method of evaluating the performance of the conventional equalizer. After noting that a direct calculation of the performance is conceptually possible but computationally impractical, we develop an alternative approach. A new computational algorithm is derived for obtaining upper and lower bounds on the performance of the conventional equalizer to any specified degree of accuracy. The implementation of this algorithm is explained, and its efficiency is studied through its application to examples of interest. Next, we present the exact performance data on the conventional equalizer when it is applied to equalization of the maximal distortion channels, as determined using this new algorithm. Section IV concludes with a discussion of the effects of equalizer length on the performance, and of the trade-off possible between signal-to-noise ratio (SNR) and equalizer length at different levels of performance.

In Sec. V, we are concerned with determining the performance characteristics of the decision-feedback equalizer. Next to its overall error rates as a function of SNR for various channels, error-propagation effects are of prime concern. Because of the nonlinear nature of the decision-feedback equalizer structure, its performance was studied through digital simulations at low and intermediate SNR. However, at high SNR, errors occur too infrequently to determine the error rates and error-propagation behavior accurately through simulations of reasonable duration. Thus, we determine the necessary modifications to our earlier algorithm to develop a second algorithm — a mixture of computation and simulation — which overcomes this difficulty, enabling us to obtain the desired error rates as well as burst and guard-space data, even at high SNR. We next present the results of our performance studies at all SNR, with discussions of overall error rates, burst and guard-space data, and the effects of equalizer length on these quantities. Finally, we conclude Sec. V with a development of an efficient method of bounding the mean burst duration, by modeling error propagation as a discrete Markov chain process, enabling us to treat equalizer recovery from the burst-error mode as a first-passage-time problem. This technique, which we find to be applicable at intermediate SNR due to the correlation properties of the distortion appearing at the output of the decision-feedback equalizer, provides us with a method of obtaining bounds on the mean recovery time without having to resort to simulations.

Section VI includes our conclusions, and suggestions for further research. After discussing threshold effects noted in the operation of the decision-feedback equalizer at low SNR, and its obvious advantages over the conventional equalizer at high SNR, we then compare both equalizer performances to upper bounds to obtain some feeling for the degree to which each is suboptimal. Differences in the performances of the two equalizers are then interpreted, and explained in terms of their respective methods of treating intersymbol interference in general, and in terms of their residual noise and intersymbol interference distortions, particularly at high SNR. Based upon our error-burst and guard-space studies, we note the additional improvements possible in the decision-feedback equalizer operation which one might realize through application of burst-error detecting and correcting coding schemes. Finally, we discuss briefly some issues which may be of interest in further research, such as extensions of the present work to handle colored noise, correlated message sequences, multilevel signaling schemes,

2

different types of decision-feedback data, and the sensitivity properties of the conventional and decision-feedback equalizers with respect to channel measurement errors.

Having outlined the purpose and content of this report, we will devote the remainder of Sec. I to presenting some background material of interest. First, we introduce an important device for implementing equalizers which has been employed in all equalization systems of recent development — the transversal filter; next, we point out the difference between channel equalization and equalization of intersymbol interference, and the desirability of the latter; finally, we present a classification of equalizers and brief descriptions of three adaptive equalizers currently under development. Two of these adaptive equalizers employ decision feedback, but both for a different purpose than the decision-feedback equalizer presented in this report.

Early efforts at channel equalization date back to 1928, when Zobel[1] published an extensive work on distortion correction using lumped RLC filters. For some time, such filters adequately provided the amplitude compensation desired for telephone circuits, for the ear proved rather insensitive to the phase distortions they generally introduced. With the development of television, and with digital communication aiming at increased data rates, phase distortion became of greater concern, leading to the work with the transversal filter reported by Kallmann[2] in 1940. The analog transversal filter may be realized using a tapped-delay-line (TDL) terminated in its characteristic impedance, with a high-input-impedance amplifier at each tap output. With the amplifier gains suitably chosen for the desired equalization properties, the amplifier outputs are summed to obtain the transversal filter output, as indicated in Fig. 1(a). Often, the TDL
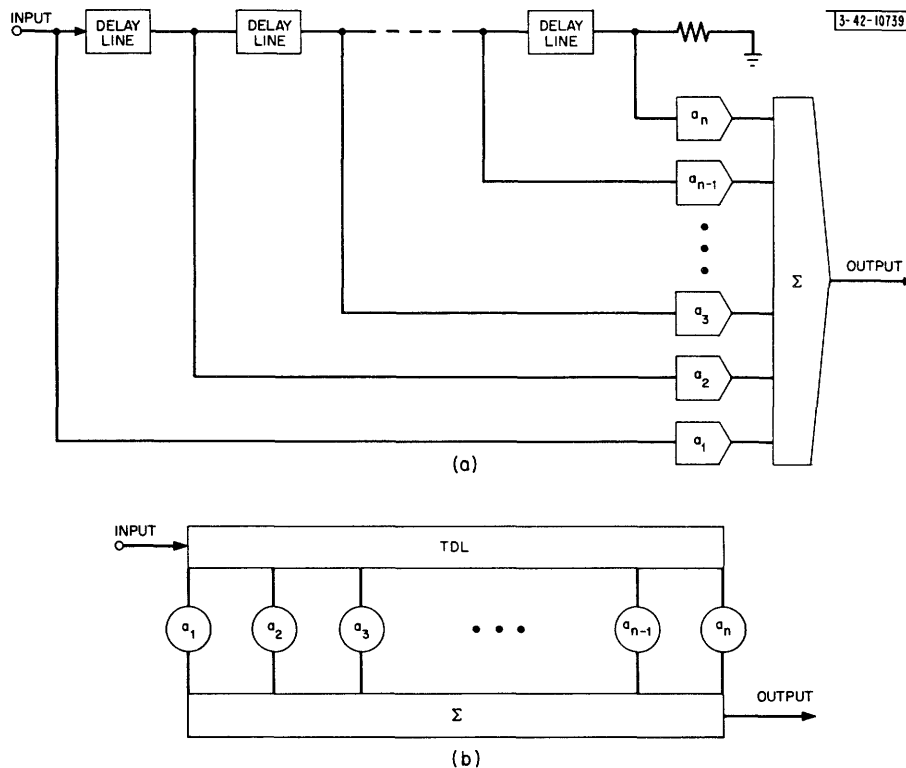

Fig. 1. Transversal filter. (a) Block diagram of filter; (b) representation in this report of both analog and digital realizations.

input is sampled, the delay lines are replaced by digital shift registers, and the weighting and summing operations are performed digitally. Throughout this report, whether considering analog or digital realizations, we will draw transversal filters as shown in Fig. 1(b). The tap gains of the transversal filter can be set to render amplitude compensation without phase distortion, phase compensation without amplitude distortion, or both amplitude and phase compensation. Such versatility, coupled with the increasing speed and availability of computers for calculating and adjusting its gains, has caused the digital transversal filter to become increasingly important in recent years, as illustrated in the adaptive equalization systems described further below.

One of the first adaptive receivers designed to equalize a dispersive channel was the RAKE system described by Price and Green.[3] This system transmits wide-band message waveforms which are correlated against their delayed replicas at the receiver to enable measurement of the amplitude and phase characteristics of the individual paths of a multipath medium such as the HF ionospheric channel. By use of these measurements to set the amplitude and phase of the tap gains of its transversal filter, the RAKE receiver achieves nearly optimum weighting of the waveforms received from each of the paths, and sums them coherently to form its output. Considering the low 45-bits/sec data rate it achieved on the HF ionospheric channel, the RAKE system represents a highly inefficient use of its 10-kHz bandwidth when compared, for example, with the less sophisticated Kineplex system which was designed for data rates of up to 3000 bits/sec with a bandwidth of only about 3.4 kHz, and without attempting channel measurement.[4,5] This serves to illustrate that, for data transmission purposes, one should not necessarily strive to equalize the channel itself, but rather should consider equalization for a particular choice of signals to be transmitted over the channel, as pointed out in the following example.

It is easily shown through the z-transform approach to inverse filtering that, in the absence of significant noise, the discrete two-path channel of Fig. 2(a) can be equalized using the transversal filter of Fig. 1(b), if its taps are spaced by the time delay between the two paths τ, and
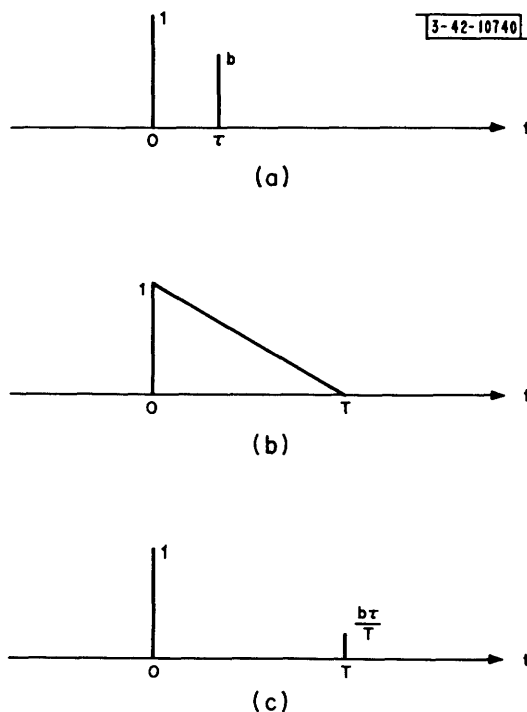

(a)

(b)

Fig. 2. Example of channel vs equivalent channel equalization. (a) Channel impulse response, (b) signaling waveform to be employed over channel, and (c) result of synchronous sampling of channel output with input waveform (b).

(c)

4

its gains are set according to the relationship $a_n = (-b)^{n-1}$ (see Ref. 6). If this equalizer is truncated after N taps, there will be residual response having magnitude $|b|^N$. On the other hand, suppose we plan instead to use the channel of Fig. 2(a) to transmit data using amplitude modulation of the signal waveform shown in Fig. 2(b), which has a baud duration $T > \tau$. Synchronous sampling of the channel output as indicated in Fig. 2(c) renders a sampled waveform which may be equalized with a transversal filter with gains $a_n = [-(b\tau/T)]^{n-1}$ and with tap spacing T. With this latter approach, it is seen that convergence of the tap gains is obtained more rapidly than before. Moreover, the tap spacings are independent of τ, an important matter if τ is a time-varying quantity, for then the channel equalization receiver must employ many more taps than are required by the intersymbol interference equalizer, which need only adjust its tap gains. This simple example points out that if one intends to transmit a signal s(t) over a dispersive channel having an impulse response g(t), it is generally more efficient to minimize the intersymbol interference distortion appearing at the receiver output through equalization of the equivalent impulse response $h(t) = s(t) \circledast g(t)$, rather than attempting to equalize the channel g(t) itself in order to be able to handle arbitrary s(t).

Equalization filters fall within three categories: fixed, automatic, and adaptive. Fixed equalizers are adjusted to provide the amplitude and phase compensation necessary to correct the average distortion characteristics of dispersive channels, while automatic and adaptive equalizers, on the other hand, have generally found application in synchronous data transmission to equalize the equivalent channel, i.e., reducing the intersymbol interference distortion at the sampling times. The automatic equalizers transmit their known pulse waveforms prior to data transmission, which they utilize in adjusting the tap gains of their transversal equalization filter (for example, see Ref. 7). Adaptive equalizers differ from the automatic equalizers in that they adjust their transversal filter parameters during data transmission, using either a sounding waveform or the message waveform itself to minimize the intersymbol interference distortion, thus indirectly obtaining equivalent channel measurement. Three such adaptive systems are described briefly below.

An adaptive equalizer named ADAPTICOM has been under study at Cardion Electronics, Inc. and has been reported by DiToro.[8] This system uses approximately a 3-kHz bandwidth to achieve a degree of equalization by using a filter which is matched to the received waveform for a single pulse transmission, in cascade with a transversal filter. ADAPTICOM's parameter settings are determined by periodically interrupting the data transmission several times per correlation time of the channel and sounding the channel, although apparently no attempt is made to exploit the correlation between the successive measurements to improve the accuracy of the resultant settings. The transversal filter centertap has unity gain, with the remaining tap gains set equal to their respective tap outputs, when a single received pulse is passed through the matched filter, at that instant when the centertap output attains its maximum value. Thus, ideally, the tap gains are set equal to the sampled autocorrelation function of the equivalent channel. DiToro states that such gains, together with proper adjustment of a single gain simultaneously affecting the total contribution of all but the centertap outputs, minimize the mean square distortion due to intersymbol interference at the output, although his mathematical basis for this has not yet been published. Performing satisfactorily in the laboratory using a multipath simulator, ADAPTICOM is being constructed for testing on an actual HF ionospheric link.

Lucky[9] reports the development and testing of an adaptive equalizer using a digital transversal filter, for application to telephone-line equalization. Similar in other respects to

his earlier automatic equalizer (Ref. 10), Lucky's adaptive equalizer uses decision feedback, enabling him to make iterative tap-gain adjustments to minimize the sum of the sidelobe magnitudes appearing at the output when the mainlobe is normalized to unity. This adaptive equalizer enabled tracking of the slowly fluctuating telephone channel, of course, but it also rendered better tap-gain settings than Lucky's automatic equalizer because a much larger number of transmitted pulses were employed in arriving at the settings than was reasonable to permit in a precall sounding signal for the automatic equalizer. The equalization algorithm used by Lucky attempts to set as many of the sidelobes to zero as is possible within the constraint of a finite TDL length, while ignoring the additive noise which is reasonably low on telephone lines. Lucky shows that this works well for channels having an initial distortion less than unity. For channels with larger initial distortion, as eventually will occur with increasing the baud rate for any channel, the convergence of Lucky's tap-gain-adjustment procedure may fail as he noted, and, in addition, large sidelobes can arise beyond the sidelobes zeroed by the transversal filter.

Another equalization system, ADEPT, is currently under development at Lincoln Laboratory, principally by Drouilhet and Niessen.[11] This system uses a 63-tap TDL for equalization of telephone lines in the transmission of 8-level, 10,000-bits/sec data. ADEPT, which has an initial training period, continues to adjust its tap settings during data transmission. A pseudo-random sequence is transmitted in addition to the message waveform and, through correlation against the same sequence at the receiver, ADEPT attempts to minimize the output distortion energy due to intersymbol interference. To minimize the degradation of the tap settings derived from correlation of the pseudo-random sequence with the message waveform, the message is subtracted out using decision feedback. Note that this represents a different, and apparently less efficient, application of decision feedback than that employed by Lucky (Ref. 9), in that the energy in the message waveform is being discarded rather than being utilized in achieving the tap-gain settings. The advantages to be obtained over Lucky's adaptive equalizer, through use of a different tap-adjustment procedure and increased filter length, will be determined in the near future when ADEPT will be tested over an actual telephone link.

II. OPTIMAL AND SUB-OPTIMAL EQUALIZATION

Here, we consider the problem of determining the structures of receivers for digital communication over a linear dispersive channel. As shown in the model of Fig. 3, during the kth-baud period of duration T, $\xi_k s(t)$ is transmitted, where s(t) vanishes outside an interval of width T and where $\xi_k = +1$ or -1, corresponding to hypotheses H_1 and H_0, respectively. We assume that the equivalent channel impulse response, $h(t) = s(t) \circledast g(t)$, is known to the receiver through prior measurement made either directly or indirectly, as in the case of the adaptive equalizers described in Sec. I. In addition, the channel has additive noise n(t) corrupting its output. Thus, the input to our receiver is

$$r(t) = \sum_k \xi_k h(t - kT) + n(t) \tag{1}$$

where here, and throughout the remainder of the report, $\underset{k}{\Sigma}$ denotes the summation for $k = -\infty$ to $+\infty$ unless otherwise noted.
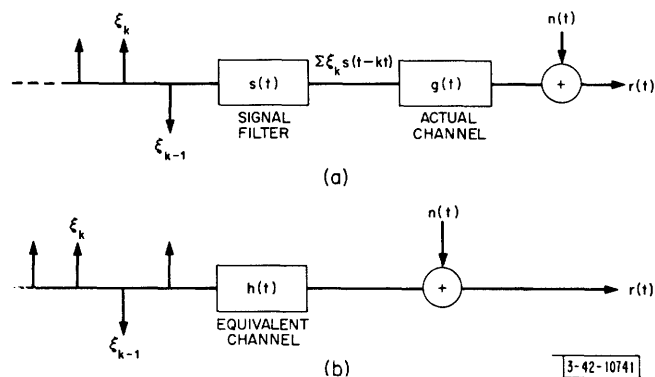
Fig. 3. Dispersive channel communication model: (a) digital communication over noisy dispersive channel; (b) equivalent channel model, $h(t) = s(t) \circledast g(t)$.

Given the received waveform Eq. (1) for all t, our problem is to obtain receivers for making decisions on the ξ_k. We first derive the optimal receiver structure, and then a simpler suboptimal receiver. We will refer to the latter receiver as the "conventional" equalizer, to distinguish it from the "decision-feedback" equalizer to be presented in Sec. III.

A. OPTIMAL EQUALIZER STRUCTURE

In deriving the optimal receiver for the problem stated above, we make the following assumptions:

(1) The ξ_k are independent,

(2) H_0 and H_1 are equally likely, and

(3) n(t) is white Gaussian noise, of double-sided spectral height $N_0/2$.

These assumptions are generally met in practice. The extension to colored Gaussian noise is straightforward, as discussed in Sec. VI. Under these assumptions, it is a well-known result

7

in statistical decision theory that, to make a decision on the zeroth baud as to the value of ξ_0, the optimal receiver computes the likelihood ratio

$$\Lambda = \frac{p[r(t)|\xi_0 = +1]}{p[r(t)|\xi_0 = -1]} \quad . \tag{2}$$

If we define for convenience of notation the sets

$$\underline{\xi}^- = \{\xi_k | k < 0\} \tag{3}$$

$$\underline{\xi}^+ = \{\xi_k | k > 0\} \tag{4}$$

then we may write

$$p[r(t)|\xi_0] = \sum_{\underline{\xi}^-} \sum_{\underline{\xi}^+} p[r(t)|\xi_0, \underline{\xi}^-, \underline{\xi}^+] \, p[\underline{\xi}^-, \underline{\xi}^+] \tag{5}$$

where the summations are over all possible message sequences occurring before and after the zeroth baud, respectively. From Eq.(1) and Assumption (3), we may write

$$p[r(t)|\xi_0, \underline{\xi}^-, \underline{\xi}^+] = K \exp\left\{-\frac{1}{N_0} \int \left[r(t) - \sum_k \xi_k h(t - kT)\right]^2 dt\right\}$$

$$= K \exp\left[-\frac{1}{N_0} \int r^2(t) \, dt\right] \exp\left[\sum_k \xi_k \frac{2}{N_0} \int r(t) \, h(t - kT) \, dt\right]$$

$$\times \exp\left[-\sum_j \sum_k \xi_j \xi_k \frac{1}{N_0} \int h(t - jT) \, h(t - kT) \, dt\right]$$

$$= K_1 \exp\left[\sum_k \xi_k a_k - \sum_j \sum_k \xi_j \xi_k b_{j-k}\right] \tag{6}$$

where we have defined $K_1 = K \exp\left[-(1/N_0) \int r^2(t) \, dt\right]$, and the quantities

$$a_k \triangleq \frac{2}{N_0} \int r(t) \, h(t - kT) \, dt = \frac{2}{N_0} \int r(t + kT) \, h(t) \, dt \tag{7}$$

and

$$b_k \triangleq \frac{1}{N_0} \int h(t) \, h(t - kT) \, dt \quad . \tag{8}$$

Note that all the information of the received waveform has been condensed into the set of sufficient statistics $\{a_k\}$, which may be generated as shown in Fig. 4. In Fig. 4(a), we see that the received waveform is input to a TDL, thus simultaneously making available the shifted versions of $r(t)$ required in Eq. (7) where it is indicated that each tap output is to be multiplied by $[(2/N_0) \times h(t)]$ and the product integrated over all time t. Each integrator output will remain constant, however, after $h(t)$ becomes zero (or negligibly small). Thus, if $h(t)$ is nonzero only over the
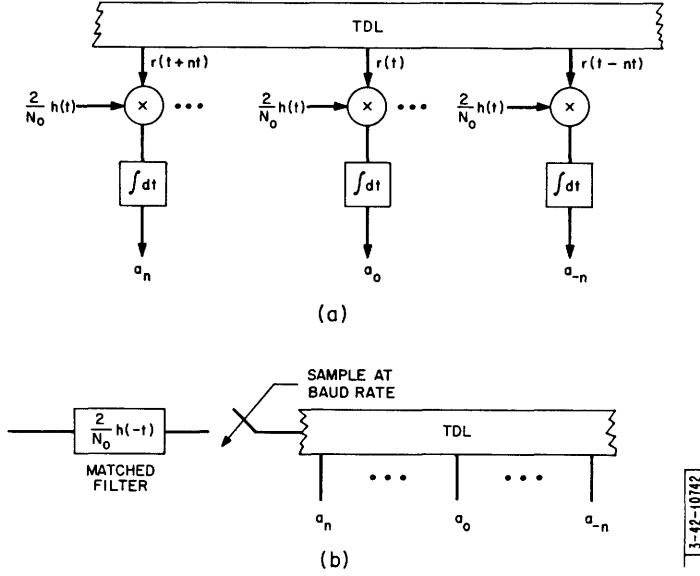
8

Fig. 4. Generation of sufficient statistics: (a) interpreting Eq. (7) directly, and (b) an alternative structure, a matched filter in cascade with a TDL.

interval $(0, T_1)$, then we may sample each integrator output at any time $t \geq T_1$ to obtain the desired a_k. Note that if we sample at $t = T_1$, then we may replace the multiplication-integration operation on each tap output by a linear filter having an impulse response $[(2/N_0) h(-t)]$, since the output of such filters will also render the desired a_k at $t = T_1$. Moreover, since the linear filters common to each tap may be replaced by a single filter operating on the received waveform $r(t)$ before it enters the TDL, and since the simultaneous sampling of each tap output may clearly be replaced by the sequential sampling of the waveform into the TDL at the baud rate $1/T$, then an equivalent method of generating the sufficient statistics is as shown in Fig. 4(b). Thus, we note that optimal reception involves passing the received waveform through a filter matched (except for the gain of $2/N_0$) to the equivalent channel impulse response $h(t)$, sampling the matched filter output at the baud rate to obtain the set of sufficient statistics $\{a_k\}$, and then passing these into a TDL. Before considering the additional operations which the optimal receiver performs on these sufficient statistics, we first consider the b_k sequence defined by Eq. (8).

From a comparison of Eqs. (7) and (8) and the discussion above, we observe that the b_k sequence may be generated using a structure identical (except for a gain of 2) to that of Fig. 4(b), if the input $r(t)$ is replaced by $h(t)$. But this corresponds to sampling the matched filter response to a single pulse transmission in the absence of noise, thus rendering (except for the gain of $1/N_0$) the samples of the equivalent channel autocorrelation function, and $b_k = b_{-k}$, as indicated in Fig. 5. Returning to Eqs. (5) and (6), we may write

$$p[r(t)|\xi_0] = \sum_{\underline{\xi}^-} \sum_{\underline{\xi}^+} K_2 \exp\left[\sum_k \xi_k a_k - \sum_j \sum_k \xi_j \xi_k b_{j-k}\right] \tag{9}$$

where $K_2 = K_1 p(\underline{\xi}^-, \underline{\xi}^+)$ is a normalization constant, independent of $\underline{\xi}^-$ and $\underline{\xi}^+$ through Assumption (1). Factoring out the remaining terms which are independent of $\underline{\xi}^-$ and $\underline{\xi}^+$, we have

9
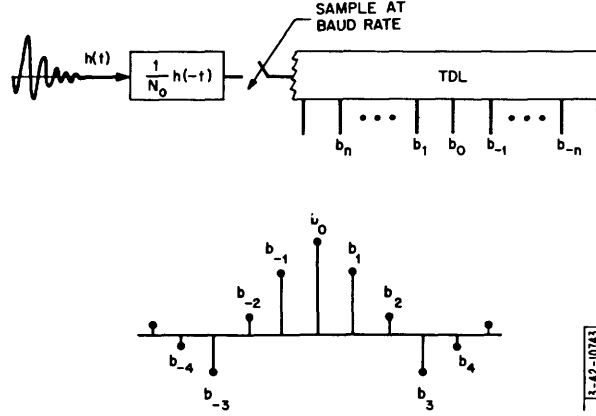
Fig. 5. Generation of b_k sequence of Eq. (8), the sampled autocorrelation function of the equivalent channel impulse response.

$$p[r(t)|\xi_0] = K_2 \exp\left[\xi_0 a_0 - \sum_i \xi_i^2 b_0\right] \sum_{\underline{\xi}^-} \sum_{\underline{\xi}^+} \exp\left[\sum_{k\neq 0} \xi_k a_k - \sum_j \sum_{k\neq j} \xi_j \xi_k b_{j-k}\right] \quad . \quad (10)$$

Using this expression in Eq. (2), and canceling factors common to the numerator and denominator, we find the likelihood ratio to be

$$\Lambda = \exp[2a_0] \frac{\left.\sum_{\underline{\xi}^-} \sum_{\underline{\xi}^+} \exp\left[\sum_{k\neq 0} \xi_k a_k - \sum_j \sum_{k\neq i} \xi_j \xi_k b_{j-k}\right]\right|_{\xi_0=1}}{\left.\sum_{\underline{\xi}^-} \sum_{\underline{\xi}^+} \exp\left[\sum_{k\neq 0} \xi_k a_k - \sum_j \sum_{k\neq i} \xi_j \xi_k b_{i-k}\right]\right|_{\xi_0=-1}} \quad . \quad (11)$$

If we denote

$$\Xi \triangleq \{\underline{\xi}^-, \xi_0, \underline{\xi}^+\}$$

$$\Xi_+ \triangleq \Xi\big|_{\xi_0=1}$$

and

$$\Xi_- \triangleq \Xi\big|_{\xi_0=-1} \quad (12)$$

and, if further, we define a function

$$C(\Xi) = \sum_j \sum_{k\neq j} \xi_j \xi_k b_{j-k} \quad (13)$$

then, noting that the optimal receiver uses the decision rule

10

$$\ln \Lambda \begin{cases} > 0 \text{ decide } H_1 \\ \\ < 0 \text{ decide } H_0 \end{cases}$$

(14)

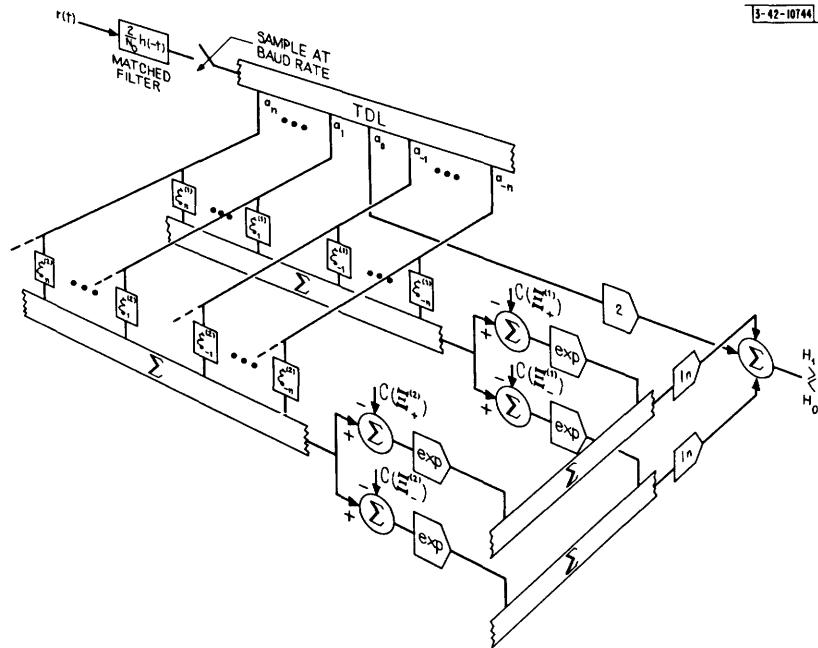we find that it may be implemented as shown in Fig. 6.

Fig. 6. Structure of optimal equalizer.

As shown above, the optimal equalizer structure passes the received waveform through a matched filter, sampler, and TDL to obtain the set of sufficient statistics $\{a_k\}$. The sufficient statistic derived from the interval upon which the decision is being made, a_0, is connected directly to the output through an amplifier of gain two. The statistics derived from all other intervals are weighted by all possible $\underline{\xi}^-$ and $\underline{\xi}^+$ sequences, as indicated. For any particular sequence, bias terms, the $C(\Xi)$, are subtracted from the weighted sum of the a_k, and the differences passed through exponentiators before summing with similar terms from all other combinations of $\underline{\xi}^-$ and $\underline{\xi}^+$. The natural logarithms of these overall sums are then added and subtracted respectively to $2a_0$, as shown in Fig. 6. This last summation result is compared with a zero threshold to decide between the hypotheses H_1 and H_0.

Next, we want to make a few observations concerning this optimal equalizer structure. First we note that if $C(\Xi_+) = C(\Xi_-) = 0$ for all choices of $\underline{\xi}^-$ and $\underline{\xi}^+$, then the inputs to their respective summations from the exponentiators will be identical, hence the logarithms of these sums will cancel with each other at the overall output. When this occurs, the decision statistic is simply $2a_0$, the other a_k do not appear, and the entire receiver degenerates to a matched filter.

There is only one way in which the $C(\text{H}_+)$ and $C(\text{H}_-)$ can vanish for all choices of $\underline{\xi}^-$ and $\underline{\xi}^+$, namely, the b_k must vanish for all $k \neq 0$. This, in turn, happens only if the channel exhibits no intersymbol interference or if the additive noise becomes sufficiently large, as we may observe from Eq. (8). Thus, as we would expect, the optimal receiver approaches a matched filter whenever the additive noise dominates the intersymbol interference.

Next, we consider the situation in which $\underline{\xi}^-$ is known exactly at the receiver. Now the $p[\underline{\xi}^-, \underline{\xi}^+]$ terms are nonzero only for this known value of $\underline{\xi}^-$, hence all the sums entering into the exponentiators have a common term $\sum_{k<0} \xi_k a_k$. This common term will therefore cancel at the overall output, and thus the a_k for $k < 0$ no longer are used in making a decision; hence, that portion of the TDL to the right of a_0 is no longer required, and the optimal equalizer weights only a_k from future baud intervals. The knowledge of $\underline{\xi}^-$ does, of course, enter the decision through the $C(\text{H})$ bias terms. Later, in Sec. IV, we will see how, in a sub-optimal equalizer, a term corresponding to that portion of the $C(\text{H})$ arising from $\underline{\xi}^-$ may be generated by means of decision feedback through a transversal filter.

The optimal equalizer structure of Fig. 6 is clearly an impractical one to realize, for two reasons. First, of course, the summations over all possible $\underline{\xi}^-$ and $\underline{\xi}^+$ are too numerous to be computed. A second impractical aspect is the requirement for numerous exponentiators, two exponentiators being required for each possible choice of $\underline{\xi}^-$ and $\underline{\xi}^+$. The purpose of Sec. B below is to obtain a receiver structure which, though sub-optimal, is much more practical to construct.

B. SUB-OPTIMAL EQUALIZATION – THE CONVENTIONAL EQUALIZER

The complexity of the optimal equalizer structure derived in Sec. A stems from the large number of terms entering into the calculation of the numerator and denominator of the likelihood ratio, a term being required for every possible message sequence $\underline{\xi}^-$ and $\underline{\xi}^+$. To simplify calculation of the likelihood ratio and obtain a less complex receiver structure, we make an additional assumption similar to that which proved fruitful in a radar resolution problem considered in Ref. 12, namely,

(4) ξ_k are Gaussian random variables of zero mean and unit variance for $k \neq 0$.

In making this assumption, of course, we have deviated from the digital communication problem of interest, the assumption being perhaps more appropriate in a PAM communication system context. Nonetheless, we will see that this assumption enables us to arrive at a much simpler, though sub-optimal, equalizer than the optimal equalizer derived in Sec. A. Moreover, we employ the assumption only in arriving at the equalizer structure and, having obtained the structure, we will later optimize its parameters for the actual digital communication problem at hand. Using this assumption, then, in addition to our earlier assumptions, the equation corresponding to Eq. (9) above becomes

$$p[r(t)|\xi_0] = \iint p[r(t)|\xi_0, \underline{\xi}^-, \underline{\xi}^+] \, p[\underline{\xi}^-, \underline{\xi}^+] \, d\underline{\xi}^- \, d\underline{\xi}^+ \tag{15}$$

12

where, from Assumptions (1) and (4), it follows that

$$p[\underline{\xi}^{-}, \underline{\xi}^{+}] = K_4 \exp\left[-\frac{1}{2} \sum_{k \neq 0} \xi_k^2\right]$$

$$= K_4 \exp\left[-\frac{1}{2} \sum_k \xi_k^2 + \frac{1}{2} \xi_0^2\right]$$

$$= K_5 \exp\left[-\frac{1}{2} \sum_j \sum_k \xi_j \delta_{jk} \xi_k\right] \tag{16}$$

where $K_5 \triangleq K_4 \, e^{1/2}$ and δ_{jk} is the Kronecker delta, zero for $j \neq k$ and unity for $j = k$. From Eqs. (6) and (16), the integrand of Eq. (15) becomes

$$p[r(t)|\xi_0, \underline{\xi}^{-}, \underline{\xi}^{+}] \, p[\underline{\xi}^{-}, \underline{\xi}^{+}] = K_1 K_5 \exp\left[\sum_k \xi_k a_k - \sum_j \sum_k \xi_j (b_{j-k} + \frac{1}{2} \delta_{jk}) \xi_k\right] \quad . \tag{17}$$

To simplify notation, it becomes convenient at this point to introduce column vectors $\underline{x}$, $\underline{a}$, and $\underline{c}$ defined by

$$\underline{x} \triangleq \begin{bmatrix} \cdot \\ \cdot \\ \cdot \\ \xi_{-2} \\ \xi_{-1} \\ \xi_1 \\ \xi_2 \\ \cdot \\ \cdot \\ \cdot \end{bmatrix} \qquad \underline{a} \triangleq \begin{bmatrix} \cdot \\ \cdot \\ \cdot \\ a_{-2} \\ a_{-1} \\ a_1 \\ a_2 \\ \cdot \\ \cdot \\ \cdot \end{bmatrix} \qquad \underline{c} \triangleq \begin{bmatrix} \cdot \\ \cdot \\ \cdot \\ c_{-2} \\ c_{-1} \\ c_1 \\ c_2 \\ \cdot \\ \cdot \\ \cdot \end{bmatrix} \tag{18}$$

where we define

$$c_k \triangleq b_k + \frac{1}{2} \delta_{k0} \tag{19}$$

and the a_k and ξ_k are as defined previously. We also introduce a matrix $\underline{Q}$ defined by its elements

$$Q_{jk} \triangleq b_{j-k} + \frac{1}{2} \delta_{jk} \tag{20}$$

for all $j, k \neq 0$. With these definitions, Eq. (17) may be written as

$$K_1 K_5 \exp[\xi_0 a_0 + \underline{x}^T \underline{a} - c_0 \xi_0^2 - 2\xi_0 \underline{x}^T \underline{c} - \underline{x}^T \underline{Q} \underline{x}] \quad . \tag{21}$$

13

Substituting Eq. (21) into Eq. (15), and ignoring the factor $K_1 K_5 \exp[-c_0 \xi_0^2]$ since it will appear in both the numerator and denominator of the likelihood ratio and thus be canceled out, we find

$$p[r(t)|\xi_0] = \exp[\xi_0 a_0] \int \exp[-\underline{x}^T \underline{Q} \underline{x} + 2\underline{x}^T (\tfrac{1}{2} \underline{a} - \xi_0 \underline{c})] \, d\underline{x}$$

$$= \exp[\xi_0 a_0 + \tfrac{1}{4} \underline{a}^T \underline{Q}^{-1} \underline{a} + \xi_0^2 \underline{c}^T \underline{Q}^{-1} \underline{c} - \xi_0 \underline{c}^T \underline{Q}^{-1} \underline{a}] \quad . \tag{22}$$

Thus, it follows from Eq. (22) that the likelihood ratio Eq. (2) becomes

$$\Lambda = \exp[2a_0 - 2\underline{c}^T \underline{Q}^{-1} \underline{a}] \tag{23}$$

hence, our decision rule is simply

$$a_0 - \underline{c}^T \underline{Q}^{-1} \underline{a} \underset{H_0}{\overset{H_1}{\gtrless}} 0 \quad . \tag{24}$$

Representing the column matrix $-\underline{Q}^{-1} \underline{c}$ by elements g_k:

$$-\underline{Q}^{-1} \underline{c} \triangleq \begin{bmatrix} \cdot \\ \cdot \\ \cdot \\ g_{-2} \\ g_{-1} \\ g_1 \\ g_2 \\ \cdot \\ \cdot \\ \cdot \end{bmatrix} \tag{25}$$

then, we may also write the decision rule (24) as

$$\sum_{k \geqslant 0} g_k a_k \underset{H_0}{\overset{H_1}{\gtrless}} 0 \tag{26}$$

where we have defined $g_0 = 1$.

Recalling our discussion in Sec. A on the generation of the sufficient statistics a_k, it is clear that the decision rule (26) may be implemented as shown in Fig. 7, where the weights g_k are seen to appear as gains on the TDL taps. This structure will be referred to as the "conventional" equalizer throughout the remainder of the report, to distinguish it from the "decision-feedback" equalizer to be derived and studied later. Further, it will prove convenient in the following discussions to denote the tap gains as a vector, defined by

$$\underline{g} \triangleq \begin{bmatrix} \cdot \\ \cdot \\ \cdot \\ g_{-1} \\ g_0 \\ g_1 \\ \cdot \\ \cdot \\ \cdot \end{bmatrix} \qquad (27)$$

which we will frequently refer to as the "tap-gain" vector.

The conventional equalizer structure with its gains as defined by Eq.(25) is, of course, only optimal under Assumption (4), hence sub-optimal for the actual binary signaling problem of interest. We would like, therefore, to next adopt this sub-optimal receiver structure, but to abandon Eq.(25) and to determine a tap-gain vector g more appropriate for the present problem.
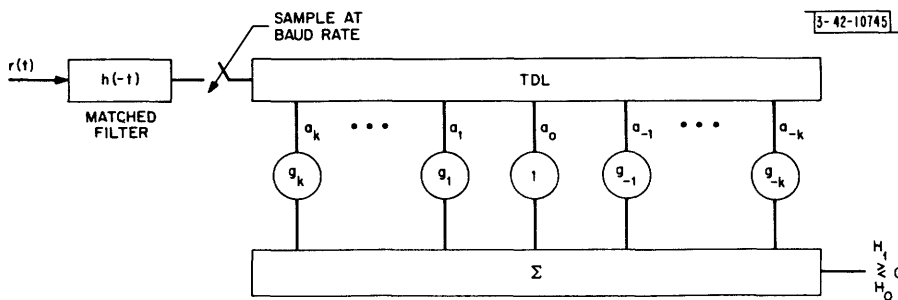

Fig. 7. Structure of conventional equalizer.

At this point, we would like to determine those tap-gain settings which optimize the equalizer performance, minimizing its probability of error. For the special case where the sum of the sidelobe magnitudes is less than unity, Aaron and Tufts[13] have done this by first minimizing the output noise variance for a given set of sidelobes, and then working through a specific example, employing a search in tap-gain space to arrive at those settings which minimize the probability of error. This approach was feasible only because they consider small numbers of sidelobes and taps, thus requiring summation over only a small number of possible message sequences. In realistic applications, as we discuss further in Sec.IV, the number of terms involved in such a probability-of-error computation becomes prohibitively large, and we therefore must be content with some other method, and with less-than-optimal tap-gain settings.

Instead of attempting to minimize the probability of error directly, authors usually attempt to minimize the intersymbol interference appearing at the receiver output. Two distortion measures are currently in use. With the mainlobe assumed unity, and the summations over the sidelobes, these measures are

$$D_\alpha = \sum q_i^2 \qquad (28)$$

15

and

$$D_\beta = \sum |q_i| \tag{29}$$

where the q_i are the output sidelobes resulting from a single pulse transmission, as shown in Fig. 8. DiToro[8] uses the D_α criterion in his ADAPTICOM receiver, while Lucky[9,10] uses the D_β criterion, although he asserts there is probably little difference in terms of performance using either criterion. In this report, we adopt a modified D_α criterion under which we include the additive noise appearing at the output, and find those tap-gain settings which minimize the total output distortion.
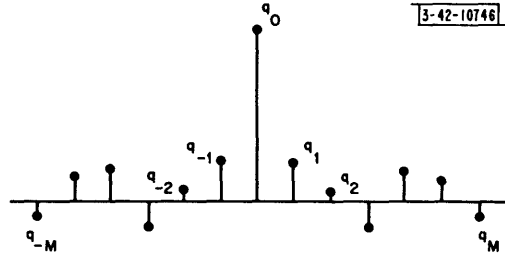

Fig. 8. Typical output sidelobes from conventional equalizer for a single $\xi_0 = +1$ pulse transmission.

We first determine an expression for the output distortion in terms of the TDL gains. For a single $\xi_0 = 1$ transmitted pulse, synchronous sampling of the matched filter output renders a sequence of samples

$$z_k = z(kT) = \int r(t)\, h(t + kT)\, dt$$

$$= \int [h(t) + n(t)]\, h(t + kT)\, dt = \varphi_k + w_k \tag{30}$$

where we have defined

$$\varphi_k = \int h(t)\, h(t + kT)\, dt \tag{31}$$

and

$$w_k = \int n(t)\, h(t + kT)\, dt \quad . \tag{32}$$

The TDL output is then a sequence of samples given by the convolution of the z_k sequence with the tap-gain vector $\underline{g}$:

$$\sum_m z_{k-m} g_m = \sum_m \varphi_{k-m} g_m + \sum_m w_{k-m} g_m$$

$$\triangleq q_k + n_k \tag{33}$$

where we have defined the first sum on the right-hand side to be q_k, and the last sum to be n_k, as indicated. In transmitting an infinite sequence of pulses modulated by the ξ_k (which we have previously assumed to be independent, of unit variance, and zero mean), the output distortion at any sample time, say, the zeroth sample time, will be given by:

$$\text{Output distortion} = \sum_k q_k^2 - q_0^2 + n_0^2 \quad . \tag{34}$$

16

Normalizing the tap gains such that $q_0 = 1$, then to minimize the average output distortion, we must minimize the quantity

$$\sum_k q_k^2 + \overline{n_0^2} \quad . \tag{35}$$

From the definition of the q_k in Eq. (33), we find that

$$\sum_k q_k^2 = \sum_k \left(\sum_m \varphi_{k-m} g_m \right) \left(\sum_v \varphi_{k-v} g_v \right)$$

$$= \sum_m \sum_v g_m \left(\sum_k \varphi_{k-m} \varphi_{k-v} \right) g_v \tag{36}$$

and

$$\overline{n_0^2} = \overline{\sum_m w_{-m} g_m \left(\sum_v w_{-v} g_v \right)}$$

$$= \sum_m \sum_v g_m \overline{w_{-m} w_{-v}} g_v$$

$$= \frac{1}{2} N_0 \sum_m \sum_v g_m \varphi_{m-v} g_v \tag{37}$$

the latter step holding since, from Eqs. (31) and (32), it follows that

$$\overline{w_{-m} w_{-v}} = \int h(t - mT) \, h(\tau - vT) \, \overline{n(t) \, n(\tau)} \, d\tau \, dt$$

$$= \frac{1}{2} N_0 \varphi_{m-v} \quad . \tag{38}$$

If we define matrices $\underline{X}$ and $\underline{Y}$ by their elements

$$X_{mv} = \sum_k \varphi_{k-m} \varphi_{k-v} \tag{39}$$

and

$$Y_{mv} = \varphi_{m-v} \tag{40}$$

then substituting these into Eqs. (36) and (37), using the tap-gain vector notation $\underline{g}$ defined in Eq. (27), we may write Eq. (35) as

$$\underline{g}^T \underline{X} \underline{g} + \frac{1}{2} N_0 \underline{g}^T \underline{Y} \underline{g} = \underline{g}^T [\underline{X} + \frac{1}{2} N_0 \underline{Y}] \underline{g} \quad . \tag{41}$$

Under the constraint that the mainlobe is unity, which we may write as

$$\underline{g}^T \underline{\varphi} = \underline{\varphi}^T \underline{g} = 1 \quad . \tag{42}$$

where we have defined the column vector

$$\underline{\varphi} = \begin{bmatrix} \cdot \\ \cdot \\ \cdot \\ \varphi_{-1} \\ \varphi_0 \\ \varphi_1 \\ \cdot \\ \cdot \\ \cdot \end{bmatrix} \qquad (43)$$

then our problem is to minimize Eq. (40) subject to the constraint Eq. (41). Introducing the Lagrange multiplier λ, we may do this by minimizing the quantity

$$J \triangleq \underline{g}^T [\underline{X} + \tfrac{1}{2} N_0 \underline{Y}] \, \underline{g} + \lambda(\underline{g}^T \underline{\varphi} - 1) \qquad (44)$$

in order to find the tap-gain vector $\underline{g}$ which is optimal under our distortion criterion. It is straightforward to show that

$$\frac{\partial J}{\partial \underline{g}} \triangleq \begin{bmatrix} \cdot \\ \cdot \\ \cdot \\ \dfrac{\partial J}{\partial g_{-1}} \\ \dfrac{\partial J}{\partial g_0} \\ \dfrac{\partial J}{\partial g_1} \\ \cdot \\ \cdot \\ \cdot \end{bmatrix} = 2[\underline{X} + \tfrac{1}{2} N_0 \underline{Y}] \, \underline{g} + \lambda \underline{\varphi} \qquad (45)$$

and, further, that $\partial J / \partial \underline{g}$ is zero for

$$\underline{g} = \frac{[\underline{X} + \tfrac{1}{2} N_0 \underline{Y}]^{-1} \underline{\varphi}}{\underline{\varphi}^T [\underline{X} + \tfrac{1}{2} N_0 \underline{Y}]^{-1} \underline{\varphi}} \qquad (46)$$

where Eq. (42) has been used to determine and replace λ.

Equation (46) is the desired solution. We next verify that it exists, is unique, and renders a minimum of Eq. (44). Since the output sample variance is always non-negative, and clearly zero only if we turn the TDL off completely by setting $\underline{g} = \underline{0}$ (for otherwise some noise at least would appear at the output), then it follows from Eq. (41) that the matrix

18

$$\underline{X} + \frac{1}{2} N_0 \underline{Y} \qquad (47)$$

is positive definite, and its inverse exists (Ref. 14, p. 46). Since the inverse of a matrix is itself unique, it follows that the solution Eq. (46) exists and is unique. Moreover, the facts that

$$\frac{\partial^2 J}{\partial \underline{g}^2} = 2[\underline{X} + \frac{1}{2} N_0 \underline{Y}] \qquad (48)$$

and that the matrix of (47) is positive definite, are sufficient conditions to guarantee that our solution Eq. (46) does indeed render a minimum of Eq. (44) (see Ref. 15, p. 227).

Having thus arrived at the tap-gain settings which minimize the total distortion at the output, we next want to determine their asymptotic behavior as the length of the TDL becomes arbitrarily large. We define a unity vector $\underline{u}$:

$$\underline{u} \triangleq \begin{bmatrix} \cdot \\ \cdot \\ \cdot \\ 0 \\ 0 \\ 1 \\ 0 \\ 0 \\ \cdot \\ \cdot \\ \cdot \end{bmatrix} . \qquad (49)$$

Noting that

$$(\underline{Y}\underline{u})_k = \sum_m Y_{km} u_m = Y_{k0} = \varphi_k \qquad (50)$$

and

$$(\underline{Y}\underline{Y})_{mv} = \sum_k Y_{mk} Y_{kv} = \sum_k \varphi_{m-k} \varphi_{k-v} = X_{mv} \qquad (51)$$

then, asymptotically, we may write

$$\underline{Y}\underline{u} = \varphi \implies \underline{Y}^{-1} \varphi = \underline{u} \qquad (52)$$

and

$$\underline{Y}\underline{Y} = \underline{X} \quad . \qquad (53)$$

Using Eqs. (52) and (53) in Eq. (46), and ignoring for the moment the denominator which is merely the normalization, we find asymptotically the solution

$$\underline{g} = [\underline{Y}\underline{Y} + \frac{1}{2} N_0 \underline{Y}]^{-1} \varphi = [\underline{Y} + \frac{1}{2} N_0 \underline{I}]^{-1} \underline{u} \quad . \qquad (54)$$

19

We next want to study this asymptotic result still further. Rewriting Eq. (54) in terms of a summation, we have

$$\sum_j [\varphi_{i-j} + \frac{1}{2} N_0 \delta_{ij}] g_j = \delta_{i0} \quad . \tag{55}$$

Subtracting the $j = 0$ term from both sides, and normalizing the tap-gain vector such that $g_0 = 1$, we find the tap gains must satisfy

$$\sum_{j \neq 0} [\varphi_{i-j} + \frac{1}{2} N_0 \delta_{ij}] g_j = -\varphi_i \tag{56}$$

for all $i \neq 0$. Dividing through by N_0, and noting by comparison of Eqs. (8) and (31) that $\varphi_i/N_0 = b_i$, then Eq. (56) becomes

$$\sum_{j \neq 0} [b_{i-j} + \frac{1}{2} \delta_{ij}] g_j = -b_i \quad i \neq 0 \quad . \tag{57}$$

But, from Eq. (19) we observe that $c_i = b_i$ for $i \neq 0$, and from Eq. (20) that $b_{i-j} + (1/2) \delta_{ij} = Q_{ij}$; hence, Eq. (57) is seen to be identical to Eq. (25). Thus, we have shown that the tap gains minimizing the total output distortion of the conventional equalizer are asymptotically the same as the tap gains obtained for the optimal receiver which was designed assuming that the interference from other bauds was Gaussian, as the length of the TDL becomes arbitrarily large.

Next, we observe that Eq. (54) may be written as

$$[\underline{Y} + \frac{1}{2} N_0 \underline{I}] \underline{g} = \underline{u} \quad . \tag{58}$$

From Eq. (40) we note that $\underline{Y}$ is a Toeplitz matrix, since the elements along any of its diagonals are the same, $Y_{ij} = Y_{i+1,j+1}$ (see, for example, Ref. 16). Thus, asymptotically, Eq. (58) becomes equivalent to convolving the row vector

$$\underline{u}^T [\underline{Y} + \frac{1}{2} N_0 \underline{I}] \tag{59}$$

with the tap-gain vector $\underline{g}$ to obtain the vector $\underline{u}$. Therefore, this may be written as a set of equations

$$\sum_m [\varphi_{k-m} + \frac{1}{2} N_0 u_{k-m}] g_m = u_k \quad . \tag{60}$$

Further, by defining transforms

$$G(\omega) \triangleq \sum_m g_m e^{-jm\omega} \tag{61}$$

$$\Phi(\omega) \triangleq \sum_m \varphi_m e^{-jm\omega} \tag{62}$$

and

$$U(\omega) \triangleq \sum_m u_m e^{-jm\omega} = 1 \tag{63}$$

it follows that we may solve Eq. (60) by first setting

$$G(\omega) = \frac{1}{\Phi(\omega) + \frac{1}{2} N_0}$$ (64)

and then inverse transforming to obtain the tap-gain vector components

$$g_m = \int G(\omega) e^{jm\omega} d\omega \quad .$$ (65)

The relation Eq. (64) was obtained previously by George,[17] except for an arbitrary gain factor he incurs by neglecting normalization. George arrived at this relation somewhat more directly by starting out initially with an unconstrained linear receiver. Later, Coll[18] adopted the resulting conventional receiver structure and, using a variational approach as George had done, determined the tap-gain equations for minimizing the output distortion for TDL of finite length. Our formulation led directly to the solution for TDL of finite length, and then asymptotically to George's result. The approach we present here enabled us to establish the existence and uniqueness of the solution, and to relate it asymptotically with the tap gains obtained in our original derivation of the conventional equalizer structure.

As explained in the Introduction of Sec. I, we will study the performance of the sub-optimal conventional equalizer in detail in Sec. IV, but first, in Sec. III we will consider another sub-optimal receiver — the decision-feedback equalizer.
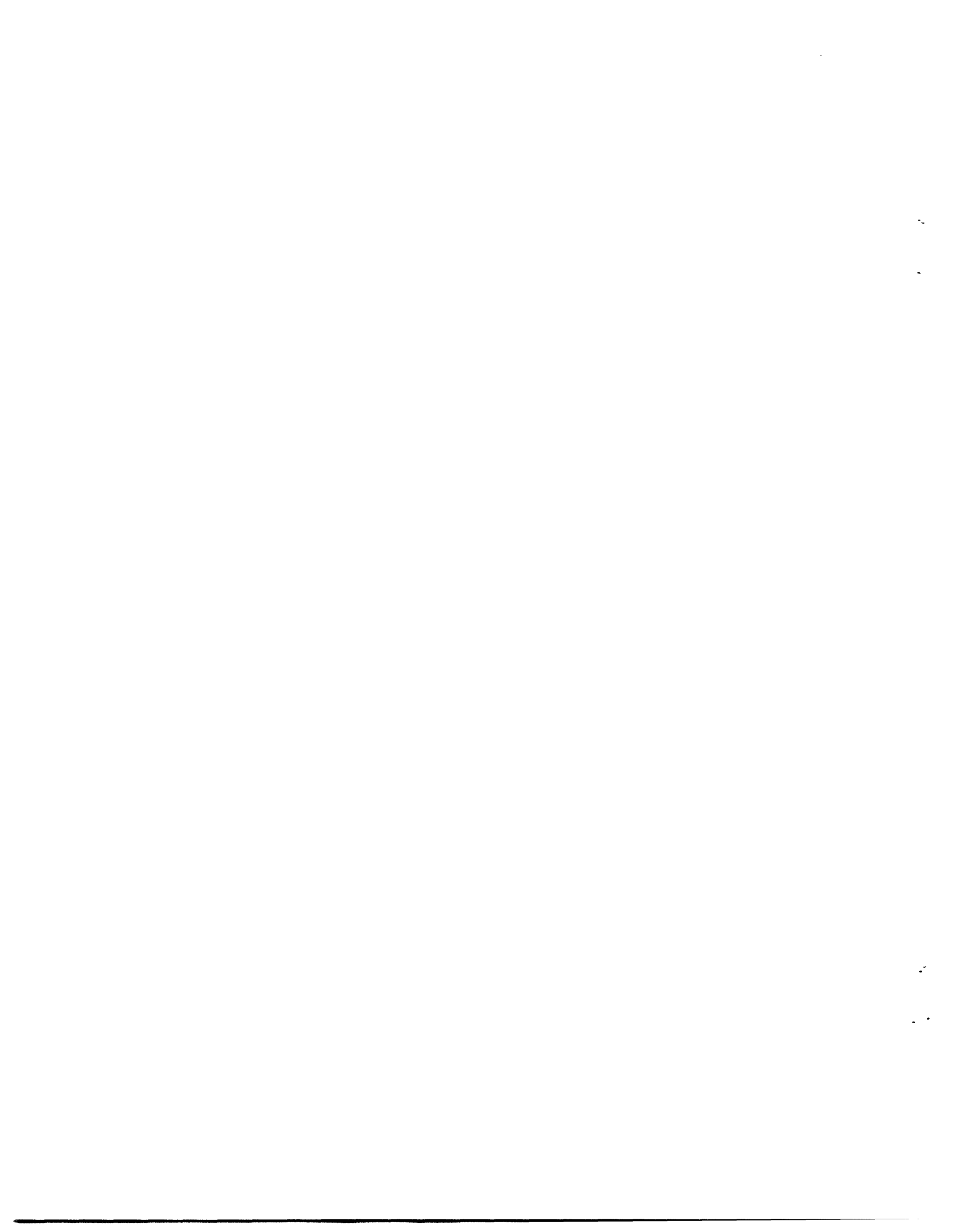
III. EQUALIZATION USING DECISION FEEDBACK

We saw in Sec. I that previous applications of decision feedback in equalization have been concerned, indirectly at least, with effectively measuring the equivalent channel in order to achieve tap-gain settings for the conventional equalizer we derived in Sec. II or its cascade equivalent. Next we derive a new equalizer structure in which the decision feedback plays a different role. We then optimize the parameters of this new structure and, finally, we briefly compare its sidelobe suppression properties with those of the conventional equalizer.

Our problem is the same as that stated in Sec. II, namely, to decide between the hypotheses H_1 and H_0 that ξ_0 is +1 or −1, respectively, given a receiver input

$$r(t) = \sum_k \xi_k h(t - kT) + n(t) \quad . \tag{66}$$

Now, under the assumptions:

(1) ξ_k are independent,

(2) H_0 and H_1 are equally likely, and

(3) $n(t)$ is white Gaussian noise, of double-sided spectral height $N_0/2$,

we found the optimal equalizer structure of Fig. 6. We now make two additional assumptions which will lead us to a sub-optimal receiver structure:

(4) ξ_k are Gaussian random variables of zero mean and unit variance for $k > 0$, and

(5) ξ_k are known for $k < 0$ (i.e., error-free decision feedback).

As we observed in making a similar assumption in Sec. II, Assumption (4) renders our model inaccurate for binary AM or PSK systems in which ξ_k = +1 or −1 for all k, while Assumption (5) is valid for decision-feedback equalizers only in the absence of decision errors.

Under our Assumption (5) that $\underline{\xi}^-$, as defined earlier by Eq. (3), is known correctly via decision feedback, the optimal receiver computes the likelihood ratio

$$\Lambda = \frac{p[r(t) \mid \underline{\xi}^-, \xi_0 = 1]}{p[r(t) \mid \underline{\xi}^-, \xi_0 = -1]}$$

$$= \frac{\int p[r(t) \mid \xi_0, \underline{\xi}^-, \underline{\xi}^+] \, p(\underline{\xi}^+) \, d\underline{\xi}^+ \big|_{\xi_0 = 1}}{\int p[r(t) \mid \xi_0, \underline{\xi}^-, \underline{\xi}^+] \, p(\underline{\xi}^+) \, d\underline{\xi}^+ \big|_{\xi_0 = -1}} \quad . \tag{67}$$

We found earlier in Eq. (6) that we could write

$$p[r(t) \mid \xi_0, \underline{\xi}^-, \underline{\xi}^+] = K_1 \exp\left[\sum_k \xi_k a_k - \sum_i \sum_j \xi_i \xi_j b_{i-j} \right] \tag{68}$$

where the a_k and b_k are defined in Eqs. (7) and (8), respectively. Ignoring constant factors independent of $\underline{\xi}^+$ and the value of ξ_0 which will come outside the integrals in Eq. (67) and cancel each other out, we may rewrite the right-hand side of Eq. (68) as

23

$$\exp\left[\xi_0 a_0 + \sum_{m>0} \xi_m a_m - 2 \sum_{k<0} \sum_{m>0} \xi_k \xi_m b_{k-m}\right.$$

$$\left. - 2\xi_0 \sum_{k<0} \xi_k b_k - 2\xi_0 \sum_{m>0} \xi_m b_m - \sum_{j>0} \sum_{m>0} \xi_j \xi_m b_{j-m}\right] \quad . \tag{69}$$

Now, under Assumption (4), we may write

$$p(\underline{\xi}^+) = K_2 \exp\left[-\frac{1}{2}\sum_{m>0}\xi_m^2\right] = K_2 \exp\left[-\sum_{j>0}\sum_{m>0}\frac{1}{2}\xi_j \delta_{jm}\xi_m\right] \quad . \tag{70}$$

Thus, by combining Eqs. (69) and (70), the numerator of Eq. (67) may be written as

$$\exp\left[\xi_0 a_0 - 2\xi_0 \sum_{k<0}\xi_k b_k\right]\int \exp\left[-\sum_{j>0}\sum_{m>0}\xi_j\left(b_{j-m} + \frac{1}{2}\delta_{jm}\right)\xi_m\right.$$

$$\left. + 2\sum_{m>0}\xi_m\left(\frac{1}{2}a_m - \sum_{k<0}\xi_k b_{k-m} - \xi_0 b_m\right)\right]d\underline{\xi}^+\Bigg|_{\xi_0=1} \quad . \tag{71}$$

By completing the square in the exponent of the integrand of Eq. (71), it is straightforward to show that this numerator of Λ is

$$\exp\left[\xi_0 a_0 - 2\xi_0 \sum_{k<0}\xi_k b_k + \sum_{j>0}\sum_{m>0}\left(\frac{1}{2}a_j - \sum_{k<0}b_{j-k}\xi_k - \xi_0 b_j\right)P_{jm}\right.$$

$$\left. \times\left(\frac{1}{2}a_m - \sum_{n<0}b_{m-n}\xi_n - \xi_0 b_m\right)\right]\Bigg|_{\xi_0=1} \tag{72}$$

where the P_{jm} are the elements of the matrix $\underline{P}$ defined by

$$\underline{P} \triangleq \underline{R}^{-1} \tag{73}$$

and where we have defined the matrix $\underline{R}$ via

$$R_{jm} = b_{j-m} + \frac{1}{2}\delta_{jm} \qquad j, m > 0 \quad . \tag{74}$$

Note that, except for the ranges of their subscripts, the matrix $\underline{R}$ defined by Eq. (74) and the matrix $\underline{Q}$ defined by Eq. (20) are otherwise identical. Since Eq. (72) evaluated at $\xi_0 = -1$ renders the denominator of Eq. (67), it is seen that the optimal receiver, under our assumptions, computes

$$\Lambda = \exp\left\{2a_0 - 4\sum_{k<0}b_k\xi_k - 4\sum_{m>0}b_m\left[\sum_{j>0}\left(\frac{1}{2}a_j - \sum_{k<0}b_{k-j}\xi_k\right)P_{jm}\right]\right\} \quad . \tag{75}$$

If we define

$$g_j \triangleq \sum_{m>0} P_{jm}b_m \tag{76}$$

$$f_k \triangleq 2b_k + 2 \sum_{j>0} g_j b_{j-k} \tag{77}$$

then the decision rule of Eq. (14) becomes

$$a_0 + \sum_{j>0} g_j a_j - \sum_{k<0} f_k \xi_k \mathrel{\underset{H_0}{\overset{H_1}{\gtrless}}} 0 \quad . \tag{78}$$

As shown in Sec. II [see Fig. 4(b)], the a_j are sufficient statistics which may be generated by matched filtering to the equivalent channel, sampling the output synchronously at the baud rate, and passing the samples into a TDL. Note, however, that with the present sub-optimal equalizer, only the a_j for $j \geqslant 0$ enter into the decision rule, just as we noted is true of the optimal equalizer whenever the previously received baud modulations ξ_k are known. Whereas the effects of these earlier-baud ξ_k were accounted for in the optimal equalizer structure by the $C(\Xi)$ constants of Eq. (13), which themselves undergo nonlinear operations before effecting the output, they enter in this sub-optimal equalizer as a weighted sum, the second term of Eq. (78). Thus, the overall decision rule of this sub-optimal receiver may be implemented as shown in Fig. 9.
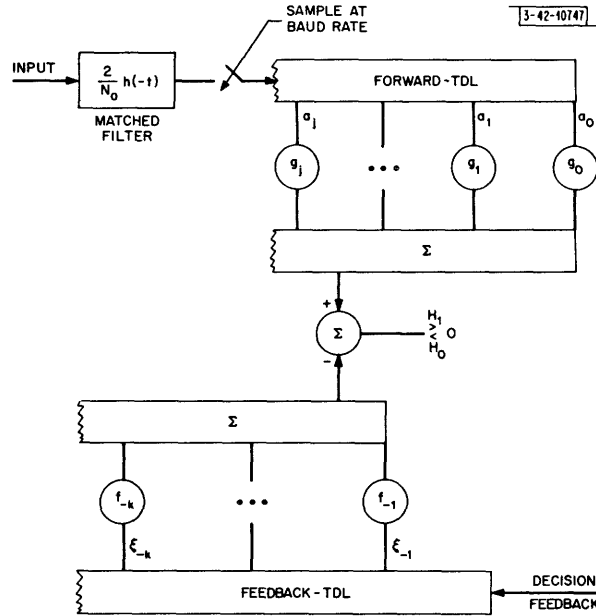
Fig. 9. Structure of decision-feedback equalizer.

It is seen to consist of a forward-TDL, which weights the sufficient statistics a_j by the tap gains g_j for $j \geqslant 0$, where we have defined $g_0 \triangleq 1$, and of a feedback-TDL through which we must pass the ξ_k upon which decisions previously have been made, where they are then weighted by the tap gains f_k.

As discussed in Sec. II when considering the conventional equalizer, the tap gains as defined by Eqs. (76) and (77) are only optimal under the assumption of Gaussian interference from future bauds. Thus, as before, we now want to adopt the equalizer structure of Fig. 9 and determine those forward- and feedback-TDL tap gains that minimize the total distortion appearing at the output in the absence of decision errors. We first introduce some additional definitions that will prove useful in the following discussion:

q_m = signal component of the forward-TDL output at the mth sample
time, when a single ξ_0 = +1 baud is transmitted (79)

$\varphi_k = \int h(t)\, h(t + kT_b)\, dt$ = sampled channel autocorrelation
function at $\tau = kT_b$ (80)

$\underline{Y}$ = matrix with elements $Y_{jk} = \varphi_{j-k}$ for $j, k \geqslant 0$ (81)

$\underline{X}$ = matrix with elements $X_{jk} = \displaystyle\sum_{m<0} \varphi_{j+m}\varphi_{k+m}$ for $j, k \geqslant 0$ (82)

$\underline{\varphi}$ = column vector with elements φ_i for $i \geqslant 0$ (83)

$\underline{g}$ = column vector with elements g_i for $i \geqslant 0$ (84)

$\underline{f}$ = column vector with elements f_{-i} for $i \geqslant 1$ (85)

A typical response of the decision-feedback equalizer to a single transmitted baud of ξ_0 = +1 is shown in Fig. 10. It is always an asymmetrical wa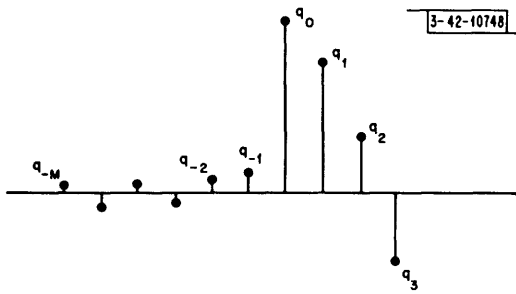veform, having M more samples occurring before the main sample (which is denoted sample number 0) than after it, where the MF output has 2M + 1 nonzero samples. This is in contrast with the typical output from the conventional MF-TDL equalizer, which was seen in Fig. 8 to always exhibit symmetry about the main sample.

Before we can proceed to determine the optimum choices of $\underline{g}$ and $\underline{f}$ under our minimum-output-sample-variance criterion, we must first understand the effect of the decision feedback on the output distortion. Consider the signal component out of the forward-TDL at the first sample time:

Fig. 10. Typical output sidelobes from decision-feedback equalizer for a single ξ_0 = +1 pulse transmission.

$$\sum_{j \geqslant 0} g_j [a_{j+1}]_{signal} = \sum_{j \geqslant 0} g_j \left[\frac{2}{N_0} \int \left\{\sum_k \xi_k h(t - kT_b)\right\} \left\{h[t - (j+1)\,T_b]\right\} dt\right] \quad . \tag{86}$$

The contribution to this component, which is due to the bauds for which decisions have already been made (that is, on all the ξ_k up to and including ξ_0), is then

$$2 \sum_{j \geqslant 0} \sum_{k \leqslant 0} g_j b_{j+1-k}\xi_k \quad . \tag{87}$$

Next, consider the output of the feedback-TDL at this same first sample time. With the use of Eq. (77) for the f_k, this becomes

$$\sum_{k<0} f_k \xi_{k+1} = \sum_{k<0} 2\left[b_k + \sum_{j>0} g_j b_{j-k}\right]\xi_{k+1} \tag{88}$$

26

and, if we let $k* = k + 1$,

$$\sum_{k<0} f_k \xi_{k+1} = 2 \sum_{k*\leqslant 0} \left[b_{k*-1} + \sum_{j>0} g_j b_{j+1-k*} \right] \xi_{k*}$$

$$= 2 \sum_{j\geqslant 0} \sum_{k*\leqslant 0} g_j b_{j+1-k*} \xi_{k*} \quad . \tag{89}$$

Here, we have used $b_{k*-1} = b_{1-k*}$ and our earlier definition, $g_0 \triangleq 1$. Thus, we see from comparing Eqs. (87) and (89) that in the absence of decision errors the feedback-TDL output is exactly the same as the contribution to the forward-TDL output at the first sample time, attributable to past bauds, hence, there is no net contribution to the distortion from those bauds upon which decisions have already been made.

In abandoning Eqs. (76) and (77) in order to optimize the tap gains under a minimum-output-distortion criterion, we wish to retain the nature and purpose of the feedback-TDL as seen above with the optimal solution – namely, to cancel out sidelobes attributable to past bauds. In the absence of decision errors, then, with the feedback-TDL tap-gain vector $\underline{f}$ suitably chosen, it is clear that the output distortion we want to minimize is given by

$$\sum_{m<0} q_m^2 + \text{output noise variance} \quad . \tag{90}$$

Under the constraint that the main sample be unity, we may include q_0 in the summation to find that

$$\sum_{m\leqslant 0} q_m^2 = \sum_{j\geqslant 0} \sum_{k\geqslant 0} g_j X_{jk} g_k = \underline{g}^T \underline{X} \, \underline{g} \tag{91}$$

while the output noise variance can be found, as in Eq. (37), to be

$$\frac{N_0}{2} \sum_{j\geqslant 0} \sum_{k\geqslant 0} g_j Y_{jk} g_k = \frac{N_0}{2} \underline{g}^T \underline{Y} \, \underline{g} \quad . \tag{92}$$

Thus, under the constraint of Eq. (42) that the mainlobe be unity, we proceed as in Sec. II to minimize the quantity

$$J = \underline{g}^T \left[\underline{X} + \frac{N_0}{2} \underline{Y} \right] \underline{g} + \lambda(1 - \underline{g}^T \underline{\varphi}) \tag{93}$$

over the choice of the forward-TDL gain vector $\underline{g}$. The unique solution is again given by

$$\underline{g} = \frac{\left[\underline{X} + \frac{N_0}{2} \underline{Y} \right]^{-1} \underline{\varphi}}{\underline{\varphi}^T \left[\underline{X} + \frac{N_0}{2} \underline{Y} \right]^{-1} \underline{\varphi}} \quad . \tag{94}$$

This result appears formally identical with that obtained for the conventional equalizer, Eq. (46). The differences are in that we have redefined the vector $\underline{\varphi}$ and the matrices $\underline{X}$ and $\underline{Y}$ in Definitions (81), (82), and (83), and now their subscript ranges differ from the ranges used in studying the conventional equalizer. Thus, while $\underline{\varphi}$ was symmetrical and $\underline{X}$ Toeplitz for the conventional equalizer, these properties do not hold for the $\underline{\varphi}$ and $\underline{X}$ for the decision-feedback

27

equalizer. Both of these differences result from the fact that sidelobes occurring after the mainlobe are ignored in the decision-feedback equalizer. In Definition (82), for example, this is reflected in that the summation is restricted to $m \leqslant 0$, whereas the corresponding summation Eq. (39) of the conventional equalizer has no such restriction.

The proper choice of the $\underline{f}$ vector now follows directly from Eq. (77), except that we have dropped the $2/N_0$ factor common to the terms of Eq. (78) (that is, the a_j contained this factor, while it has not been included in the MF output in the present discussion), and thus the $2b_k$ become replaced by the φ_k of Definition (80):

$$f_k = \sum_{j \geqslant 0} g_j \varphi_{j-k} \qquad \text{for } k < 0 \quad . \tag{95}$$

If we define a matrix $\widetilde{\underline{Y}}$ with elements

$$\widetilde{Y}_{jk} = \varphi_{j-k} \qquad \text{for } \begin{cases} j \geqslant 0 \\ k < 0 \end{cases} \tag{96}$$

[note that it is the range of k which distinguishes this matrix from the $\underline{Y}$ matrix of Definition (81)], then the feedback-TDL tap-gain vector may be conveniently written as

$$\underline{f} = \widetilde{\underline{Y}} \underline{g} \quad . \tag{97}$$

Thus, once the sampled channel autocorrelation function and the additive noise level have been specified, we can use Eqs. (94) and (97) to determine the tap gains of the minimum-output-distortion decision-feedback equalizer. Moreover, using the same arguments we presented for the conventional equalizer, we can show that the solutions to these equations exist, are unique, and render a minimum of Eq. (90).

We want next to compare the operation of the decision-feedback equalizer of Fig. 9 with that of the conventional equalizer structure shown in Fig. 7. Since in actual implementation, equalizer cost is directly related to the number of delay elements and amplifiers required, then our comparisons will be based on equalizers having the same number of taps. The conventional equalizer, of course, uses its allotment of taps on its single TDL, while the decision-feedback equalizer must devote part of its taps to the feedback-TDL and the remainder to the forward-TDL.

Before proceeding, we want to consider the number of taps required on the feedback-TDL. We may rewrite Eq. (95) as

$$f_{-k} = \sum_{m \geqslant k} \varphi_m g_{m-k} \qquad \text{for } k > 0 \tag{98}$$

and thus, for a channel where the maximal dispersion is over, say, N bauds (that is, where $\varphi_n = 0$ for $n \geqslant N$), then from Definition (83) it is clear that

$$f_{-k} \equiv 0 \qquad \text{for all } k \geqslant N \quad . \tag{99}$$

Thus, at most, $N - 1$ taps are required in the feedback-TDL of the decision-feedback equalizer, and any additional taps which are available may be employed in the forward-TDL.

The sampled MF output for a single pulse transmitted is always symmetrical, thus it follows from Eq. (38) that a conventional equalizer having an odd number of taps always has a symmetrical tap-gain vector. Hence, a $(2M + 1)$-tap conventional equalizer really has only M degrees of
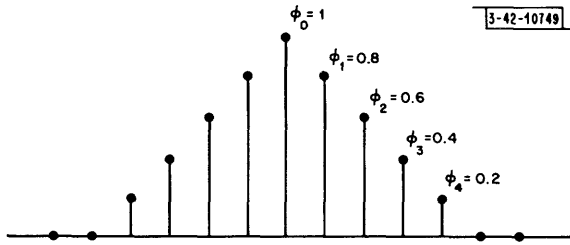
Fig. 11. Example sampled channel autocorrelation function for illustrating sidelobe suppression in conventional and decision-feedback equalizers.

freedom, assuming that the centertap gain is normalized to unity. With these M degrees of freedom, the conventional equalizer must simultaneously attempt to suppress the sidelobes attributable to both past and future baud transmissions. On the other hand, as we noted above, the decision-feedback equalizer feedback-TDL requires only $N - 1$ taps for a channel with a maximal dispersion of N bauds, leaving $2M + 2 - N$ taps and degrees of freedom available for the forward-TDL. Moreover, the forward-TDL gains are computed without regard to the q_m for $m > 0$, and only the q_m for $m < 0$ are taken into account (see Fig. 10). Thus, the forward-TDL need only be concerned with suppressing the sidelobes attributable to future bauds, that is, those bauds upon which decisions have not yet been made.

To illustrate the advantages resulting from the greater degrees of freedom available to the decision-feedback equalizer, we will consider the sampled channel autocorrelation function shown in Fig. 11. Using a 21-tap TDL in the conventional equalizer, with the tap gains given by Eq. (46), the tap-gain vector has a limiting solution with increasing SNR and, accordingly, there is a limiting sidelobe behavior at the output for a single pulse transmission, as shown in Fig. 12(a). The forward-TDL output of the equivalent decision-feedback equalizer, with its tap gains computed according to Eq. (94), is shown in Fig. 12(b). In this example, the conventional equalizer has $M = 10$ degrees of freedom compared with $2M + 2 - N = 17$ degrees of freedom available to the forward-TDL of the decision-feedback equalizer. The resulting sidelobes q_m for $m < 0$ for the decision-feedback equalizer are seen to be considerably smaller under either a D_α or D_β distortion criterion [defined in Eqs. (28) and (29), respectively] than are the sidelobes of the conventional equalizer. As we discuss further in Secs. IV, V, and VI, this greater sidelobe-suppression behavior results in a large improvement in the performance of the decision-feedback equalizer over that of the conventional equalizer.

As expected, the sidelobes q_m for $m > 0$ at the output of the decision-feedback equalizer forward-TDL are very large, since they were not involved in the tap-gain optimization. In the absence of decision errors, these large sidelobes are exactly subtracted out by the feedback-TDL component of the output, as we observed previously.

(a) CONVENTIONAL EQUALIZER
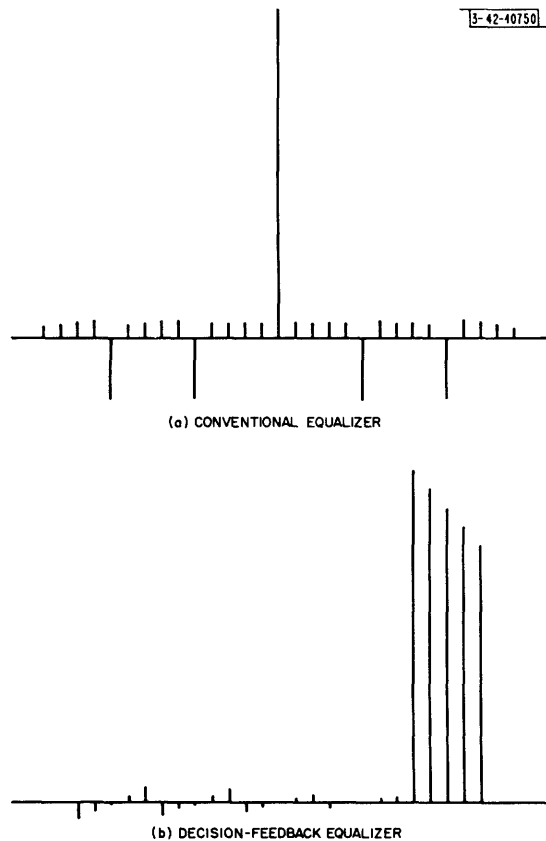
(b) DECISION-FEEDBACK EQUALIZER

Fig. 12(a-b). Limiting sidelobes with increasing SNR of 21-tap conventional and decision-feedback equalizers, applied to channel of Fig. 11.

29

When an error does occur, however, this same feedback-TDL output then enhances these large sidelobes rather than eliminating them. As a consequence, on the next decision an additional sidelobe of magnitude $2q_1$ appears as distortion at the decision-feedback equalizer output. This large distortion term results in a greatly increased probability of a decision error on the next baud and, in fact, on the next $N - 1$ bauds, since the feedback-TDL has $N - 1$ taps for a channel spread over N bauds or less. It therefore follows that one error can lead to a second error which, in turn, causes another, etc. This is referred to as "error propagation," an issue which we examine in detail in Sec. V, where we fully investigate the performance of the decision-feedback equalizer derived above. For purposes of comparison, however, we first consider the performance of the conventional equalizer in Sec. IV.

IV. PERFORMANCE OF THE CONVENTIONAL EQUALIZER

We now evaluate the performance of the conventional equalizer structure derived in Sec. II, with a view to comparing it with the performance of the decision-feedback equalizer derived in Sec. III. Such a comparison, however, necessarily involves consideration of a specific channel, or class of channels. We describe next the class of channels which we have chosen (the maximal distortion channels), after which we present an algorithm for the efficient evaluation of the conventional equalizer performance; finally, we present the results obtained by applying this new algorithm to the maximal distortion channels.

A. MAXIMAL DISTORTION CHANNELS

We want to determine those channels which, for a given overall dispersion of N baud intervals, exhibit the maximum realizable distortion, as measured under the D_β criterion of Eq. (29). Thus, as indicated in Fig. 13 (where the baud duration T has been normalized to unity for convenience), our problem is to determine the sampled channel autocorrelation functions having the largest D_β. Other than normalizing d_0 to unity, the only constraint on the d_i is that of realizability, namely, that the transform of the autocorrelation function defined by

$$D(\omega) \triangleq \sum_{n=-N+1}^{N-1} d_n e^{-jn\omega} = 1 + 2 \sum_{n=1}^{N-1} d_n \cos(n\omega) \tag{100}$$

be non-negative over the interval $\omega \in (0, \pi)$. (The transform must be non-negative for all ω, of course, but $D(\omega)$ is symmetrical about the origin and of period 2π, so we only need consider the interval indicated.)
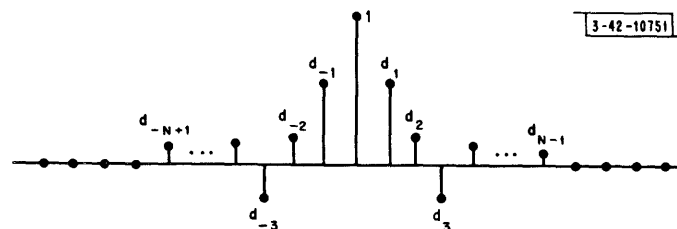

Fig. 13. Sampled autocorrelation function of an Nth-order dispersive channel, that is, where the dispersion extends over N bauds.

At this point, we want to visualize an $(N-1)$-dimensional "sidelobe space," with the d_n as the coordinates. We then define that portion of this sidelobe space within which $D(\omega)$ is non-negative over $(0, \pi)$ as the "region of realizability." This region always includes the origin, since all the sidelobes may be set equal to zero, corresponding to a nondispersive channel. Moreover, since it is a well-known property of autocorrelation functions that they attain their maximum at the point corresponding to the center sample d_0 in Fig. 13, which we have normalized to unity, it then follows that the region of realizability is bounded, being within a hypercube having sides of length two centered at the origin. By its very definition, it follows that, at points outside the region of realizability, $D(\omega)$ becomes negative. Since, from Eq. (100) we observe that $D(\omega)$ is a continuous function of the d_n, then it clearly must just vanish at its minima on the boundary of

the region of realizability. Moreover, the quantity we want to maximize subject to realizability, D_β, is recognized to be constant over hyperplanes in each hyperquadrant of sidelobe space. Since D_β increases with the distance of these hyperplanes from the origin, it is clear that any point maximizing D_β must lie on the boundary of the region of realizability, for the maximum D_β will be attained on the hyperplane which is just tangent to the region of realizability. From this and our above result, we conclude that $D(\omega)$ must vanish at its minima for the desired maximal distortion channel.

We next consider the minima of $D(\omega)$. Let ω_i be a frequency at which $D(\omega)$ has a minimum. Then, ω_i must satisfy the two equations

$$D'(\omega_i) = -2 \sum_{n=1}^{N-1} n d_n \sin(n\omega_i) = 0 \qquad (101)$$

$$D''(\omega_i) = -2 \sum_{n=1}^{N-1} n^2 d_n \cos(n\omega_i) > 0 \qquad (102)$$

where Eq. (101) requires that ω_i correspond to a critical point, and Eq. (102) insures that it is a minimum rather than a maximum or inflection point. Now, since

$$\sin(n\omega_i) = \sin(\omega_i) \, p^{(n-1)}[\cos(\omega_i)] \qquad (103)$$

where $P^{(n)}[x]$ denotes an nth-order polynomial in x, then clearly two of the critical points are always at $\omega_i = 0$ and $\omega_i = \pi$. Now, $n \leqslant N - 1$ in Eq. (101); thus, from Eq. (103) the highest order polynomial in $\cos(\omega_i)$ encountered there is of order $N - 2$. Moreover, since $\cos(\omega_i)$ is single valued over the $(0, \pi)$ interval of interest, then this polynomial will render exactly $N - 2$ additional critical frequencies ω_i, giving a total number of N critical frequencies for the Nth-order channel of Fig. 13. N/2 of these, or the largest integer in N/2, correspond to minima of $D(\omega)$.

Now, imposing the constraint arrived at earlier that $D(\omega)$ vanish at its minima for the maximal distortion channel, we want to maximize the quantity

$$J = D_\beta + \sum_{i=1}^{[N/2]} \lambda_i D(\omega_i) \qquad (104)$$

where we have introduced the Lagrange multipliers λ_i, [N/2] denotes the largest integer in N/2, and the summation is seen to be taken over all those ω_i corresponding to the minima of $D(\omega)$. Noting from Eq. (29) that

$$\frac{\partial D_\beta}{\partial d_n} = 2 \, \text{sgn}(d_n) \qquad (105)$$

and from Eq. (100) that

$$\frac{\partial D(\omega_i)}{\partial d_n} = 2 \cos(n\omega_i) + \left. \frac{\partial D(\omega)}{\partial \omega} \right|_{\omega=\omega_i} \left(\frac{\partial \omega_i}{\partial d_n} \right) \qquad (106)$$

where, at the minima points ω_i, the quantity $\partial D(\omega)/\partial \omega$ vanishes, we may combine Eqs. (104) to (106) to find $\partial J/\partial d_n$. Doing this, and recalling our constraints, we find the set of equations which the maximal distortion solutions must satisfy:

$$\frac{\partial J}{\partial d_n} = \text{sgn}(d_n) + \sum_{i=1}^{[N/2]} \lambda_i \cos(n\omega_i) = 0 \qquad (107)$$

$$D(\omega_i) = 1 + 2 \sum_{n=1}^{N-1} d_n \cos(n\omega_i) = 0 \quad . \qquad (108)$$

Next, we observe that if $\tilde{d}_1, \ldots, \tilde{d}_{N-1}$ is a solution to Eqs. (107) and (108), then, from the relation

$$\tilde{D}(\omega) \triangleq 1 + 2 \sum_{n=1}^{N-1} \tilde{d}_n \cos(n\omega)$$

$$= 1 + 2 \sum_{n=1}^{N-1} (-1)^n \tilde{d}_n \cos[n(\pi - \omega)] \triangleq D(\pi - \omega) \qquad (109)$$

we can conclude that defining

$$d_n = (-1)^n \tilde{d}_n \qquad (110)$$

also renders a maximal distortion solution, since from Eq. (109) it is seen that $D(\omega)$ is simply $\tilde{D}(\omega)$ reversed within the interval $(0, \pi)$. Thus, we conclude that the odd-numbered sidelobes of a maximal distortion solution may all be reversed in sign to obtain a second maximal distortion solution. We henceforth refer to this as the "symmetry" property with respect to the odd-numbered sidelobes.

We now want to apply all of the above, and to determine the class of maximal distortion channels. Considering first the simplest case where the channel is spread over two bauds ($N = 2$), we have a single sidelobe d_1. Because Eq. (107) involves $\text{sgn}(d_1)$, there are two situations to consider. However, one of these can be obtained from the symmetry property shown above, thus we need only consider the case where d_1 is positive. In this case, Eqs. (107), (108), (101), and (102) become, respectively,

$$\frac{\partial J}{\partial d_1} = 1 + \lambda_1 \cos(\omega_1) = 0$$

$$D(\omega_1) = 1 + 2d_1 \cos(\omega_1) = 0$$

$$D'(\omega_1) = -2d_1 \sin(\omega_1) = 0$$

$$D''(\omega_1) = -2d_1 \cos(\omega_1) > 0 \quad . \qquad (111)$$

This set of equations has the unique solution

$$\lambda_1 = 1$$

$$\cos(\omega_1) = -1$$

$$\sin(\omega_1) = 0$$

$$d_1 = \frac{1}{2} \quad . \qquad (112)$$

33

Thus, by using the symmetry property, the two maximal solutions are $d_1 = \pm 1/2$, both rendering a distortion $D_\beta = 1$. The corresponding sampled channel autocorrelation functions and a cycle of their transforms are shown in Figs. 14(a) and (b), respectively. These will be discussed further below.
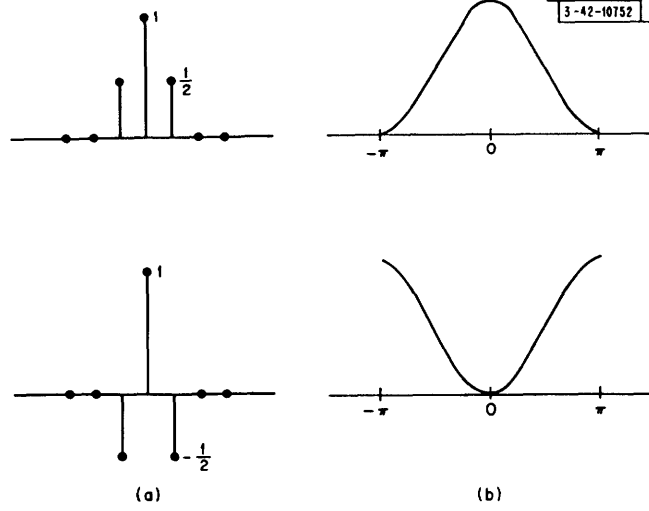

Fig. 14. Second-order maximal distortion channels: (a) sampled autocorrelation functions, and (b) corresponding frequency spectra.

For the $N = 3$ case, there are four situations, two of which may be found from the symmetry property. Remaining then are case (1) where d_1 and d_2 are both positive, and case (2) where d_1 is positive and d_2 is negative. For case (1), the equations we must solve become

$$\frac{\partial J}{\partial d_1} = 1 + \lambda_1 \cos(\omega_1) = 0$$

$$\frac{\partial J}{\partial d_2} = 1 + \lambda_1 \cos(2\omega_1) = 0$$

$$D(\omega_1) = 1 + 2d_1 \cos(\omega_1) + 2d_2 \cos(2\omega_1) = 0$$

$$D'(\omega_1) = -2d_1 \sin(\omega_1) - 4d_2 \sin(2\omega_1) = 0$$

$$D''(\omega_1) = -2d_1 \cos(\omega_1) - 8d_2 \cos(2\omega_1) > 0 \tag{113}$$

which has the unique solution

$$\lambda_1 = 2$$

$$\cos(\omega_1) = \cos(2\omega_1) = -\frac{1}{2}$$

$$\sin(\omega_1) = -\sin(2\omega_1) = \frac{\sqrt{3}}{2}$$

$$d_1 = \frac{2}{3}$$

$$d_2 = \frac{1}{3} \tag{114}$$

34

corresponding to a $D_\beta = 2$. For case (2), all the above equations still hold except that for $\partial J/\partial d_2$, which becomes

$$\frac{\partial J}{\partial d_2} = -1 + \lambda_1 \cos(2\omega_1) = 0 \tag{115}$$

leading to the non-unique solution

$$\lambda_1 = 1$$

$$\cos(\omega_1) = -\cos(2\omega_1) = -1$$

$$\sin(\omega_1) = \sin(2\omega_1) = 0$$

$$2d_1 - 2d_2 = 1 \quad . \tag{116}$$

But this last equation simply states that $D_\beta = 1$, which is less than that obtained with case (1). Applying the symmetry property, it therefore follows that the maximal distortion solutions are $d_1 = \pm 2/3$, $d_2 = 1/3$. The corresponding sampled channel autocorrelation functions and a cycle of their transforms are shown in Figs. 15(a) and (b), respectively.

From Figs. 14(a) and 15(a), one might suspect that perhaps one of the maximal distortion solutions always has a triangular envelope, as indicated in Figs. 16(a) and (b) for the N = 2 and N = 3 cases considered above. This may be investigated for arbitrary N by considering the triangular channel autocorrelation function $\varphi_{hh}(\tau)$ shown in Fig. 16(c). Its conventional Fourier transform is given by
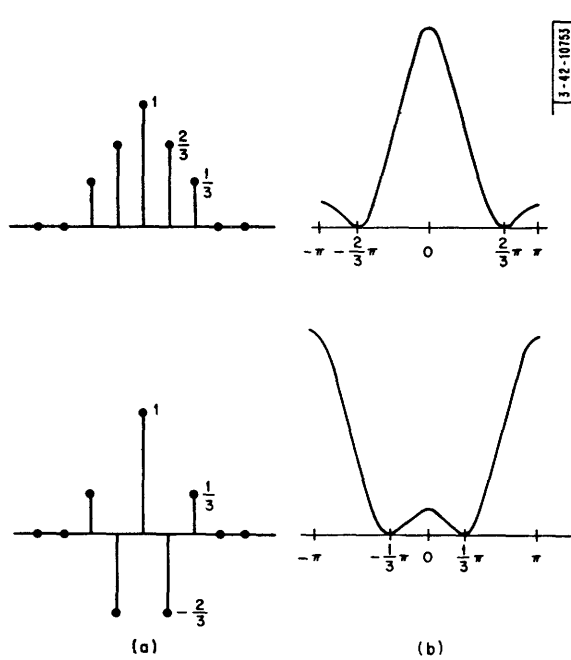

Fig. 15. Third-order maximal distortion channels: (a) sampled autocorrelation functions, and (b) corresponding frequency spectra.
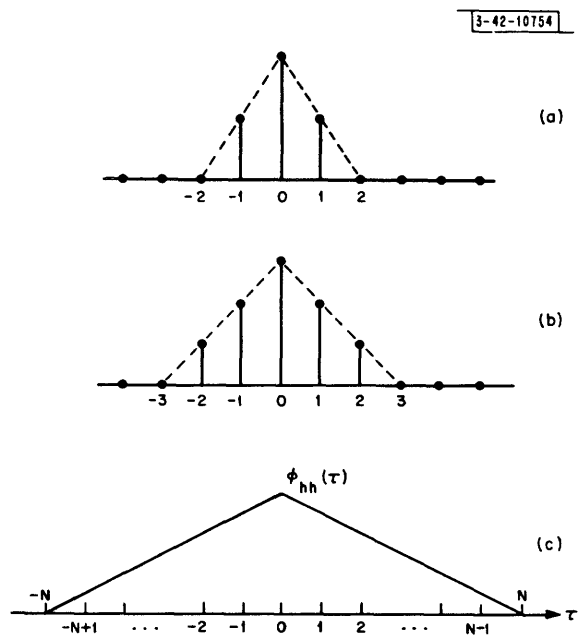

Fig. 16. Autocorrelation functions with triangular envelopes: (a) second-order maximal distortion channel; (b) third-order maximal distortion channel; (c) continuous N^{th}-order channel autocorrelation function.

$$\Phi_{hh}(\omega) = \int_{-\infty}^{\infty} \varphi_{hh}(\tau)\, e^{-j\omega\tau}\, d\tau = N\,[\frac{\sin(N\omega/2)}{N\omega/2}]^2 \qquad (117)$$

as sketched in Fig. 17(a).   The equivalent to the sampled version of Fig. 16(b) may be obtained by multiplying it with an impulse train whose Fourier transform, also an impulse train, is shown in Fig. 17(b).   The transform of the resulting sampled channel autocorrelation function
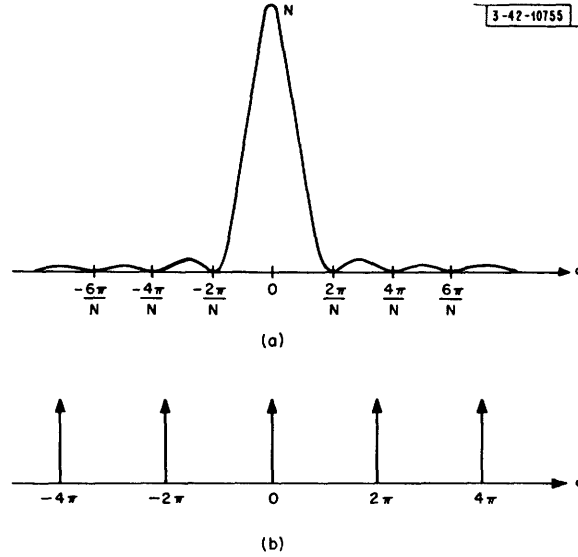

Fig. 17.   Transforms used in derivation of maximal distortion channels:
(a) transform of autocorrelation function of Fig. 16(c), and (b) transform
of an impulse train.

may then be found through convolution of the waveforms in Figs. 17(a) and (b).   The resulting transform $D(\omega)$ has, by inspection, the following properties:

(1) $D(\omega)$ has minima at $\omega_i = 2\pi i/N$ for $i = 1, \ldots, N - 1$

(2) $D(\omega)$ vanishes at all such minima ω_i

(3) $D(\omega)$ is periodic with period 2π.

It therefore follows that sampled channel autocorrelation functions with triangular envelopes satisfy conditions of Eqs. (101), (102), and (108).   To show they are indeed maximal distortion solutions, we must show that Eq. (107) is satisfied as well.   As explained earlier, only the minima occurring within the interval $(0, \pi)$ need be considered, which from property (1) above means summing over $1 \leqslant i \leqslant N/2$ in Eq. (107):

$$\frac{\partial J}{\partial d_n} = 1 + \sum_{i=1}^{[N/2]} \lambda_i \cos(2\pi ni/N) = 0 \qquad (118)$$

for $1 \leqslant n \leqslant N - 1$, where we have applied $\mathrm{sgn}(d_n) = 1$ for the present case.   Moreover, since

$$\cos[2\pi(N - n)\,i/N] = \cos(2\pi ni/N)$$

then, to prove that the sampled channel autocorrelation function having a triangular envelope vanishing at $\tau = N$ is the maximal distortion channel, we need only to show that a set of Lagrange multipliers λ_i exists to satisfy Eq. (118) for $n = 1, \ldots, [N/2]$.

36

If we define a matrix $\underline{A}$ with elements

$$A_{ij} = \cos(2\pi ij/N) \qquad 1 \leqslant i, j \leqslant N/2 \tag{119}$$

then Eq. (118) may be written as the matrix equation

$$\left[A_{ij}\right]
\begin{bmatrix}
\lambda_1 \\
\lambda_2 \\
\cdot \\
\cdot \\
\cdot \\
\lambda_{[N/2]}
\end{bmatrix}
=
\begin{bmatrix}
-1 \\
-1 \\
\cdot \\
\cdot \\
\cdot \\
-1
\end{bmatrix}
\tag{120}$$

where we recall that $[N/2]$ is defined to be the largest integer in $N/2$. A solution to Eq. (120) exists whenever $\underline{A}$ is nonsingular, having a nonzero determinant. While we have not been able to establish this for general N, it appears true, as shown below for N = 2 through N = 7:

$$N = 2 \qquad \det\underline{A} = |\cos(2\pi/2)| = -1 \neq 0$$

$$N = 3 \qquad \det\underline{A} = |\cos(2\pi/3)| = -1/2 \neq 0$$

$$N = 4 \qquad \det\underline{A} = \begin{vmatrix} \cos(2\pi/4) & \cos(4\pi/4) \\ \cos(4\pi/4) & \cos(8\pi/4) \end{vmatrix} = -1 \neq 0$$

$$N = 5 \qquad \det\underline{A} = \begin{vmatrix} \cos(2\pi/5) & \cos(4\pi/5) \\ \cos(4\pi/5) & \cos(8\pi/5) \end{vmatrix} = -0.559 \neq 0$$

$$N = 6 \qquad \det\underline{A} = \begin{vmatrix} \cos(2\pi/6) & \cos(4\pi/6) & \cos(6\pi/6) \\ \cos(4\pi/6) & \cos(8\pi/6) & \cos(12\pi/6) \\ \cos(6\pi/6) & \cos(12\pi/6) & \cos(18\pi/6) \end{vmatrix} = 3/2 \neq 0$$

$$N = 7 \qquad \det\underline{A} = \begin{vmatrix} \cos(2\pi/7) & \cos(4\pi/7) & \cos(6\pi/7) \\ \cos(4\pi/7) & \cos(8\pi/7) & \cos(12\pi/7) \\ \cos(6\pi/7) & \cos(12\pi/7) & \cos(18\pi/7) \end{vmatrix} = 0.875 \neq 0 \quad .$$

Granting that sampled channel autocorrelation functions having triangular envelopes (such as we have drawn in Fig. 18) render maximal distortion (as we showed above, at least for channels with dispersions up to N = 7 bauds duration), we find from the symmetry property that a second maximal distortion solution may be obtained by changing the signs of the odd-numbered sidelobes. From Eq. (46), however, it is easily established for the conventional equalizer that its optimal tap-gain vectors corresponding to these two choices of maximal distortion channels
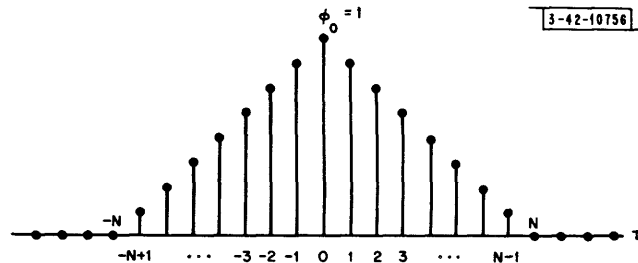

Fig. 18. N^{th}-order maximal distortion channel sampled autocorrelation function.

37

are identical, except that the polarity of their odd-numbered gains is reversed. Moreover, this renders output sidelobes which are identical except for a polarity reversal of the odd-numbered sidelobes. Consequently, the output distortion with either choice of sampled channel autocorrelation function is the same. From Eq. (94), we see that this is also true for the decision-feedback equalizer; thus, in the cases to be considered later in this Section and again in Sec. V, we will arbitrarily choose the first case, where the d_n are taken as positive.

B. ERROR TREE ALGORITHM

We next want to determine the performance of the conventional equalizer derived in Sec. II. As we noted previously, the input to the conventional equalizer TDL for a single $\xi_0 = 1$ transmitted pulse is the symmetrical sampled channel autocorrelation function, resulting in a symmetrical tap-gain vector and symmetrical output sidelobes, as sketched in Fig. 8. If there are a total of 2M such sidelobes (M on either side of the mainlobe), then in making a decision on, say, ξ_0 when a continuous message sequence has been transmitted, these sidelobes are weighted by the ξ_k to render the intersymbol interference distortion D appearing at the output:

$$D = \sum_{k=-M}^{M}{}' q_{-k}\xi_k \qquad (121)$$

where the prime on the summation denotes that the k = 0 term is to be omitted from the sum. For any given distortion D and output additive noise variance σ^2, we may determine the conditional probability of error from

$$p(\text{error}|D) = \frac{1}{2}\ \text{erfc}\left(\frac{1+D}{\sqrt{2}\ \sigma}\right) \qquad (122)$$

where

$$\text{erfc}(z) = \frac{2}{\sqrt{\pi}} \int_z^\infty e^{-t^2}\ dt \qquad (123)$$

is the complementary error function. Thus, noting that, for a given set of sidelobes, D depends only upon the ξ_k, it is clear that we could (at least conceptually) determine the probability of error via the relation

$$p(\text{error}) = \sum_{\underline{\xi}^-} \sum_{\underline{\xi}^+} p(\text{error}|\underline{\xi}^-, \underline{\xi}^+)\ p(\underline{\xi}^-, \underline{\xi}^+) \qquad (124)$$

where we have here modified Definitions (3) and (4) to cover only the desired M bauds into the past and future:

$$\underline{\xi}^- \triangleq \{\xi_k | -M \leqslant k \leqslant -1\} \qquad (125)$$

$$\underline{\xi}^+ \triangleq \{\xi_k | 1 \leqslant k \leqslant M\} \qquad (126)$$

and where

$$p(\underline{\xi}^-, \underline{\xi}^+) = 2^{-2M} \qquad (127)$$

since the ξ_k were assumed to be independent binary random variables.

38

The difficulty with this straightforward approach (adopted for a simple case in Ref. 13) is that the summation of Eq. (124) involves a total of 2^{2M} terms which, for practical channel dispersions and equalizer lengths of interest, can become prohibitively large. For example, in one of the cases considered below, M = 19, corresponding to $2^{38} = 2.7 \times 10^{11}$ terms to be included in the summation of Eq. (124).

We may simplify matters somewhat by first rewriting Eq. (121):

$$D = \sum_{k=1}^{M} (q_{-k}\xi_k + q_k\xi_{-k}) \quad . \tag{128}$$

Then, since $q_k = q_{-k}$ from sidelobe symmetry, it follows that the kth term of Eq. (128) may assume three values:

$$(q_{-k}\xi_k + q_k\xi_{-k}) = \begin{cases} 2q_k & \text{with probability } \frac{1}{4} \\ 0 & \text{with probability } \frac{1}{2} \\ -2q_k & \text{with probability } \frac{1}{4} \end{cases} . \tag{129}$$

Thus, if we define new "equivalent" sidelobes

$$\tilde{b}_k \triangleq 2|q_k| \tag{130}$$

and new independent random variables

$$\tilde{\eta}_k \triangleq \begin{cases} 1 & \text{with probability } \frac{1}{4} \\ 0 & \text{with probability } \frac{1}{2} \\ -1 & \text{with probability } \frac{1}{4} \end{cases} \tag{131}$$

then an intersymbol interference distortion statistically equivalent to Eq. (128) is

$$D = \sum_{k=1}^{M} \tilde{b}_k\tilde{\eta}_k \tag{132}$$

and, thus, an alternative expression for Eq. (124) is

$$p(\text{error}) = \sum_{\tilde{\underline{\eta}}} p(\text{error}|\tilde{\underline{\eta}})\, p(\tilde{\underline{\eta}}) \tag{133}$$

where we have defined $\tilde{\underline{\eta}} = \{\tilde{\eta}_k\}$. The summation of Eq. (133) has 3^M terms, since the M different η_k may each assume the three values indicated in Eq. (131). Since $3^M < 2^{2M} = 4^M$, it is seen that Eq. (133) represents a large reduction in computation over Eq. (124), indeed by a factor of $(4/3)^M = 235$ for our M = 19 case. Unfortunately, however, $3^{19} = 1.1 \times 10^9$ is still far too large a number of terms to sum in practice. Therefore, we next derive a new algorithm which, as we will see later in this Section, reduces further the summation requirements to the point where obtaining arbitrarily close upper and lower bounds on Eq. (133) becomes computationally feasible.

We begin by rearranging the sidelobes of Eq. (130), defining a new set of sidelobes denoted by $b_1, b_2, \ldots, b_M$ which correspond one-to-one with the $\tilde{b}_k$ of Eq. (130), but where now they are ordered such that

$$b_1 \geqslant b_2 \geqslant \ldots \geqslant b_M \quad . \tag{134}$$

These sidelobes, just as those of Eq. (130), are all positive, corresponding to the doubled magnitudes of the original set of sidelobes q_k except for ordering. Also, defining $\underline{\eta} = \{\eta_1, \eta_2, \ldots, \eta_M\}$ to be the corresponding rearrangement of $\underline{\tilde{\eta}}$, we may write Eqs. (132) and (133) as

$$D = \sum_{k=1}^{M} b_k \eta_k \tag{135}$$

$$p(\text{error}) = \sum_{\underline{\eta}} p(\text{error} | \underline{\eta}) \, p(\underline{\eta}) \quad . \tag{136}$$

Because the weightings b_k in Eq. (135) are non-increasing and usually decreasing with k, we would expect that many of the $\underline{\eta}$ appearing in Eq. (136) will have distortions D essentially determined by their first few components. If this were strictly true, we could compute the combined contribution to Eq. (136) from all $\underline{\eta}$ having identical first few components, thereby reducing the overall number of terms to be included in Eq. (136). Since the latter components of $\underline{\eta}$ cannot be legitimately ignored altogether, however, we instead consider upper and lower bounds on their contribution.

Let $\underline{\eta}^*$ denote $\{\eta_1^*, \eta_2^*, \ldots, \eta_K^*, \eta_{K+1}, \ldots, \eta_M\}$, where the η_k^* have been specified and the η_k are arbitrary. We may then define quantities

$$D_L(K) \triangleq \sum_{k=1}^{K} b_k \eta_k^* + \sum_{k=K+1}^{M} b_k \tag{137}$$

$$D_U(K) \triangleq \sum_{k=1}^{K} b_k \eta_k^* - \sum_{k=K+1}^{M} b_k \tag{138}$$

which correspond to the largest and smallest distortions which any such $\underline{\eta}^*$ can cause. The subscripts L and U are adopted because use of these distortions in Eq. (122) renders "lower" and "upper" bounds on the conditional probability of error for any such $\underline{\eta}^*$, respectively:

$$P_L(K) \triangleq \frac{1}{2} \operatorname{erfc} \left[\frac{1 + D_L(K)}{\sqrt{2}\,\sigma} \right] \tag{139}$$

$$P_U(K) \triangleq \frac{1}{2} \operatorname{erfc} \left[\frac{1 + D_U(K)}{\sqrt{2}\,\sigma} \right] \quad . \tag{140}$$

Next, we let $\underline{\eta} \in \underline{\eta}^*$ denote that the first K components of $\underline{\eta}$ are identical with those of $\underline{\eta}^*$. Then, from the discussion above, we may write for any such $\underline{\eta}$:

$$P_L(K) \leqslant p(\text{error} | \underline{\eta}) \leqslant P_U(K) \quad . \tag{141}$$

Further, observing that

40

$$\sum_{\underline{\eta} \in \underline{\eta}^*} p(\underline{\eta}) = \prod_{k=1}^{K} p(\eta_k^*) \sum_{\eta_{K+1}} \cdots \sum_{\eta_M} \prod_{j=K+1}^{M} p(\eta_j)$$

$$= \prod_{k=1}^{K} p(\eta_k^*) \qquad (142)$$

then, if we define

$$W(K) = \prod_{k=1}^{K} p(\eta_k^*) \qquad (143)$$

to be the probability of any such $\underline{\eta}$ taking on these initial K components, from Eqs. (141) to (143) we may write

$$W(K) \, P_L(K) \leqslant \sum_{\underline{\eta} \in \underline{\eta}^*} p(\text{error} | \underline{\eta}) \, p(\underline{\eta}) \leqslant W(K) \, P_U(K) \quad . \qquad (144)$$

The inequalities of Eq. (144) provide lower and upper bounds on the total contribution to Eq. (136) from all those $\underline{\eta} \in \underline{\eta}^*$. If these bounds are sufficiently close in some sense (which we consider further below), then we need not bother summing over all the additional components of these $\underline{\eta}$ (that is, over the η_k for $k > K$), for the result of such additional computations cannot change the net contribution to Eq. (136) from all such $\underline{\eta}$ by more than the bounds of Eq. (144) allow.

Since we may rewrite Eq. (136) as

$$p(\text{error}) = \sum_{\underline{\eta}^*} \sum_{\underline{\eta} \in \underline{\eta}^*} p(\text{error} | \underline{\eta}) \, p(\underline{\eta}) \qquad (145)$$

where the first summation is over distinct $\underline{\eta}^*$, then from Eqs. (144) and (145) the desired probability of error for the conventional equalizer may be bounded above and below via

$$\sum_{\underline{\eta}^*} W(K) \, P_L(K) \leqslant p(\text{error}) \leqslant \sum_{\underline{\eta}^*} W(K) \, P_U(K) \qquad (146)$$

where in general, of course, the value of K required to bring the bounds of Eq. (144) sufficiently close together will differ for the different choices of $\underline{\eta}^*$. The actual computation of the bounds in Eq. (146) is accomplished through the sequential searching procedure described below.

Consider the tree-like structure shown in Fig. 19. Starting at the left, we trace through the tree to the right, determining a particular sequence $\eta_1^*, \eta_2^*, \ldots$ by our choice of paths. At each node, we want to stop and compute the lower and upper bounds of Eq. (144). To accomplish this, we need to keep track of $W(K)$, $D_L(K)$, and $D_U(K)$ as we progress through the tree. This is done conveniently by means of the recursive relationships

$$W(K + 1) = W(K) \, p(\eta_{K+1}) \qquad (147)$$

$$D_L(K + 1) = D_L(K) + (\eta_{K+1} - 1) \, b_{K+1} \qquad (148)$$

$$D_U(K + 1) = D_U(K) + (\eta_{K+1} + 1) \, b_{K+1} \qquad (149)$$

41

$P_L(0)$
$P_U(0)$
$\eta_1 = 1$
$\eta_1 = 0$
$\eta_1 = -1$
$P_L(1)$
$P_U(1)$
$\eta_2 = 1$
$\eta_2 = 0$
$\eta_2 = -1$
$P_L(2)$
$P_U(2)$
$P_L(3)$
$P_U(3)$

Fig. 19. Error tree algorithm.

where K is the number of branches separating the present node from the first node, and where we define the initial values

$$W(0) \triangleq 1$$

$$D_L(0) \triangleq \sum_{k=1}^{M} b_k \triangleq -D_U(0) \quad . \tag{150}$$

If, in arriving at a node, we find the bounds of Eq. (144) are sufficiently close together, we add them into the appropriate summations of Eq. (146). We then reverse direction, traveling to the left, reducing K accordingly until arriving at a node having one or two paths which we have not yet taken (such paths are recognized by the status of "flags" left at each node as we pass through it). Since un-traveled paths represent distinct $\underline{\eta}^*$ which must be taken into account in the summations of Eq. (146), we proceed along them to the right, continuing our search. If, on the other hand, in traveling to the right we arrive at a node and find the lower and upper bounds of Eq. (144) are not sufficiently close, then we continue tracing out $\underline{\eta}^*$ by proceed-ing from the node along one of the three untraveled paths leading from it to the right.

The above procedure is carried out by always choosing next to be taken, that path which is most likely to lead to a decision error, in order to insure the most rapid convergence of the al-gorithm possible. We stop at a particular node to reverse direction only when the upper and lower bounds of Eq. (144) differ by less than a fixed percentage of (1) each other, or (2) the total accumulated up to that point toward the lower bound summation of Eq. (146). By proceeding in this way, each of the distinct paths $\underline{\eta}^*$ is searched out and the bounds on the conventional equal-izer probability of error are obtained.

Of interest is the efficiency of this "error tree" algorithm described above. The overall number of paths in the tree is easily shown to be $(3^{M+1} - 1)/2$, which for large M is only 3/2 as many paths as the number of terms required in the calculation of Eq. (136). This algorithm was applied to the maximal distortion channels derived in Sec. IV-A, for various channel disper-sion spreads of N bauds, and for different conventional equalizer TDL lengths. The searches were conducted requiring an accuracy of 0.001 percent. Figures 20(a) and (b) illustrate the typ-ical behavior of the algorithm for 11- and 21-tap TDL, respectively. They show the percentage of paths searched vs SNR for various values of N and the corresponding values of M. Com-parison of these figures indicates that, generally, the larger the total number of possible paths, the smaller the percentage of them which must be investigated using our algorithm. We note from Figs. 20(a) and (b) that the algorithm searches only a relatively small percentage of the tree in all cases at low SNR because here the additive noise dominates the intersymbol inter-ference, the probability of error is only weakly dependent upon the particular message sequence transmitted, and hence the values of K required to bring the two bounds of Eq. (144) sufficiently
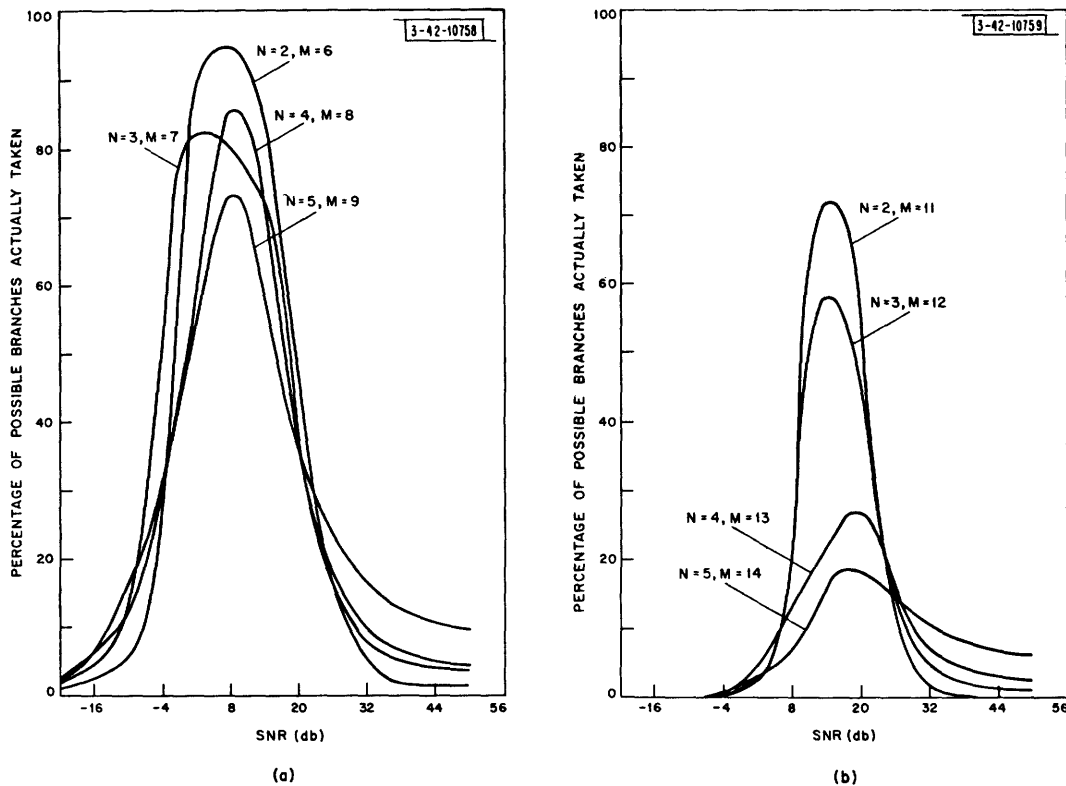
Fig. 20.   Efficiency of error tree algorithm in determining performance of conventional equalizer
applied to maximal distortion channels: (a) 11-tap equalizer, (b) 21-tap equalizer.

close together are small, resulting in a brief and efficient search of the tree.   For intermediate
SNR this no longer holds, for there are many combinations of message sequences and additive
noises which can lead to an error, thus requiring that the algorithm search out a much larger
percentage of the tree.   Finally, at high SNR, unless the intersymbol interference is rather
strongly opposed to a correct decision, an error is unlikely to occur and, since there are a
relatively small number of sidelobe combinations leading to strong opposition, then, here again
(as at low SNR), the algorithm need only search a small percentage of the total number of pos-
sible paths in the tree.

   We observe at this point that a possible alternative to our error tree algorithm approach
would be to determine the performance of the conventional equalizer through digital simulations,
as we do in Sec. V when considering the decision-feedback equalizer performance.   This would
work out well at low and intermediate SNR, but at high SNR, when the error rates are generally
low, this alternative approach would require simulations of prohibitively long duration.   Thus,
it is in the high SNR cases where the algorithm proves most useful, for it efficiently and accu-
rately renders the bounds required in Eq. (146).

   Section C below presents the results obtained through applying our algorithm to conventional
equalizer performance calculations for the maximal distortion channels described in Sec. A.

C.   CONVENTIONAL EQUALIZER PERFORMANCE

   We now present performance data obtained when the conventional equalizer which we de-
rived in Sec. II is applied to the equalization of the maximal distortion channels described in

43

Sec. A above. In the following discussions, we will denote by L the number of taps used on the conventional equalizer TDL, frequently referring to L as the TDL length. We denote by N the order of the maximal distortion channel, where N is the number of bauds over which the channel dispersion extends. Also, we may occasionally refer to the situation where a maximal distortion channel of order N is equalized using a TDL having L taps as the "N-L case." We considered several different cases, for various N, L, and SNR, as described below.

For each case studied, we first performed the calculations indicated by Eq. (46) to arrive at the optimal tap-gain settings of the conventional equalizer under our distortion criterion. That is, we computed those gains which minimized the total distortion encountered at the output, the sum of the sidelobe energy and output noise variance. With these tap gains, we then calculated the additive noise variance appearing at the output. Next, we determined the output sidelobes for a single pulse transmission, and the corresponding distortion measures D_α and D_β. Finally, using this set of sidelobes and the output noise variance, we applied the error tree algorithm developed in Sec. B to determine the performance of the conventional equalizer.

In this Section, we will be chiefly concerned with the effects of N, L, and SNR upon the conventional equalizer performance, its probability of error. The remaining data we obtained on tap-gain and sidelobe behavior will prove of interest as well in Sec. VI, when we compare the conventional equalizer operation with that of the decision-feedback equalizer.

The results of our performance calculations are summarized in Tables I to IV, which contain the probability-of-error data obtained with the maximal distortion channels of orders N = 2 to N = 5, respectively. As these tables show, we permitted the SNR to range between −16 and +50 db for each combination of N and L chosen. This rather broad range of SNR enabled us to observe the performance of the conventional equalizer at two extremes: (1) at low SNR, where the performance is essentially noise limited and independent of the intersymbol interference, and (2) at high SNR, where it becomes noise independent and limited only by the TDL length, as we discuss further below.

The data of Tables I to IV are presented in two sets of curves. The first set, comprising Figs. 21(a) to (d), shows performance vs SNR for the different TDL lengths L, with a separate figure for each order maximal distortion channel. We have also included in each of these figures the curve corresponding to the nondispersive N = 1 case. This latter curve, of course, provides a performance bound, representing the best performance we could obtain for any order maximal distortion channel, if we were to separate the transmitted pulses sufficiently in time that the channel dispersion no longer caused intersymbol interference. The second set of curves, consisting of Figs. 22(a) to (d), plots performance vs L for different values of SNR, again with a separate figure for each order maximal distortion channel. Other combinations are, of course, possible (e.g., plotting L vs SNR for different performance levels and N), but these appear to lend little additional insight into the conventional equalizer operation over that already afforded by Figs. 21(a) to 22(d).

In Fig. 21(a) for the maximal distortion channel of order N = 2, we note that at very low SNR the performance depends upon the SNR only, and becomes independent of the length of the TDL employed. This, of course, is true because at very low SNR all the tap gains approach zero except that of the centertap on the TDL; thus, whether or not additional taps are available is unimportant, since their gains would be virtually zero anyhow. These same comments are seen to apply to Figs. 21(b) to (d). Secondly, comparison of Figs. 21(a) to (d) (or equivalently,

TABLE I
PROBABILITY OF ERROR OF THE CONVENTIONAL EQUALIZER WHEN APPLIED TO THE MAXIMAL DISTORTION CHANNEL OF ORDER N = 2

SNR (db)	L = 3	L = 7	L = 11	L = 21
−16	4.3742E-01	4.3742E-01	4.3742E-01	4.3742E-01
−10	3.7871E-01	3.7871E-01	3.7871E-01	3.7871E-01
−4	2.8026E-01	2.8021E-01	2.8021E-01	2.8021E-01
2	1.5729E-01	1.5481E-01	1.5477E-01	1.5476E-01
8	6.7533E-02	5.2207E-02	5.0739E-02	5.0471E-02
14	3.4307E-02	1.1122E-02	7.5639E-03	6.2770E-03
20	3.1251E-02	2.9832E-03	8.2527E-04	1.9785E-04
26	3.1250E-02	1.9572E-03	1.7364E-04	4.3707E-06
32	3.1250E-02	1.9531E-03	1.2211E-04	3.2424E-07
38	3.1250E-02	1.9531E-03	1.2206E-04	1.2026E-07
44	3.1250E-02	1.9531E-03	1.2207E-04	1.1919E-07
50	3.1250E-02	1.9531E-03	1.2205E-04	1.1918E-07

TABLE II
PROBABILITY OF ERROR OF THE CONVENTIONAL EQUALIZER WHEN APPLIED TO THE MAXIMAL DISTORTION CHANNEL OF ORDER N = 3

SNR (db)	L = 5	L = 7	L = 11	L = 21
−16	4.3788E-01	4.3788E-01	4.3788E-01	4.3788E-01
−10	3.8182E-01	3.8182E-01	3.8181E-01	3.8182E-01
−4	2.9515E-01	2.9504E-01	2.9503E-01	2.9503E-01
2	1.9299E-01	1.9072E-01	1.9033E-01	1.9026E-01
8	1.0395E-01	9.5034E-02	8.8843E-02	8.6879E-02
14	5.6339E-02	4.3839E-02	2.7950E-02	2.0839E-02
20	4.0142E-02	2.7355E-02	9.5650E-03	2.5208E-03
26	3.5796E-02	2.3558E-02	5.4858E-03	4.1724E-04
32	3.5113E-02	2.3219E-02	4.5145E-03	1.7321E-04
38	3.5131E-02	2.3020E-02	4.2275E-03	1.3429E-04
44	3.5143E-02	2.2713E-02	4.1558E-03	1.3214E-04
50	3.5146E-02	2.2483E-02	4.1503E-03	1.3143E-04

TABLE III
PROBABILITY OF ERROR OF THE CONVENTIONAL EQUALIZER WHEN APPLIED TO THE MAXIMAL DISTORTION CHANNEL OF ORDER N = 4

SNR (db)	L = 7	L = 11	L = 21	L = 31
−16	4.3834E-01	4.3834E-01	4.3834E-01	4.3834E-01
−10	3.8475E-01	3.8474E-01	3.8474E-01	3.8474E-01
−4	3.0708E-01	3.0693E-01	3.0690E-01	3.0690E-01
2	2.1701E-01	2.1501E-01	2.1461E-01	2.1461E-01
8	1.2710E-01	1.1542E-01	1.1325E-01	1.1300E-01
14	7.0315E-02	4.3566E-02	3.6097E-02	3.5769E-02
20	4.9133E-02	1.7326E-02	8.1159E-03	6.9431E-03
26	4.2939E-02	1.0665E-02	2.5972E-03	1.2222E-03
32	4.1450E-02	9.0423E-03	1.5769E-03	4.4200E-04
38	4.1007E-02	8.7043E-03	1.3377E-03	2.7296E-04
44	4.0629E-02	8.6284E-03	1.2408E-03	2.2638E-04
50	4.0646E-02	8.5907E-03	1.1941E-03	2.1884E-04

TABLE IV
PROBABILITY OF ERROR OF THE CONVENTIONAL EQUALIZER WHEN APPLIED TO THE MAXIMAL DISTORTION CHANNEL OF ORDER N = 5

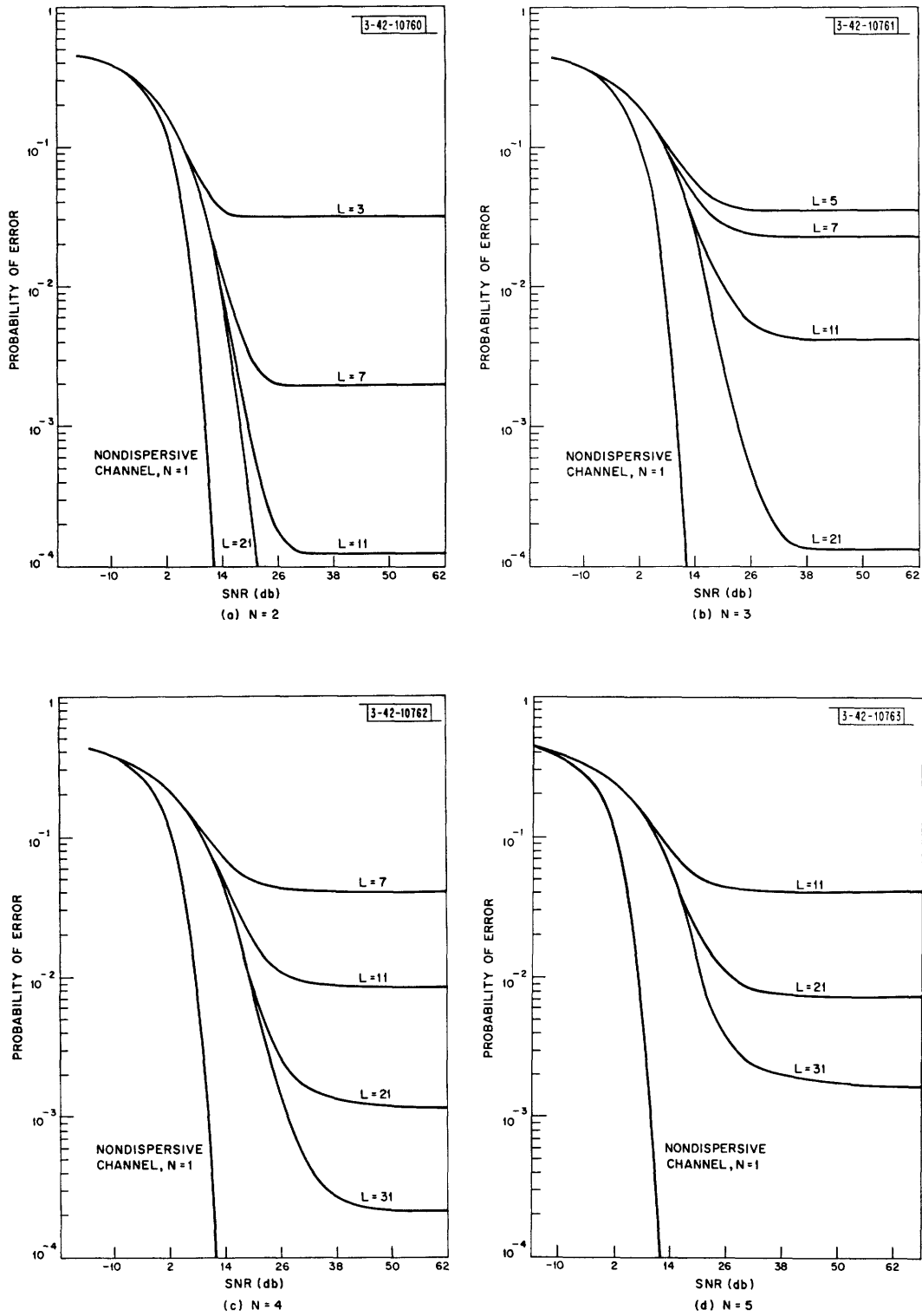| SNR (db)	L = 11	L = 21	L = 31
−16	4.3879E-01	4.3879E-01	4.3879E-01
−10	3.8744E-01	3.8743E-01	3.8743E-01
−4	3.1651E-01	3.1646E-01	3.1646E-01
2	2.3346E-01	2.3255E-01	2.3253E-01
8	1.4275E-01	1.3403E-01	1.3354E-01
14	7.8867E-02	5.3350E-02	5.0958E-02
20	5.2988E-02	2.0410E-02	−
26	4.4980E-02	1.0824E-02	−
32	4.2787E-02	8.3894E-03	−
38	4.2253E-02	7.7529E-03	−
44	4.2120E-02	7.6684E-03	1.8502E-03
50	4.2095E-02	7.6446E-03	1.7749E-03

Fig. 21(a–d).   Probability of error vs SNR for conventional equalizer having L-tap TDL, applied to maximal distortion channels of orders N = 2 to N = 5.
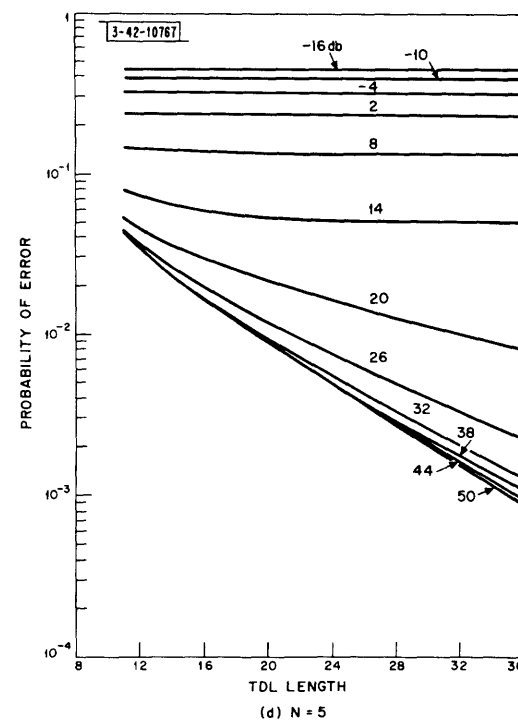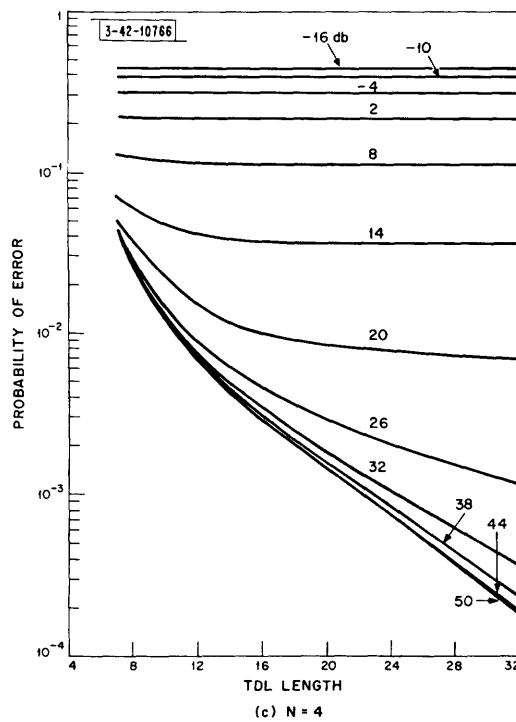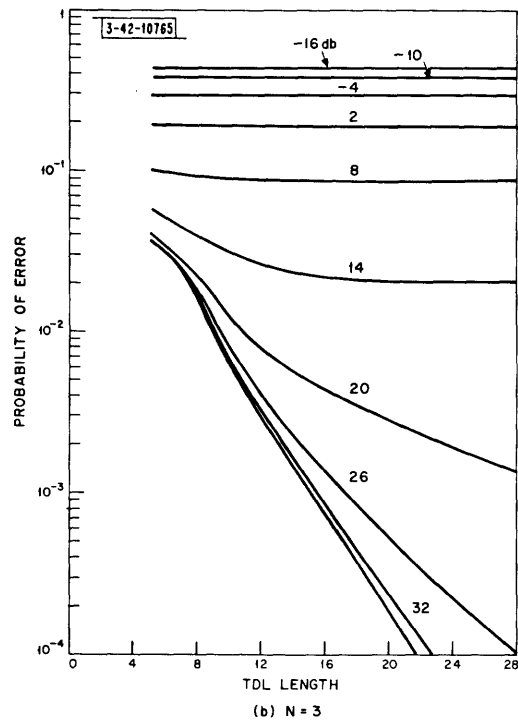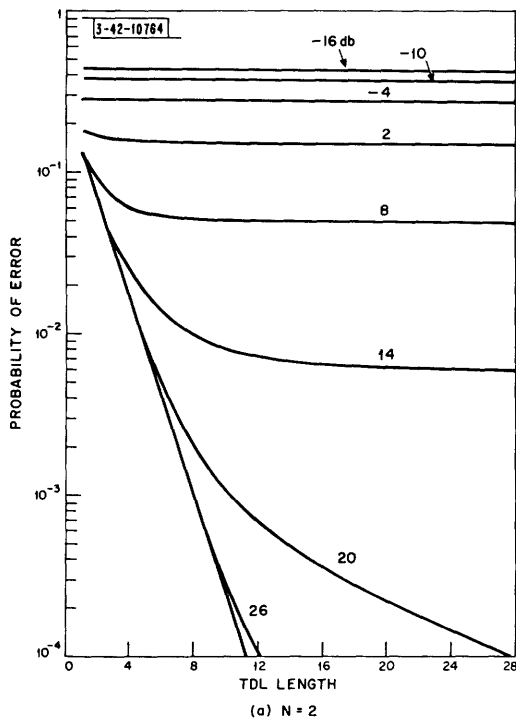
47

Fig. 22(a-d). Probability of error vs TDL length for conventional equalizer when applied to maximal distortion channels of orders N = 2 to N = 5.

48

Tables I to IV) shows that with decreasing SNR the performance becomes gradually independent of the channel distortion, and the performance for all orders of maximal distortion channels approaches that which we would obtain using a matched filter operating with the nondispersive $N = 1$ channel. In brief, then, we observe just what we would expect at very low SNR: the performance becomes essentially noise limited, and independent of both the TDL length L and the channel dispersion N.

With increasing SNR, we note in Fig. 21(a) that the first observable effect regarding the conventional equalizer performance is that due to the channel dispersion, as the curves for all L are no longer able to stay with the nondispersive $N = 1$ curve beyond about -5 db, but instead exhibit an increasingly greater probability of error relative to it. The TDL length L does not become a noticeable factor for the lengths considered until the SNR reaches about 2 db. Beyond this point, the shorter TDL one-by-one exhibit performances which cannot continue to match that of the longer TDL with increasing SNR. We likewise see from Figs. 21(b) to (d) that these observations hold for the higher-order maximal distortion channels, the main differences being that their increased dispersions cause even greater SNR losses over the $N = 1$ curve. We therefore conclude that at low SNR the channel dispersion, as well as the SNR, becomes a limiting factor on the conventional equalizer performance, while at intermediate SNR the TDL length becomes of importance as well, and for any TDL there is always some SNR above which we begin to suffer a loss in performance due to its finite length.

Finally, at high SNR, each of the curves in Figs. 21(a) to (d) exhibits a limiting performance level, which we see is strongly dependent upon the number of TDL taps used. This effect of TDL length is better seen through reference to Figs. 22(a) to (d) which plot probability of error vs L directly, for different SNR. For any given L, we find there exists a minimum probability of error which can be achieved, regardless of how high the SNR becomes. These limiting values of the probability of error depend upon the residual output sidelobes which we incur even in the absence of any additive noise, for any TDL of finite length. The residual sidelobes remaining at the conventional equalizer output are considerably larger, under both the D_α and D_β distortion measures, than those at the decision-feedback equalizer output, as we discuss further in Sec. VI.

Note that the low SNR curves in Figs. 22(a) to (d) have very small slopes, illustrating the point we made earlier that at low SNR the length of the TDL is relatively unimportant. With increasing SNR, the slopes of the curves increase until attaining that of the limiting performance curve determined by the TDL length L. These curves enable us to examine the advantages, if any, of increasing the TDL length with a given SNR, or of increasing the SNR with a given TDL length, at different performance levels. For example, with $L = 5$ in Fig. 22(a), there is little performance advantage in a SNR increase from 20 to 26 db, while with 21 taps it can make an improvement in probability of error by nearly two orders of magnitude. On the other hand, for a SNR of 14 db in Fig. 22(a), if we double the TDL length from $L = 12$ to $L = 24$, we gain a factor of only 1.16 improvement in performance, while the same doubling of the TDL length operating at 26 db would improve our performance by a factor of about 46. By viewing things in this way, Figs. 22(a) to (d) can thus enable us to evaluate the effects of variations in SNR and L under different operating conditions.

Having determined the conventional equalizer performance and obtained curves illustrating the relationships between TDL length L and SNR for the maximal distortion channels of different orders, we next investigate the operation of the decision-feedback equalizer in Sec. V, before going on to compare the two equalizers in Sec. VI.

V. PERFORMANCE OF THE DECISION-FEEDBACK EQUALIZER

As we anticipated earlier in Sec. III and will confirm later in this section, a decision error by the decision-feedback equalizer can lead to error propagation, or error "bursts": the situation where the initial decision error causes additional errors on succeeding bauds with high probability, these errors in turn cause still more errors, etc. The probability of error on any baud, of course, depends upon both the forward-TDL output distortion and upon the "state" of the feedback-TDL, that is, the number and location of the erroneous decisions it contains. Lacking knowledge of the probabilities of occurrence of the different feedback-TDL states and of the corresponding probabilities of error, we could not make a direct performance calculation for the decision-feedback equalizer as we had done previously in Sec. IV for the conventional equalizer. Instead, we determined the decision-feedback equalizer performance through digital simulations.

The N-L cases we simulated were the same cases we considered in Sec. IV with the conventional equalizer where, recall, N is the number of bauds over which the channel dispersion extends, and L is the number of taps available for equalization. With the decision-feedback equalizer, of course, L now represents the sum of the taps on both the forward- and feedback-TDL filters. Our first step in each case was to solve Eqs. (94) and (97) for the forward- and feedback-TDL tap-gain vectors, respectively, thus minimizing the total output distortion — just as we had done previously for the conventional equalizer.

Using the sampled channel autocorrelation function appropriate to the order of the maximal distortion channel of interest, we next found the response of the forward-TDL to a single $\xi_0 = +1$ pulse transmission. We then took these resulting output samples and used them as the tap-gain settings on a single transversal filter, providing us with a filter whose response to an input sample of +1 was identical with that obtained when passing the $\xi_0 = +1$ impulse into the cascade of our equivalent channel, matched filter, sampler, and forward-TDL. This is illustrated by the upper branches of Figs. 23(a) and (b), where we have labeled this single transversal filter as the "equivalent signal filter."
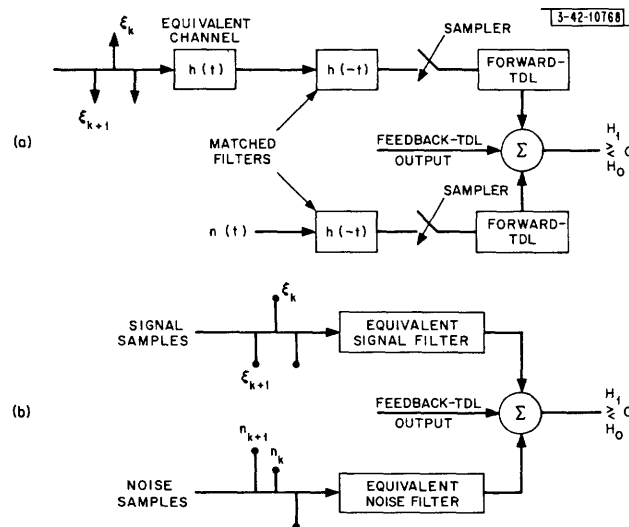

Fig. 23. Equivalent filters for simulating decision-feedback equalizer: (a) model of digital communication using decision-feedback equalizer; (b) equivalent model used in digital simulations.

Similarly, we replaced the noise branch of Fig. 23(a) by its cascade equivalent. For any given sampled channel autocorrelation function, there were, of course, an infinite number of equivalent impulse responses h(t) which we could have chosen in arriving at the matched filter in this noise branch. The choice, however, may be made arbitrarily, since the noise statistics at the forward-TDL output depend not upon our choice of a particular h(t), but rather only upon its sampled autocorrelation function. Thus, for convenience, we chose an h(t) of constant amplitude over the N bauds, in arriving at the "equivalent noise filter" for the Nth-order maximal distortion channel. Having done this, we then used the filters shown in Fig. 23(b) in our simulation studies.

After each simulation, we printed out an "Error Occurrence Photo," a sequence of digits indicating the performance on many successive bauds, with a "0" for a correct decision, and a "1" for an incorrect decision. Typical results are shown in Figs. 24(a) and (b), for the 5-21 case at 8 and 14 db, respectively. We see that errors occur in groups, called "bursts," separated by error-free regions known as "guard spaces." The bursting effect is brought out a little more clearly in Figs. 25(a) and (b), where we have blocked out the error bursts. In determining burst durations, we must keep in mind that for the N-L case there are $N - 1$ taps on the feedback-TDL, thus a decision error affects the succeeding $N - 1$ decisions. Hence, if a group of errors is followed by $N - 1$ or more error-free decisions, that error burst is over, and any subsequent errors are due to the noise and intersymbol interference arising from future bauds alone.

As we had expected, our digital simulations of the decision-feedback equalizer proved an efficient means of determining its performance, burst statistics, and guard-space data at low and intermediate SNR, where its error rates were reasonably high. As indicated by Figs. 24(b) and 25(b), however, with increasing SNR the error rates for the different cases began to fall off rapidly, until finally so few errors were occurring that we could not obtain sufficiently accurate data with simulations of reasonable duration. Our solution which overcame this difficulty, and enabled us to determine the desired data on the decision-feedback equalizer operation at all SNR, is developed in the discussion below. We begin in Sec. A with consideration of the probability of occurrence of an initial error while the feedback-TDL is operating in the "error-free" state. We then proceed to discuss our algorithm for determining the overall probability of error and error-burst statistics at all SNR. Next, in Sec. B, we present the data obtained using the normal simulations at low and intermediate SNR, and this new algorithm at high SNR. Concluding, in Sec. C we propose an alternative approach one might adopt to bound the mean error-burst duration, without the need of simulations.

A. ALGORITHM FOR OBTAINING HIGH SNR PERFORMANCE

In the absence of previous decision errors, the determination of the probability of an error is analogous to that presented in Sec. IV for the conventional equalizer. The output intersymbol interference distortion for M sidelobes before the mainlobe is given by

$$D = \sum_{k=1}^{M} q_{-k} \xi_k \tag{151}$$

-42-10769

-42-10770

(a)

(b)

Fig. 24. Error occurrence photos for 5-21 case: (a) SNR = 8 db; (b) SNR = 14 db.

Fig. 25. Error occurrence photos with bursts blocked out for 5-21 case: (a) SNR = 8 db; (b) SNR = 14 db.

54

which differs from the corresponding distortion at the conventional equalizer output, as given by Eq.(121), in that the distortion arising from the ξ_k for $k < 0$ has been eliminated through the decision feedback. Equation (122) applied to the probability of an initial error occurring, is still valid:

$$p(\text{initial error} \mid D) = \frac{1}{2} \, \text{erfc} \left[\frac{1 + D}{\sqrt{2}\sigma} \right] \tag{152}$$

where we recall that σ^2 is the output noise variance. Analogous to our earlier derivation of Sec. IV, we define

$$\tilde{b}_k = \left| q_{-k} \right| \qquad k = 1, \ldots, M \tag{153}$$

and $b_1, b_2, \ldots, b_M$ to be the ordered version of $\tilde{b}_1, \tilde{b}_2, \ldots, \tilde{b}_M$, so that Eq. (134) still holds. Defining $\eta_1, \eta_2, \ldots, \eta_M$ to be the corresponding rearrangement of the $\xi_1, \xi_2, \ldots, \xi_M$, the output distortion in the absence of decision errors becomes

$$D = \sum_{k=1}^{M} b_k \eta_k \tag{154}$$

which is formally identical with Eq.(135). The difference now, of course, is that the η_k are independent binary random variables, with $\eta_k = \pm 1$ with equal probability for all k. If we denote the occurrence of an initial error by e_i, Eq.(136) becomes:

$$p[e_i] = \sum_{\underline{\eta}} p[e_i \mid \underline{\eta}] \, p(\underline{\eta}) \tag{155}$$

except that Eq.(155) involves 2^M terms, compared with the 3^M terms of Eq.(136). Since this is still an impractical number of terms to sum over directly, we may proceed as in Sec. IV, where Eqs. (137) through (146) still apply, to arrive at upper and lower bounds on the probability of an initial error, given by

$$\sum_{\underline{\eta}^*} W(K) \, P_L(K) \leqslant p[e_i] \leqslant \sum_{\underline{\eta}^*} W(K) \, P_U(K) \quad . \tag{156}$$

Thus, by modifying appropriately the error tree algorithm derived in Sec. IV, we may compute the upper and lower bounds of Eq.(156) to any desired closeness to one another. The description of the modified algorithm is nearly identical with that given earlier, the only differences in its implementation being: (1) the number of paths leading to the right from each node is now only two, corresponding to η_k which are binary rather than ternary random variables, thus reducing the "flagging" requirements at each node, and (2) the weight W(K) of Eq. (143) now becomes

$$W(K) = 2^{-K} \tag{157}$$

which is independent of the particular $\underline{\eta}^*$ sequence taken (i.e., the particular path selected in searching the tree), and only depends upon K, the distance between the present and the first node. This means the sequential computation of W(K) as given by Eq. (147) is no longer necessary. These two differences thus result in a somewhat more simplified implementation of the algorithm than we incurred previously for the conventional equalizer.

55

Next, we want to consider conceptually what is occurring during a simulation. As we noted above, errors tend to occur in bursts with the decision-feedback equalizer. Therefore, referring to Fig. 26, we define

$$g_i = \text{length of } i^{th} \text{ guard space in bauds}$$

$$c_i = \text{length of } i^{th} \text{ error burst in bauds}$$

$$n_i = \text{number of errors occurring in } i^{th} \text{ burst.}$$
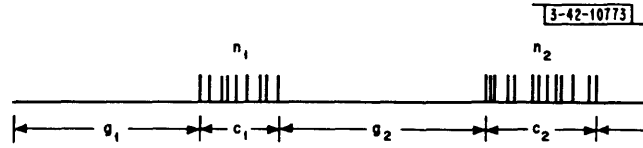

Fig. 26. Error-burst notation used in simulations of decision-feedback equalizer.

Note that, except for the 2-L cases, c_i and n_i may differ, since not all decisions occurring during a burst of errors are necessarily incorrect — as we can observe from Fig. 24(a), for example, in the 5-21 case. To estimate the overall probability of error, we want to compute the ratio of the number of bauds in error to the total number of bauds, as given by

$$p(\text{error}) = \frac{\Sigma n_i}{\Sigma g_i + \Sigma c_i} \tag{158}$$

as the number of error bursts encountered, P, becomes large. Normalizing by dividing through the numerator and denominator of Eq.(158) by P, we find that

$$p(\text{error}) = \frac{\overline{B}_e}{\overline{S}_g + \overline{T}_r} \tag{159}$$

where we have introduced the abbreviated notation:

$$\overline{B}_e \triangleq \frac{1}{P} \sum n_i = \text{mean number of errors per burst} \tag{160}$$

$$\overline{S}_g \triangleq \frac{1}{P} \sum g_i = \text{mean guard space (in bauds)} \tag{161}$$

$$\overline{T}_r \triangleq \frac{1}{P} \sum c_k = \text{mean recovery time, or mean burst length (in bauds)} \tag{162}$$

Now, the mean guard space is simply the reciprocal of the probability of an initial error

$$\overline{S}_g = \frac{1}{p[e_i]} \tag{163}$$

which we are able to determine to any desired accuracy using Eq.(156) implemented by our modified error tree algorithm. Next, we may write the mean recovery time after an initial decision error as

$$\overline{T}_r = \sum_{\underline{\eta}} [\overline{T}_r | e_i, \underline{\eta}] \; p[\underline{\eta} | e_i] \tag{164}$$

and, since

$$p[\underline{\eta} | e_i] = \frac{p[e_i | \underline{\eta}] \; p(\underline{\eta})}{p(e_i)} \tag{165}$$

we may substitute Eqs.(165) and (163) into Eq.(164) to find that

$$\overline{T}_r = \overline{S}_g \sum_{\underline{\eta}} [\overline{T}_r | e_i, \underline{\eta}] \; p[e_i | \underline{\eta}] \; p[\underline{\eta}]$$

$$= \overline{S}_g \sum_{\underline{\eta}^*} \sum_{\underline{\eta} \epsilon \underline{\eta}^*} [\overline{T}_r | e_i, \underline{\eta}] \; p[e_i | \underline{\eta}] \; p[\underline{\eta}] \tag{166}$$

where, just as with Eqs.(145) and (146), the first summation is to be taken over all distinct $\underline{\eta}^*$. Now, for $\underline{\eta} \epsilon \underline{\eta}^*$,

$$p(\underline{\eta}) = W(K) \; 2^{-M+K} \tag{167}$$

where W(K) is as given in Eq.(157). If we define for convenience

$$\overline{T}_r^* = \sum_{\underline{\eta} \epsilon \underline{\eta}^*} [\overline{T}_r | e_i, \underline{\eta}] \; 2^{-M+K} \tag{168}$$

and note that Eq.(141) applied to the present problem renders bounds on the probability of an initial error for any $\underline{\eta} \epsilon \underline{\eta}^*$:

$$P_L(K) \leqslant p[e_i | \underline{\eta}] \leqslant P_U(K) \tag{169}$$

then we may substitute Eqs. (167) through (169) in Eq. (166) to obtain the bounds on the mean recovery time

$$\overline{S}_g \sum_{\underline{\eta}^*} P_L(K) \; W(K) \; \overline{T}_r^* \leqslant \overline{T}_r \leqslant \overline{S}_g \sum_{\underline{\eta}^*} P_U(K) \; W(K) \; \overline{T}_r^* \quad . \tag{170}$$

Using Eq.(170), we could obtain arbitrarily close upper bounds on the mean recovery time, if only we knew the quantities $\overline{T}_r^*$ defined by Eq.(168). But, for each $\underline{\eta}^*$ there are 2^{M-K} different $\underline{\eta} \epsilon \underline{\eta}^*$, thus Eq.(168) represents the mean recovery time averaged over the equiprobable $\underline{\eta} \epsilon \underline{\eta}^*$. Hence, for a given $\underline{\eta}^*$, we want to take the various $\underline{\eta} \epsilon \underline{\eta}^*$ and determine the mean recovery time after an initial error has taken place. One way in which we may do this is through quasi-simulations, which we now describe.

We randomly select an $\underline{\eta} \epsilon \underline{\eta}^*$ and put it into the equivalent signal filter, "freezing" the η_k in their respective positions. With no errors in the feedback-TDL, we then pass a sequence of samples into the equivalent noise filter of Fig. 23(b) until a decision error occurs. After this

initial error, we then "unfreeze" the $\underline{\eta}$ sequence within the equivalent signal filter of Fig. 23(b) by permitting new signals to enter it, and normal simulation continues until the error burst is over. Through performing a sufficient number of these quasi-simulations, we may obtain the conditional recovery time of Eq.(168) as accurately as desired. Further, by doing this for each distinct $\underline{\eta}^*$, we may weight these expressions of Eq.(168) to obtain the bounds of Eq.(170) as closely as desired.

All this is conveniently achieved through further modification of our error tree algorithm. Recalling our previous discussion of its implementation in Sec. IV, the major difference now is that, in arriving at a node where the bounds of Eq.(167) are sufficiently close, we then perform the quasi-simulations described above for the current value of $\underline{\eta}^*$. The mean recovery times of Eq.(168) are weighted appropriately by $P_L(K) W(K)$ and $P_U(K) W(K)$ and accumulated, to form the lower and upper bounds of Eq.(170), respectively, as we search through the tree. Simultaneously, of course, we accumulate the bounds of Eq.(156), thus obtaining bounds on the probability of an initial error (and then to the mean guard space) via Eq.(163).

It is clear that we may obtain bounds on the mean number of errors per burst in exactly the same way as we have just shown for the mean recovery time. Again, the computations fit conveniently into our modified error tree algorithm, and we must further determine only the average number of errors per burst occurring for our quasi-simulations for each $\underline{\eta}^*$. Denoting this average as $\overline{B}_e^*$, we may then use an expression identical with Eq.(170), except with $\overline{T}_r$ and $\overline{T}_r^*$ replaced by $\overline{B}_e$ and $\overline{B}_e^*$, respectively, to obtain the desired bounds on the mean number of errors per burst. Similarly, we can determine bounds on the mean square recovery time, which we did in order to study the variance of the burst lengths, as we discuss later in this Section.

The rationale behind all this is as follows. The difficulty with high SNR simulations, as we noted earlier, is the low error rates we encounter. These, in turn, are due to the small distortions appearing at both the equivalent signal filter and equivalent noise filter outputs. In particular, at high SNR both D_β and the output noise variance σ^2 are generally sufficiently small that most of the time neither the intersymbol interference nor the additive noise acting alone can cause a decision error. This is strictly true for the intersymbol interference acting alone whenever $D_\beta < 1$, which it always becomes at high SNR with the decision-feedback equalizer, as we will see further below. Similarly, the probability of noise causing an error in the absence of intersymbol interference is negligible compared with its probability of causing an error in the presence of intersymbol interference opposed to a correct decision. Thus, at high SNR, errors occur most of the time only through a collaboration of intersymbol interference and noise distortion. All this, of course, is true only in the absence of decision errors, for with decision errors in the feedback-TDL, D_β can easily exceed unity and error propagation can occur due to intersymbol interference alone, a matter we describe in more detail below. Thus, in the absence of previous decision errors, an error in our simulation involves the simultaneous occurrence of a "harmful" intersymbol interference distortion and a "large" noise distortion, which, both being low probability events, means such errors occur infrequently. The quasi-simulation approach described above effectively determines those intersymbol interference sidelobe combinations which are most strongly opposed to a correct decision, through the efficient selection of $\underline{\eta}^*$ via the error tree algorithm. The noise is then permitted to cause an error, which eventually occurs. However, we must have the noise correlation correct at the time of the initial error, so, in general, the possibility of "inserting an error" is not a valid approach. At very

high SNR, however, as we will observe below, the noise distortion becomes virtually uncorrelated; thus, inserting an error at high SNR is a legitimate approach. Both methods were adopted, where appropriate, in our quasi-simulations to determine the decision-feedback equalizer performance at high SNR using Eq.(159). At low SNR, of course, normal simulations were performed, as explained earlier.

B.   DECISION-FEEDBACK EQUALIZER PERFORMANCE

We present the resulting error-rate data in Tables V to VIII for the maximal distortion channels of orders N = 2 to N = 5, respectively. The burst and guard-space data we obtained will be presented and discussed further below. In Figs. 27(a) to (d), we plot this error-rate data vs SNR for various L, where L is the total number of taps on both the forward- and feedback-TDL, with a separate figure for each of the maximal distortion channels considered.

At very low SNR, the performance becomes noise-limited, independent of both the channel distortion and the number of taps used. This is seen to be true in Fig. 27(a) for SNR less than about -10 db. Beyond this point, we note that the error rate curves gradually become worse than the nondispersive N = 1 bound. The effective loss in SNR for a given error rate is seen to reach a limiting value with increasing SNR, however, becoming approximately 4 db with L = 3, and 3 db for L = 7 at an error rate of 10^{-4}. To further investigate this matter, we greatly compressed the vertical scales, enabling us to plot the 2-L error rates down to 10^{-35}, as shown in Fig. 28 where we observe that the effective loss in SNR does become constant with respect to the N = 1 bound at high SNR, being about 2.8 db, for example, in the 2-21 case. We see that these observations also apply to Figs. 27(b) to (d), except that the loss in SNR is seen to become greater as the channel dispersion becomes larger.

There are two major reasons for the degradation in SNR with the decision-feedback equalizer operating at high SNR. For any finite length of the forward-TDL, with increasing SNR its tap gains (which are set to minimize the total output distortion energy) approach limiting values which are determined solely by the intersymbol interference and the length of the forward-TDL, independent of the noise. These limiting tap-gain settings result in (1) a limiting noise enhancement effect, and (2) a limiting set of output sidelobes which give rise to the intersymbol interference (these two factors are shown in Figs. 29 and 30). In Fig. 29, we have plotted the degradation in SNR due to noise enhancement vs the forward-TDL length for the maximal distortion channels of orders N = 2 to N = 5, where we recall that the forward-TDL has a length given by $L - N + 1$, since $N - 1$ of the total of L taps are required on the feedback-TDL. In Fig. 30, we have plotted the limiting value of the intersymbol interference distortion measure D_β with increasing SNR, again vs the length of the forward-TDL.

The intersymbol interference distortion remains nonzero, of course, for any forward-TDL of finite length, although from Fig. 30 it appears to approach zero asymptotically with increasing forward-TDL length. As we observed above from Fig. 28 for the 2-21 case, the loss in SNR compared with the nondispersive N = 1 curve is about 2.8 db. However, from Fig. 29 we find for this 2-21 case, where the forward-TDL has 20 taps, that about 2.6 db of this loss is directly attributable to the noise enhancement, with the remaining loss caused by the residual intersymbol interference distortion which has a $D_\beta = 0.065$ as we find from Fig. 30 for this case. Thus, for a decision-feedback equalizer having a long forward-TDL, the loss in SNR it suffers compared with the nondispersive N = 1 channel performance is essentially determined by the noise enhancement of the forward-TDL at high SNR. Throughout this discussion, of course, we have

TABLE V
DECISION-FEEDBACK EQUALIZER ERROR RATE WHEN APPLIED TO THE MAXIMAL DISTORTION CHANNEL OF ORDER N = 2

SNR (db)	L = 3	L = 7	L = 11	L = 21
−16	4.34E-01	4.39E-01	4.27E-01	4.35E-01
−10	3.84E-01	3.78E-01	3.74E-01	3.80E-01
−4	2.82E-01	2.81E-01	2.94E-01	2.80E-01
2	1.58E-01	1.72E-01	1.69E-01	1.60E-01
8	4.54E-02	4.36E-02	3.79E-02	3.42E-02
14	1.71E-03	1.93E-04	1.40E-04	1.36E-04
20	4.73E-09	6.48E-12	3.87E-13	−
26	1.80E-30	1.96E-39	8.13E-43	9.67E-47
32	−	−	−	−

TABLE VI
DECISION-FEEDBACK EQUALIZER ERROR RATE WHEN APPLIED TO THE MAXIMAL DISTORTION CHANNEL OF ORDER N = 3

SNR (db)	L = 5	L = 7	L = 11	L = 21
−16	4.42E-01	4.34E-01	4.40E-01	4.39E-01
−10	3.81E-01	3.90E-01	3.82E-01	3.89E-01
−4	3.09E-01	3.05E-01	3.09E-01	3.06E-01
2	2.09E-01	2.09E-01	2.07E-01	2.12E-01
8	8.41E-02	7.91E-02	7.86E-02	7.15E-02
14	8.44E-03	3.41E-03	1.82E-03	1.54E-03
20	7.63E-06	2.06E-07	1.10E-08	1.03E-09
26	9.53E-17	8.65E-23	3.44E-26	2.55E-30
32	2.51E-59	−	−	−

TABLE VII
DECISION-FEEDBACK EQUALIZER ERROR RATE WHEN APPLIED TO THE MAXIMAL DISTORTION CHANNEL OF ORDER N = 4

SNR (db)	L = 7	L = 11	L = 21	L = 31
−16	4.39E-01	4.39E-01	4.41E-01	4.43E-01
−10	3.92E-01	3.86E-01	3.89E-01	3.93E-01
−4	3.18E-01	3.24E-01	3.18E-01	3.21E-01
2	2.35E-01	2.83E-01	2.43E-01	2.46E-01
8	1.28E-01	1.20E-01	1.18E-01	1.06E-01
14	2.12E-02	8.93E-03	6.20E-03	4.90E-03
20	2.16E-04	6.42E-06	1.79E-07	−
26	1.06E-10	1.77E-15	3.17E-21	−
32	9.30E-35	1.74E-50	2.69E-69	−
38	−	−	−	−

TABLE VIII
DECISION-FEEDBACK EQUALIZER ERROR RATE WHEN APPLIED TO THE MAXIMAL DISTORTION CHANNEL OF ORDER N = 5

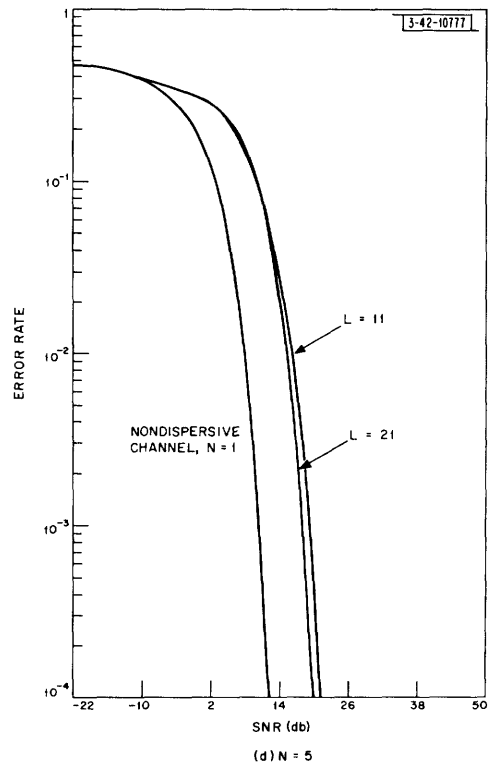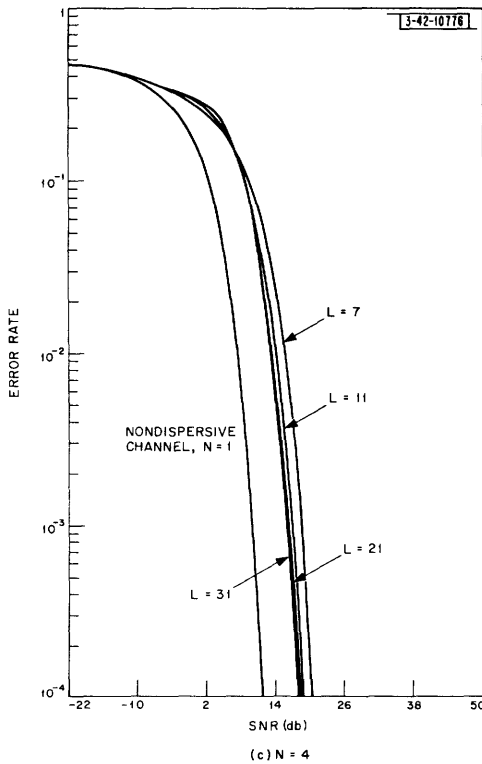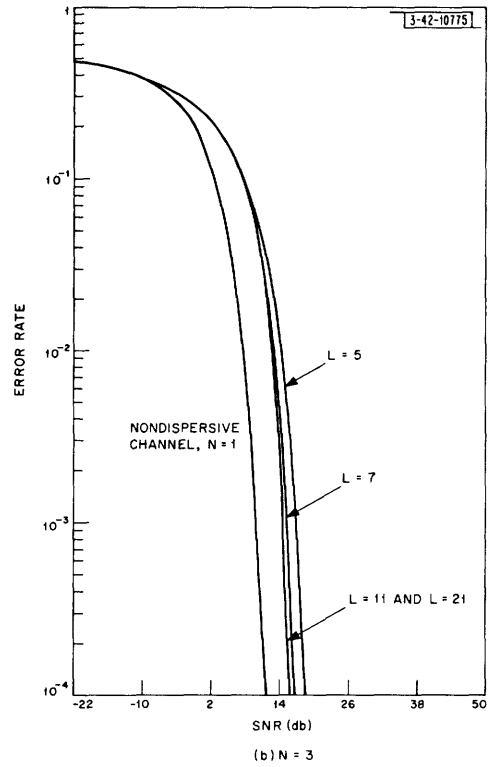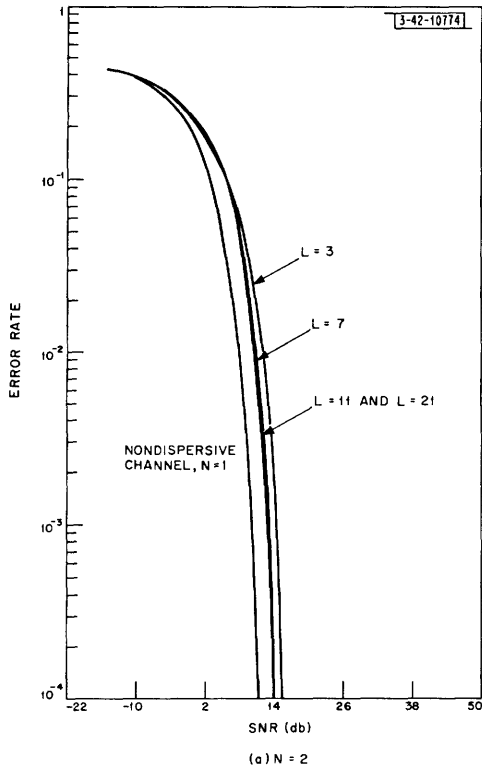| SNR (db)	L = 11	L = 21	L = 31
−16	4.38E-01	4.38E-01	4.38E-01
−10	3.92E-01	3.92E-01	3.96E-01
−4	3.33E-01	3.36E-01	3.41E-01
2	2.54E-01	2.73E-01	2.65E-01
8	1.38E-01	1.43E-01	1.44E-01
14	2.49E-02	1.45E-02	−
20	3.36E-04	6.72E-06	−
26	7.13E-09	4.67E-15	−
32	6.88E-25	1.46E-45	−

Fig. 27(a-d). Error rate vs SNR for decision-feedback equalizer applied to maximal distortion channels of orders N = 2 to N = 5, for L taps.

Fig. 28. Decision-feedback equalizer error rate for second-order maximal distortion channel.
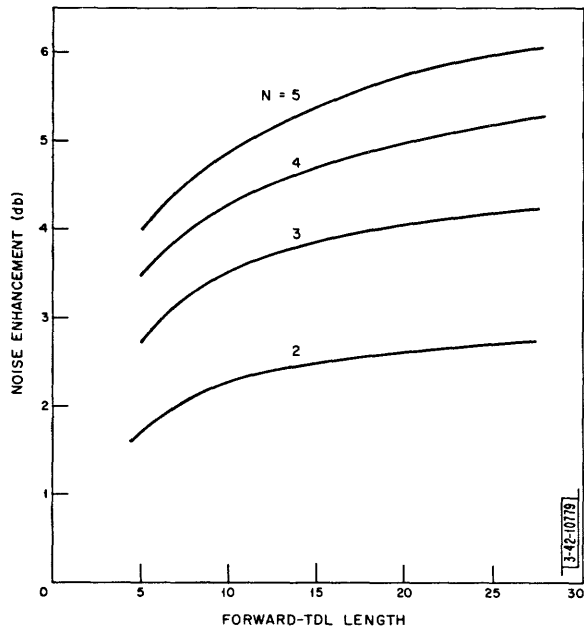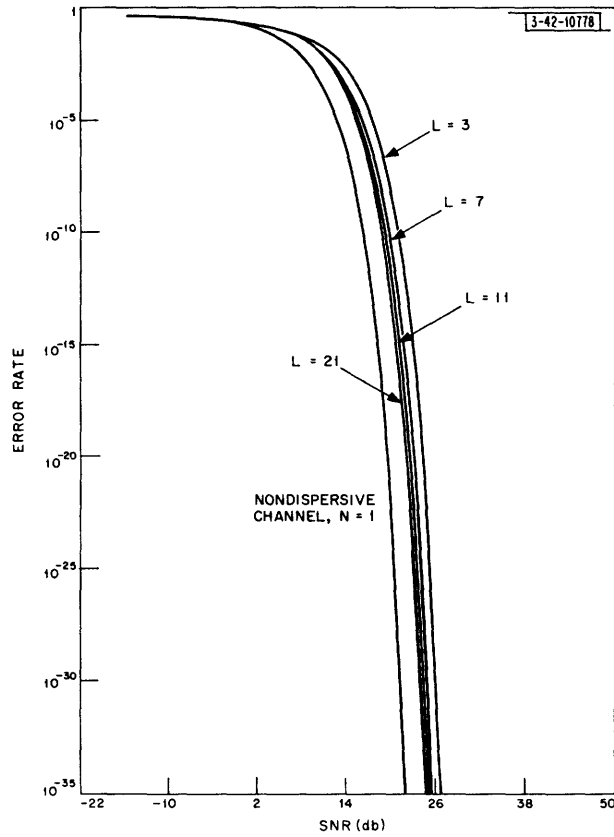

Fig. 29. Noise enhancement vs forward-TDL length in decision-feedback equalizer, applied to maximal distortion channels of order N.
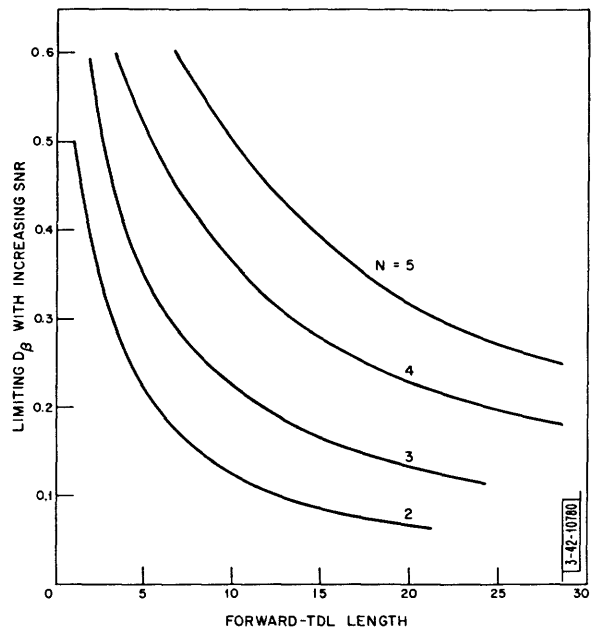

Fig. 30. Limiting distortion D_β vs forward-TDL length in decision-feedback equalizer, applied to maximal distortion channels of order N.

63

considered D_β to be measured in the absence of decision errors. When such errors occur, the D_β become large, and bursts result even at high SNR, as indicated in Figs. 25(a) and (b) for the 5-21 case. Such bursts, however, merely increase the error rate beyond the probability of an initial error by a factor equaling the mean number of errors per burst. This is true because in Eq. (159) the mean recovery time becomes negligible compared with the mean guard space as we will see below, and the mean guard space and the probability of an initial error are directly related via Eq. (163). As we consider next, the burst and guard-space data obtained from our simulations and quasi-simulations using the modified error tree algorithm are such that, given the steepness of the error-rate curves in Figs. 27 and 28 at high SNR, the further degradation due to bursting effects becomes negligible compared with the losses arising from the forward-TDL noise enhancement.

In the course of our normal simulations at low SNR, we obtained error-burst data, recording the relative frequency of occurrence of the various burst lengths and then computing the average burst duration, or mean recovery time $\overline{T}_r$ as we referred to it above. We also computed the recovery time variance from these data. In our high SNR quasi-simulations, of course, the $\overline{T}_r$ was necessary for our evaluation of Eq. (159) in order to obtain the overall error rate of the decision-feedback equalizer, and we further recorded the recovery time variance. Typical mean recovery time data are shown in Figs. 31(a) and (b) where we have plotted the mean recovery time in bauds vs SNR for the N-11 and N-21 cases, respectively.
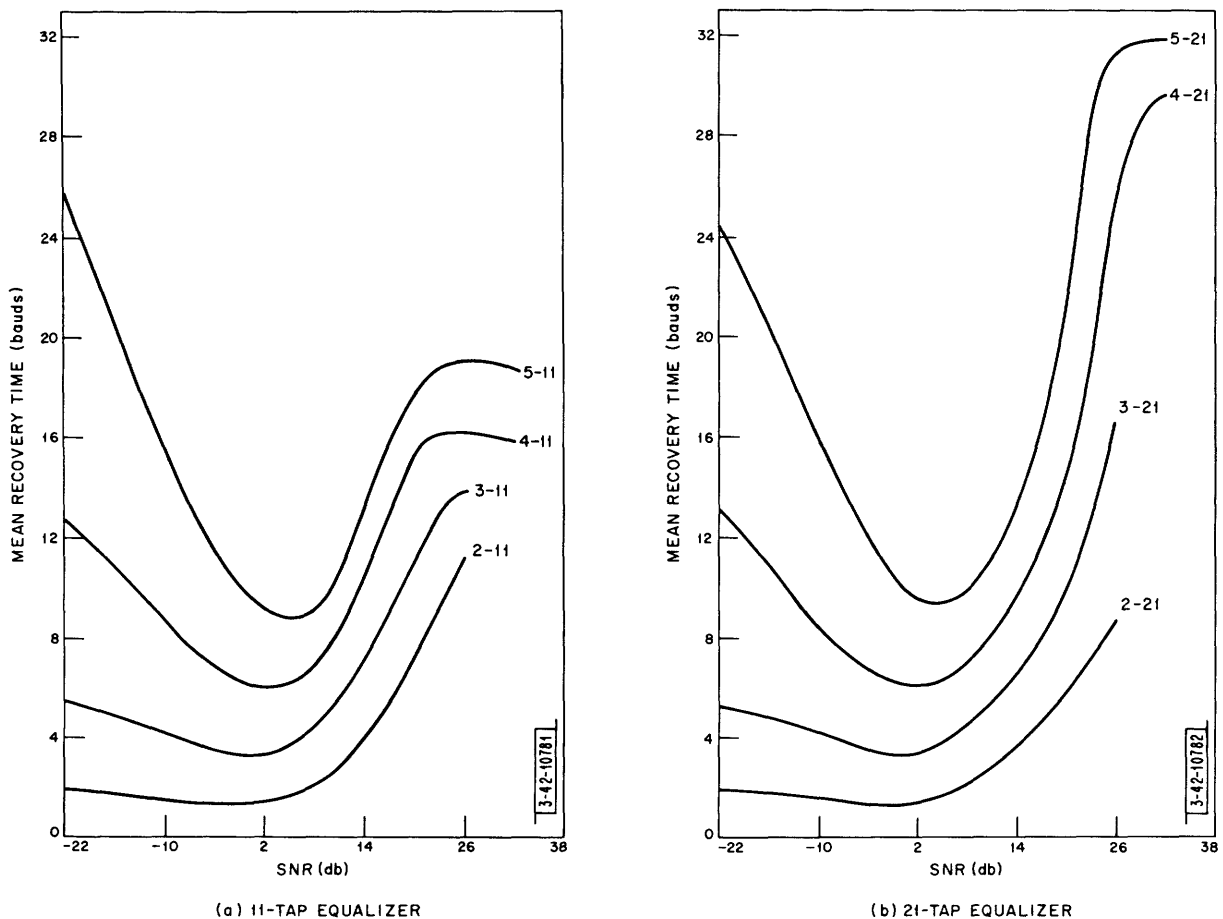

Fig. 31(a-b). Mean recovery time vs SNR after an initial decision error with 11- and 21-tap decision-feedback equalizers, applied to maximal distortion channels.

64

As we observed earlier, at very low SNR the noise dominates both the channel dispersion and the length of equalizer being employed. Correspondingly, even after a decision error has been made, the length of time until recovery is essentially determined by the additive noise, asymptotically with decreasing SNR. As a result, the mean recovery time approaches asymptotically the mean time required before the receiver makes enough correct "guesses" that the feedback-TDL once again contains no errors. The average time to recovery through guessing with an Nth-order channel may be handled using the simple Markov chain flow diagram of Fig. 32(b) where we have let the "state" of the feedback-TDL correspond to the number of the rightmost tap position containing an error. Thus, referring to Fig. 32(a), an initial decision error becomes positioned at the first tap, corresponding to state 1 of Fig. 32(b). If the next decision is correct, the initial error shifts to tap 2, or state 2 of Fig. 32(b), etc. Since the feedback-TDL has $N - 1$ taps, then clearly upon reaching state N, recovery is complete. In Fig. 32(b), the transitions from the Kth state are, on a "guessing" basis, equally likely to result in states 1 or $K + 1$ on the next decision, as indicated by the factor of $1/2$ on each transition. The z appearing on each transition represents a unit delay, corresponding to a decision interval, the baud period. If we let p_i be the probability of recovering after exactly i bauds, then defining the z-transform of the $p_1, p_2, \ldots$ sequence as

$$P(z) = \sum_{i=1}^{\infty} p_i z^i \qquad (171)$$

it follows that

$$\left. \frac{dP(z)}{dz} \right|_{z=1} = \sum_{i=1}^{\infty} i p_i \qquad (172)$$

which is precisely the mean recovery time we desire. It is a straightforward exercise in flow-chart manipulation to find that for Fig. 32(b)

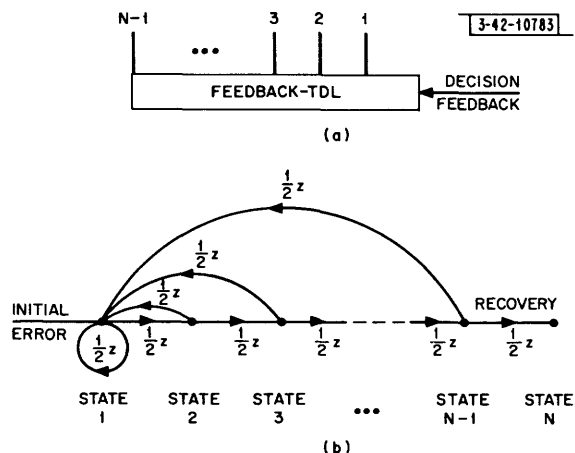$$P(z) = \frac{(\frac{1}{2}z)^{N-1} (1 - \frac{1}{2}z)}{1 - z + (\frac{1}{2}z)^N} \qquad (173)$$

Fig. 32. Error-state transitions while in guessing mode: (a) numbering taps on feedback-TDL, and (b) flow diagram of error states in guessing mode.

65

and thus

$$\overline{T}_r = \frac{dP(z)}{dz}\bigg|_{z=1} = 2^N - 2 \qquad (174)$$

is the mean recovery time we would encounter through guessing. We can see from Figs. 31(a) and (b) that the decision-feedback equalizer mean recovery time does indeed approach asymptotically the values given by Eq. (174) for the different order channels, as the $N = 2$ channel $\overline{T}_r$ approaches 4 bauds, the $N = 3$ channel $\overline{T}_r$ approaches 6 bauds, etc., with decreasing SNR.

With increasing SNR, the mean recovery time decreases up until about 2 db, as we observe from Figs. 31(a) and (b), mainly because the additive noise is decreasing; hence, the decisions are becoming better than those obtained through guessing. In addition, however, there is a compensation effect which we now describe. The occurrence of an initial error generally requires that the additive noise be opposed to a correct decision. That is, for the decision-feedback equalizer to make an error in determining ξ_0, say, when ξ_0 in fact is +1, requires in general that the output of the equivalent noise filter of Fig. 23(b) be negative. On the other hand, on the succeeding decision this error results in an additional sidelobe of $2q_1\xi_0$ because, referring to Fig. 10, the feedback-TDL now enhances the q_1 sidelobe appearing at the forward-TDL output rather than subtracting it out. Because q_1 is positive for the maximal distortion channels, this enhanced sidelobe is seen to oppose the noise on the succeeding decision, since the noise correlation properties are such that the negative noise which caused the initial error is still likely to be negative on the next few decisions at low SNR. Moreover, this compensation effect is not limited to the maximal distortion channels. This follows because at low SNR all but one of the tap gains on the forward-TDL are relatively small, hence the sidelobes occurring after the mainlobe still strongly resemble the sampled channel autocorrelation function. Likewise, the noise at the output still has a correlation function determined nearly by the matched filter alone, and it also strongly resembles the sampled channel autocorrelation function. Thus, we observe that this compensation effect will take place at low SNR, regardless of the particular channel we might care to consider.

Referring again to Figs. 31(a) and (b), we observe that the mean recovery time increases rapidly beyond about 2 db, for two reasons. The first factor is that the compensation effect we discussed in the preceding paragraph becomes less as the SNR becomes higher, since gradually the forward-TDL gains increase, causing a mismatched filter whose output noise correlation no longer agrees with the sidelobes occurring after the mainlobe. The second (and more important) factor, however, is tied in with the properties of the correlation functions of the output distortions, of the noise and of the intersymbol interference, in the absence of decision errors, and with an error-propagation effect. We will therefore interrupt our discussion of the mean recovery time of Figs. 31(a) and (b) to consider these other issues in more detail.

In Figs. 33(a) and (b), we illustrate typical behavior of the output distortion correlation functions, in the absence of decision errors, by drawing them for the 5-21 case for various SNR. At each SNR, we have indicated the intersymbol interference distortion correlation function, the output noise distortion correlation function, and the total output distortion correlation function (which is the sum of these two). All the correlation functions are shown in normalized form, with actual values of their distortion energy as indicated. At low SNR, we see that the total distortion correlation function is the same as that of the noise, since the output noise

energy greatly exceeds that of the intersymbol interference distortion. With increasing SNR, however, the noise distortion continually decreases, while the intersymbol interference attains a limiting value, for any forward-TDL of finite length. Thus, with increasing SNR, the total distortion correlation becomes identical with the limiting distortion correlation function of the intersymbol interference alone, as we may observe from Fig. 33(b). There are two aspects of these correlation functions we want to bring out at this time. The first concerns the noise distortion, for, as we see in Figs. 33(a) and (b), it is becoming nearly uncorrelated from one decision to another as the SNR increases. Our second observation is similar, namely, that the total distortion is seen to become virtually uncorrelated at intermediate SNR, from about 8 to 20 db, as the intersymbol interference and noise distortion correlation functions tend to cancel one another out. The fact that the noise becomes nearly uncorrelated at high SNR enabled us to determine error-rate and burst statistics at high SNR by "inserting an error" to initiate a burst in the course of our quasi-simulations using our modified error tree algorithm. As mentioned earlier, such an approach is not legitimate at lower values of SNR, where the noise distortion is seen to be highly correlated from one decision to the next. The fact that the total distortion tends to become uncorrelated at intermediate SNR enables us to obtain performance data in that region, by assuming that the total distortion is indeed exactly uncorrelated, without having to resort to simulations or quasi-simulations, as we will discuss in some detail below.

Returning to our mean recovery time discussion of Figs. 31(a) and (b), we next want to account for the steep increase in mean recovery time beyond about 2 db which we encountered with the maximal distortion channels. As we will see in Sec. VI, the value of D_β is always less than unity beyond about 2 db; thus, the initial error of a burst cannot arise from harmful intersymbol interference alone, but the additive noise must also be strongly opposed to a correct decision. As we observed above from Figs. 33(a) and (b), the noise becomes virtually uncorrelated beyond about 2 db; hence, after a "large" noise sample occurs to initiate the error burst, the noise tends to resume its typically small values and, thus, error propagation is seen to take place because of decision errors alone, and virtually without the further assistance of the noise which initiated it.

To better understand how error propagation can occur, we consider a typical situation (the 5-21 case at 20 db) and show that those future baud message sequences $\xi_1, \xi_2, \ldots$ which are likely to give rise to a decision error, also are prone to exhibit strong error-propagation behavior. In Fig. 34(a), we indicate the decision-feedback equalizer forward-TDL response to a single $\xi_0 = +1$ pulse transmission, denoting each sidelobe by its polarity only, with the mainlobe position located between the parallel lines. The sidelobes after the mainlobe are canceled out by the feedback-TDL in the absence of decision errors. The worst possible message sequence is as shown on the first line of Fig. 34(b), where the ξ_k for k < 0 have been replaced by zeros since their effect is assumed to have been eliminated through error-free decision feedback. The result of weighting this message sequence by the sidelobes of Fig. 34(a) is shown in the second line of Fig. 34(b), where all the products are seen to oppose the mainlobe and a correct decision through our choosing the worst possible message sequence. Suppose a decision error occurs with this sequence, resulting on the next decision in the shifted sequence indicated in the first line of Fig. 34(c). The leftmost position is now occupied by +1 or −1 with equal probability, which we have indicated with a question mark. The decision error has caused the feedback-TDL to enhance rather than eliminate the q_1 sidelobe contribution, as noted by the + sign immediately after the mainlobe position.
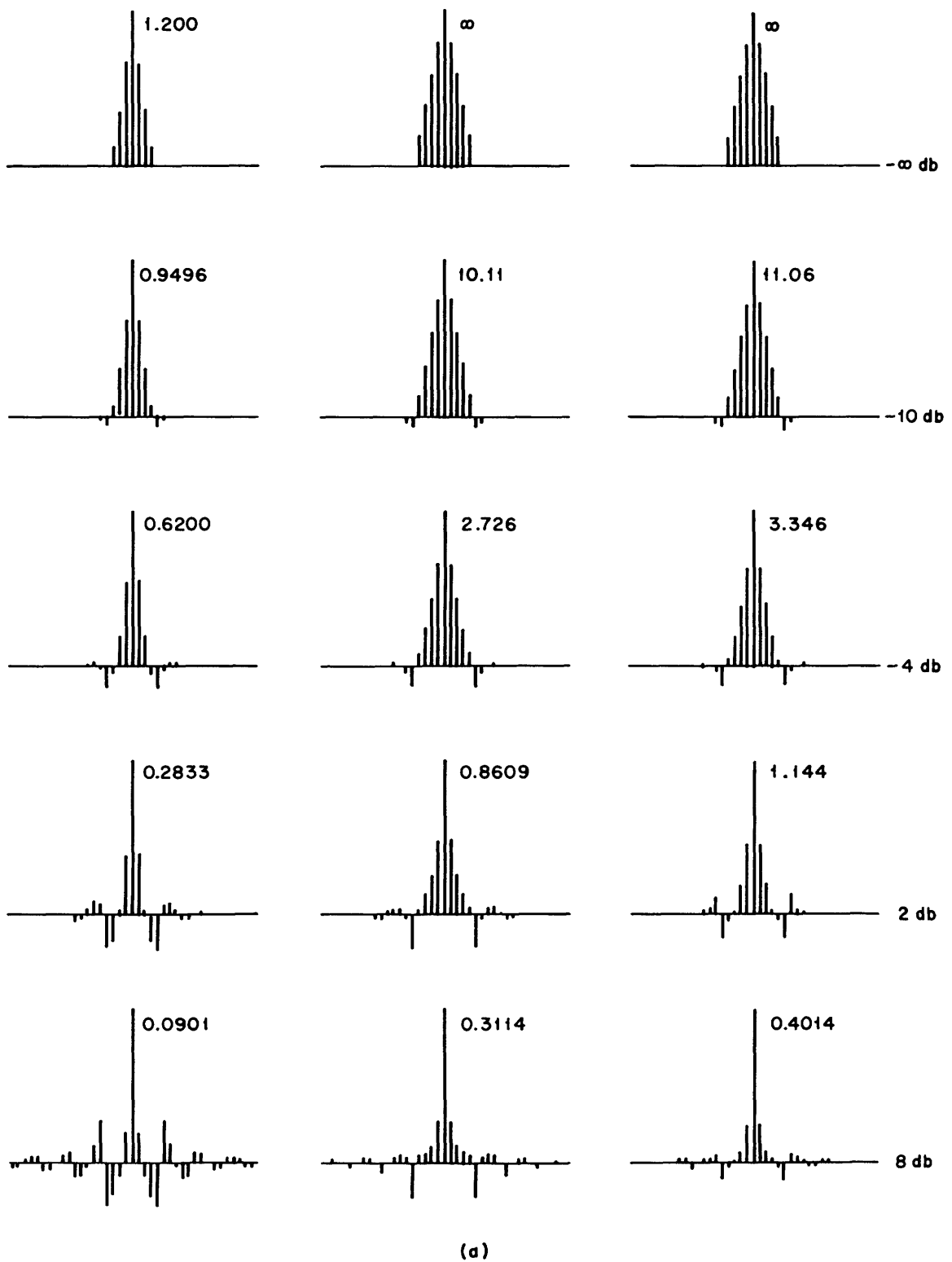
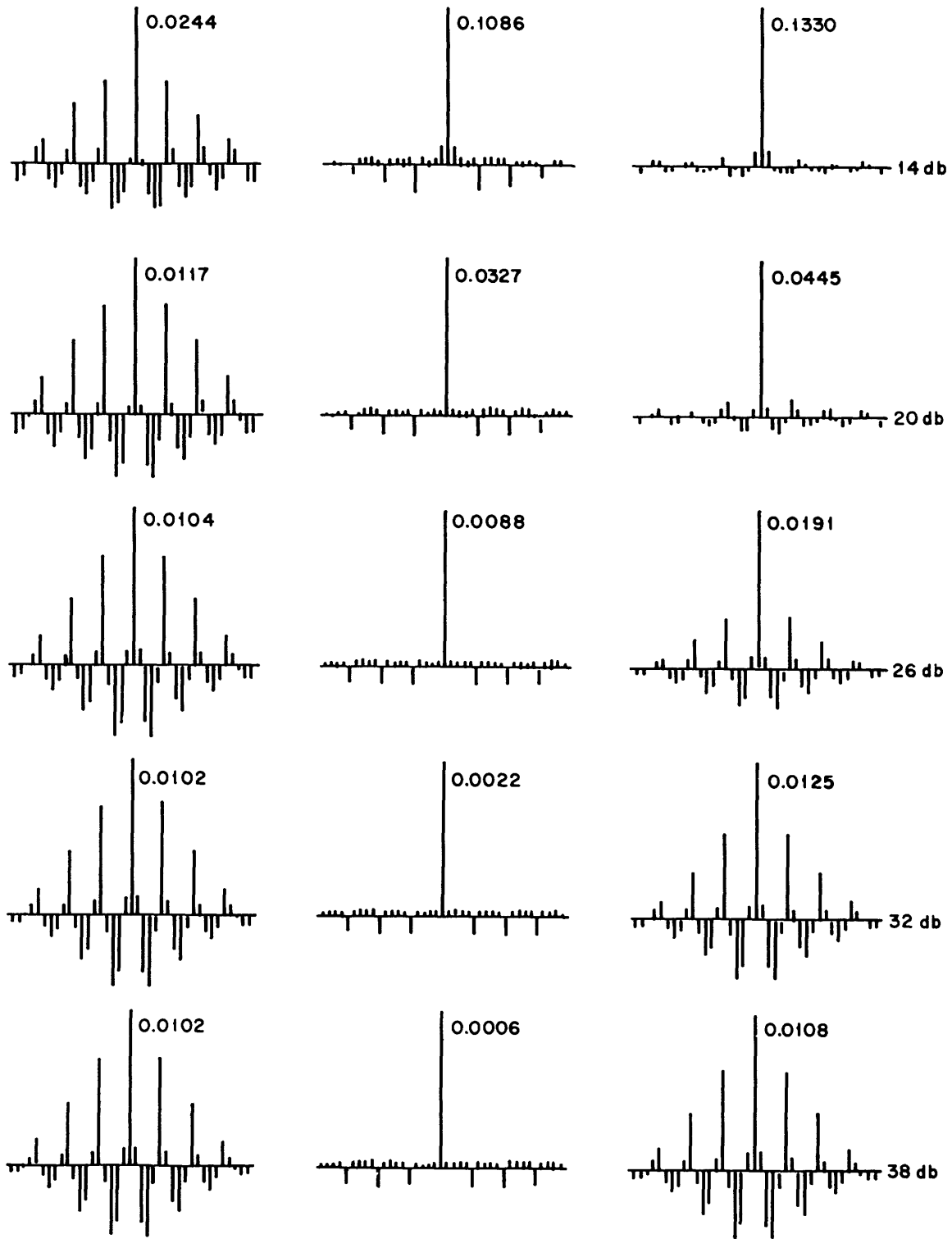Fig. 33(a-b). Distortion correlation functions for 5-21 case. Left column: intersymbol interference alone; center column: noise alone; right column: total distortion, sum of intersymbol interference and noise distortions.

0.0244　　　0.1086　　　0.1330

0.0117　　　0.0327　　　0.0445

0.0104　　　0.0088　　　0.0191

0.0102　　　0.0022　　　0.0125

0.0102　　　0.0006　　　0.0108

14 db

20 db

26 db

32 db

38 db

(b)

Fig. 33(a-b). Continued.

```
                                                  MAINLOBE
                                                     ↓
(a)   -  -  -  +  +  -  -  -  +  +  -  -  -  +  +  -  -  -  +  + │ + │ +  +  +  +      3-42-10786

      +  +  +  -  -  +  +  +  -  -  +  +  +  -  -  +  +  +  -  - │ + │ 0  0  0  0
(b)
      -  -  -  -  -  -  -  -  -  -  -  -  -  -  -  -  -  -  -  - │ + │ 0  0  0  0

      ?  +  +  +  -  -  +  +  +  -  -  +  +  +  -  -  +  +  +  - │ - │ +  0  0  0
(c)
      ?  -  -  +  -  +  -  -  +  -  +  -  -  +  -  +  -  -  +  - │ - │ +  0  0  0

      ?  ?  +  +  +  -  -  +  +  +  -  -  +  +  +  -  -  +  +  + │ - │ -  +  0  0
(d)
      ?  ?  -  +  +  +  +  -  +  +  +  +  -  +  +  +  +  -  +  + │ - │ -  +  0  0

      ?  ?  ?  +  +  +  -  -  +  +  +  -  -  +  +  +  -  -  +  + │ + │ -  -  +  0
(e)
      ?  ?  ?  +  +  -  +  +  +  +  -  +  +  +  +  -  +  +  +  + │ + │ -  -  +  0
```
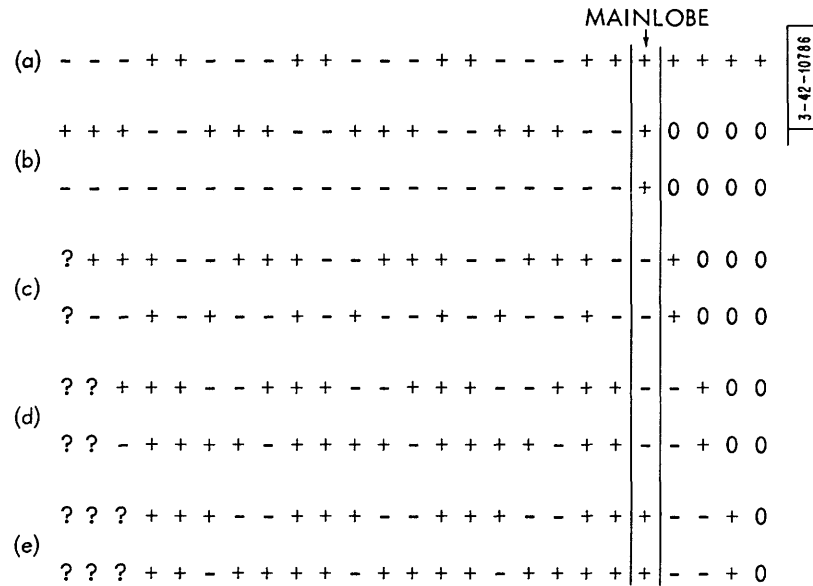
Fig. 34. Error propagation example using 5-21 case at 20 db. (a) Equivalent signal filter output for single +1 input sample; (b) worst possible message sequence for making decision on $\xi_0 = 1$, and their corresponding weightings of sidelobes of (a); and (c) to (e), shifted versions of this sequence on successive bauds, with errors on each decision, and with corresponding sidelobe weightings.

The result of weighting this message sequence by the corresponding sidelobes of Fig. 34(a) is shown in the second line of Fig. 34(c). Now, not all the distortions of the intersymbol interference are opposing the correct decision; in fact, the majority are aiding a correct decision. Note, however, that our previous decision error has caused an additional sidelobe of $2q_1$, which being large and positive leads to a decision error on the present baud with probability close to unity. Proceeding to Fig. 34(d), the first two errors have led to sidelobes $-2q_1$ and $2q_2$, which are both large, but fortunately tending to cancel one another out. Unfortunately, the majority of the other sidelobes are now in opposition to a correct decision, thus a third error is likely to occur with some high probability. Matters continue on in this way, with decreasing but high probabilities of error on successive bauds, until reaching the point where the first question mark comes up for a decision. At this point, all the sidelobes occurring before the mainlobe are being weighted by messages which are independent of the initial message sequence which helped initiate the burst; thus, the probability of error on each baud once again becomes no worse than 1/2 and, in fact, it is generally much less than 1/2 due to the relatively low noise levels in this region. Similar comments are seen to apply to Fig. 34(e). Thus, summarizing, an initial error caused by the collaboration of harmful intersymbol interference and additive noise is seen capable of propagating, virtually without further assistance from the additive noise, due to the particular message sequence which gave rise to the initial error, coupled with the erroneous decision feedback. This is what is happening in Figs. 31(a) and (b), where the mean recovery time is seen to increase beyond about 2 db for each of the cases studied, eventually reaching maximum values as shown in these two figures. Note that the mean recovery times of Fig. 31(b) become longer than the times in the corresponding cases of Fig. 31(a), since the number of taps on the equivalent signal filter is larger in the N-21 than in the N-11 cases, leading to correspondingly longer periods of error propagation such as that encountered in our example above. At this

point, we should note that the error-propagation effect leading to increased mean recovery times will not occur, in general, with an arbitrary choice of a message sequence; hence, if an initial error were to be caused by noise acting alone (perhaps by impulse noise on a telephone line, for example), the mean recovery time would generally be considerably shorter than those indicated in Figs. 31(a) and (b) which were obtained for bursts arising, to a great extent at least, from the intersymbol interference itself.

Having plotted the mean recovery time and explained its behavior to some extent as a function of SNR, the most encouraging conclusion we may draw from Figs. 31(a) and (b) is that in all cases the mean recovery time is bounded, and that on the average no error burst will last indefinitely. Coupled with the mean recovery time, of course, is the question of recovery time variance or, correspondingly, its standard deviation. We have plotted the standard deviations of the mean recovery times for the N-11 and N-21 cases in Figs. 35(a) and (b), respectively.

The general behavior of Figs. 35(a) and (b) is similar to that of Figs. 31(a) and (b) which show the mean recovery time. In all cases, moreover, we find that the standard deviation of the recovery time is less than its mean. Also, due to the longer forward-TDL lengths involved, the error propagation leads not only to greater mean recovery times in the N-21 than in the N-11 cases as noted previously, but it also results in a slightly greater recovery time variance. The recovery time standard deviation decreases at very high SNR, since only a small number of side-lobe combinations can result in a decision error, and since the noise is small, the resulting error burst is virtually deterministic for the next several succeeding bauds, becoming progressively less deterministic as new and independent binary signal samples enter into the equivalent signal filter. We see that the mean recovery time and the recovery time variance are both well-behaved, thus error propagation will not continue indefinitely with any finite probability. This conclusion is supported also by our simulation studies, as we illustrate in Figs. 36(a) and (b) which show the maximum recovery times in bauds which we encountered in our simulations, plotting them vs SNR for the N-11 and N-21 cases, respectively. From these figures, we note that in all cases
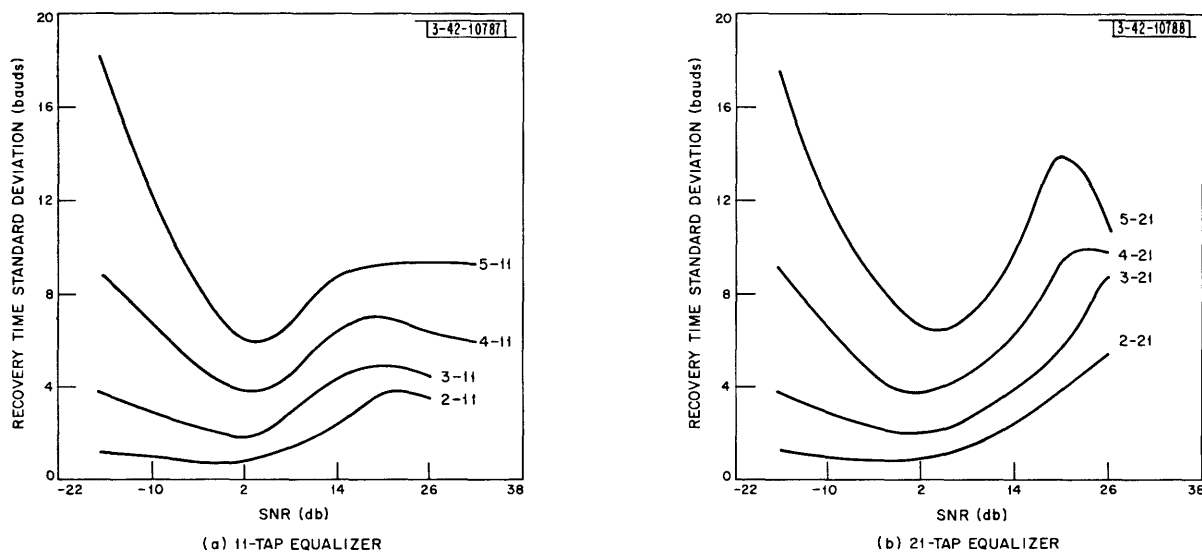

Fig. 35(a-b). Recovery time standard deviation vs SNR for 11- and 21-tap decision-feedback equalizers, applied to maximal distortion channels.
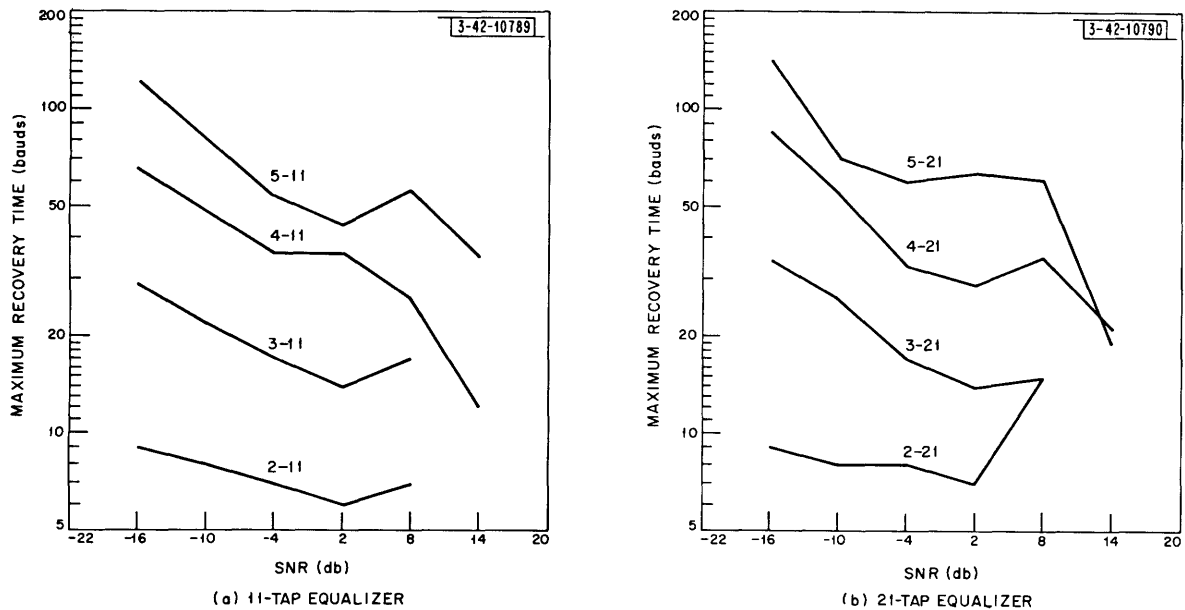
Fig. 36(a-b). Maximum recovery time vs SNR encountered in simulations of 11- and 21-tap decision-feedback equalizers for maximal distortion channels.

the maximum recovery times encountered were less than about 5 or 6 times the corresponding mean recovery times, as shown in Figs. 31(a) and (b), confirming further our conclusion that recovery of the decision-feedback equalizer will indeed occur, and that error bursts of indefinite duration do not pose a real problem in its operation.

Next, we want to consider the guard-space data obtained during our quasi-simulations of the decision-feedback equalizer. We have plotted the mean guard space as defined in Eq.(161) in Figs. 37(a) and (b) for the N-11 and N-21 cases, respectively. We observe from these figures that the mean guard space increases rapidly beyond about 14 db. This is to be expected, since the mean guard space is the reciprocal of the probability of an initial error which, in turn, is of the same order of magnitude as the overall probability of error, the two being related by a factor equal to the mean number of errors per burst at high SNR, which is even less than the mean recovery time. Thus, as asserted earlier in this Section, the mean guard space dominates the mean recovery time in the denominator of Eq.(159) at high SNR. The large guard spaces encountered with the decision-feedback equalizer are very desirable in terms of detecting and correcting the error bursts through coding techniques, a matter we will discuss further in Sec. VI.

C. BOUNDING MEAN RECOVERY TIME

We now present a method of obtaining bounds on the mean recovery time of the decision-feedback equalizer without having to perform simulations, whenever the total output distortion may be assumed uncorrelated from one decision to another, which we noted earlier was a valid assumption at intermediate SNR for the maximal distortion channels. Briefly stated, the method we will develop is to model the error propagation as a discrete Markov chain process, with "states" corresponding to the contents at the feedback-TDL positions. To obtain the mean recovery time exactly, we would have to consider a total of 3^{N-1} such states with an Nth-order
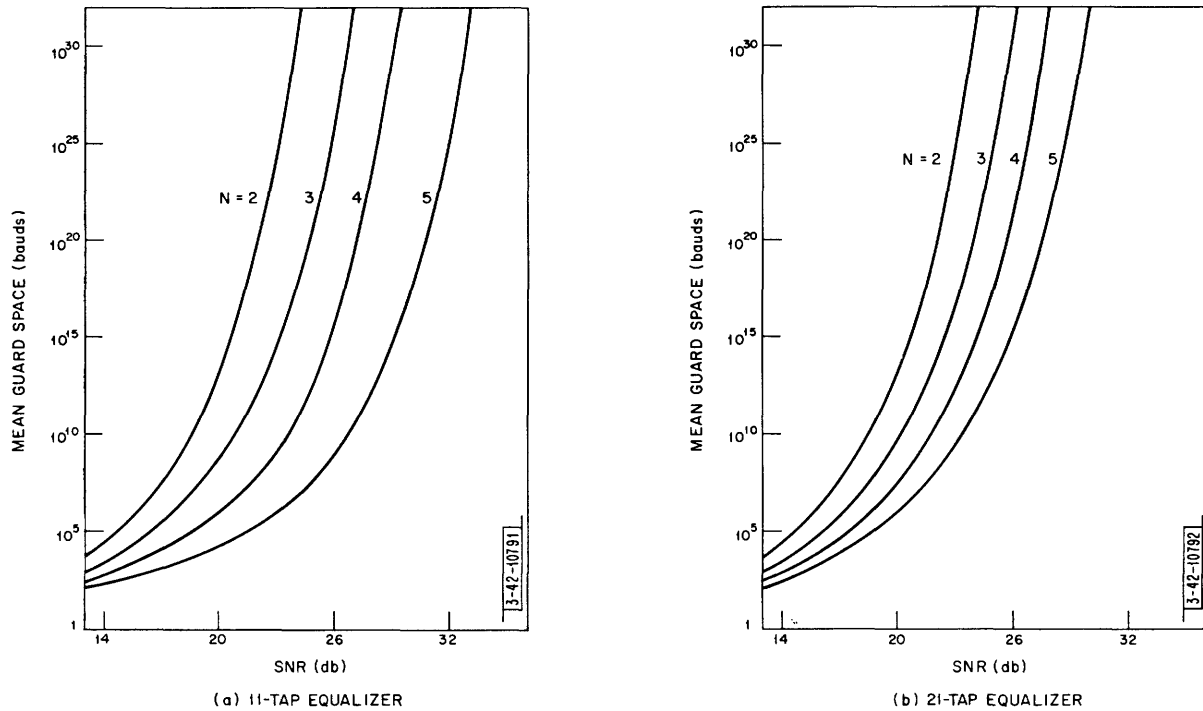
Fig. 37(a-b). Mean guard space vs SNR for 11- and 21-tap decision-feedback equalizers, applied to maximal distortion channels.

channel, since each of the N − 1 feedback-TDL positions may contain no error, a positive error, or a negative error. Instead, we will ignore the signs of the errors, thus reducing the total number of states to 2^{N-1}, with the N − 1 positions either containing an error or not. This leads us to a means of bounding the mean recovery time by solving the first-passage-time problem in the associated discrete Markov chain representation of the feedback-TDL state, using appropriate bounds on the transition probabilities from one state to another. The mathematical formulation of the problem developed in the following will apply as well to the original set of states, however, simply by replacing our bounds by the actual transition probabilities.

For an Nth-order channel, the feedback-TDL has N − 1 taps, which we number from right to left, as shown in Fig. 32. We will represent the state of the feedback-TDL on the nth decision by a sequence of digits

$$k_{N-1}^{(n)} \cdots k_2^{(n)} \, k_1^{(n)} \tag{175}$$

where $k_i^{(n)} = 1$ if the ith position of the feedback-TDL is occupied by an error on the nth decision, and where $k_i^{(n)} = 0$ otherwise. We will number these 2^{N-1} states, for convenience assigning numbers 1 and 2^{N-1} to the error-free and initial-error states, respectively:

$$\text{state 1:} \qquad 000 \ldots 00 \tag{176}$$

$$\text{state } 2^{N-1}: \qquad 000 \ldots 01 \quad . \tag{177}$$

The remaining state numbers we assign arbitrarily. Thus, state 1 is the desired operating state in which no errors are contained in the feedback-TDL, while state 2^{N-1} is entered when the initial error of a burst occurs. After each decision, the contents of the feedback-TDL shift to the left, thus

73

$$k_i^{(n+1)} = k_{i-1}^{(n)}$$ (178)

for $i = 2, \ldots, N - 1$. The value of k_1, of course, depends upon whether or not a decision error has occurred, thus we see that each state can undergo a transition to exactly two other states. This is illustrated by the example shown in Fig. 38, where we have indicated the possible transitions for a fifth-order channel. We see there that in the error-free mode of operation the decision-feedback equalizer occupies the leftmost state shown, the 0000 state. A transition out of this state to the 0001 state occurs with an initial error. The problem then of determining the mean recovery time is thus seen to be equivalent to determining the mean first-passage time from the 0001 state back to the 0000 state in Fig. 38 or, more generally, from state 2^{N-1} back to state 1, in view of our assignments (176) and (177). Assuming that an initial error has just
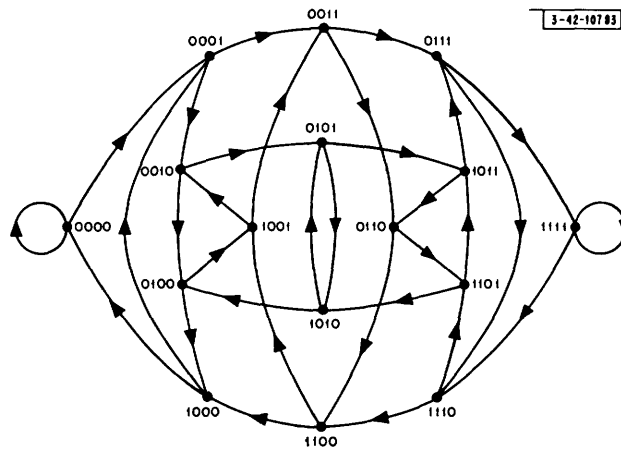

Fig. 38. Error-state transition diagram for Markov chain model of error propagation in decision-feedback equalizer for fifth-order channel.

occurred, we next solve this mean first-passage-time problem, first introducing some notation which is generally consistent with that discussed more fully in Ref. 19:

p_{ij} = probability of a transition from state i to state j after a decision has been made   (179)

$\pi_i(n)$ = probability that the feedback-TDL is in state i after n transitions, given that it was initially in state 2^{N-1} (180)

$\underline{P}$ = process transition matrix, with elements p_{ij} (181)

$\underline{\pi}(n)$ = state occupation probability vector after n transitions, given the initial state 2^{N-1}, a row vector with elements $\pi_i(n)$.   (182)

As noted above, recovery of the decision-feedback equalizer is equivalent to reaching state 1 after an initial error has put it in state 2^{N-1}. Since we are interested in the first-passage times back to state 1, we want to consider state 1 as a trapping state. We further want to prevent self-looping in state 1 from being counted as "first-passages" and, thus, to prevent all transitions after state 1 has once been entered, we define modified transition probabilities

$$p_{ij}^* = \begin{cases} p_{ij} & \text{for } i \neq 1 \\ 0 & \text{for } i = 1 \end{cases} \tag{183}$$

with a corresponding modification of the transition matrix:

$$\underline{P}^* = \text{modified process transition matrix, elements } p_{ij}^* \quad . \tag{184}$$

From definition of the transition matrix, we have that under these modifications

$$\underline{\pi}(n) = \underline{\pi}(n-1)\,\underline{P}^* = \underline{\pi}(0)\,\underline{P}^{*\,n} \tag{185}$$

as the state occupation vector after n transitions, where

$$\underline{\pi}(0) = (0, 0, \ldots, 0, 1) \tag{186}$$

since initially the feedback-TDL is in state 2^{N-1}. If we further define a column vector $\underline{e}_0$ with 2^{N-1} components via

$$\underline{e}_0 \;\triangleq\; \begin{bmatrix} 1 \\ 0 \\ 0 \\ . \\ . \\ . \\ 0 \end{bmatrix} \tag{187}$$

then, from notation (182) and Eq.(187), it follows that

$$\pi_1(n) = \underline{\pi}(n)\,\underline{e}_0 \tag{188}$$

which is simply the probability that we are in state 1 after n transitions, conditioned on the fact that we have not previously entered state 1, through our use of $\underline{P}^*$ instead of $\underline{P}$ in Eq. (185). Thus, we conclude that the mean first-passage time $\overline{T}_{fp}$ may be expressed by

$$\overline{T}_{fp} = \sum_{n=1}^{\infty} n\pi_1(n) \tag{189}$$

which, through substituting in from Eqs.(185) and (188), becomes

$$\overline{T}_{fp} = \sum_{n=1}^{\infty} n\underline{\pi}(0)\,\underline{P}^{*\,n}\underline{e}_0 = \underline{\pi}(0)\left[\sum_{n=1}^{\infty} n\underline{P}^{*\,n}\right]\underline{e}_0 \quad . \tag{190}$$

Now, it is straightforward to show that

$$\sum_{n=1}^{\infty} n\underline{P}^{*\,n} = [\underline{I} - \underline{P}^*]^{-2}\,\underline{P}^* \tag{191}$$

where $\underline{I}$ is the $2^{N-1} \times 2^{N-1}$ identity matrix, simply by multiplying both sides by $[\underline{I} - \underline{P}^*]^2$ and reducing Eq.(191) to an identity. Similarly, noting that the first row of $\underline{P}^*$ contains all zeros and that the elements in each of the remaining rows sum to unity since some transition must occur after each decision, then we can verify that

$$[\underline{I} - \underline{P}^*]^{-1} \, \underline{P}^* \, \underline{e}_0 = \begin{bmatrix} 0 \\ 1 \\ 1 \\ \cdot \\ \cdot \\ \cdot \\ 1 \end{bmatrix} \triangleq \underline{e}_0^* \tag{192}$$

and thus, using Eqs.(191) and (192) in Eq.(190), we find the mean first-passage time is given by

$$\overline{T}_{fp} = \underline{\pi}(0) \, [\underline{I} - \underline{P}^*]^{-1} \, \underline{e}_0^* \tag{193}$$

where, again, $\underline{\pi}(0)$, $\underline{P}^*$, and $\underline{e}_0^*$ are as defined in Eqs. (186), (184), and (192), respectively.

Next, we want to apply Eq. (193) in order to obtain a bound on the mean recovery time of the decision-feedback equalizer. To do this, we must specify the appropriate bounds on the p_{ij}^*, the elements of the modified transition matrix $\underline{P}^*$. There are a number of ways in which we might do this. We will describe one method, convenient for its simplicity, which has proved useful in practice. First we observe that the net sum of the uncanceled sidelobes is either tending to assist or oppose a correct decision. Clearly then, we may determine an upper bound to the probability of error by first defining for each state a quantity Q via

$$Q = \begin{cases} 0 & \text{if the net sum of the uncanceled sidelobes tends} \\ & \text{to assist a correct decision} \\ D_e & \text{otherwise} \end{cases} \tag{194}$$

where we have defined the distortion measure due to errors as

$$D_e = -2 \sum |q_i| \tag{195}$$

the summation being over the uncanceled sidelobes, and the factor of two arising from the fact that these sidelobes were doubled rather than canceled through the erroneous decision feedback. Then, since under our assumptions the two situations of Eq. (194) are equally probable, we may write down a bound on the probability of error while in any state:

$$p(\text{error} \mid \text{state } i) \leqslant \frac{1}{2} \, p(\text{error} \mid Q = 0) + \frac{1}{2} \, p(\text{error} \mid Q = D_e) \tag{196}$$

where D_e and Q, of course, are dependent upon i, the number of the state being considered. The calculation of the quantities $p(\text{error} \mid Q)$ appearing in Eq.(196) is a straightforward application of our modified error tree algorithm, being identical with our discussion of finding the probability of the initial error of a burst, with the exception that the mainlobe $q_0 = 1$ used there

76

must now be replaced by a mainlobe of $q_0^* = 1 + Q$. This renders the desired bounds on the probability of error in each of the feedback-TDL states which, in turn, render the p_{ij}^* needed in Eq.(193) to determine the bound we desire on the mean recovery time.

The approach indicated in the preceding discussion can thus enable us to arrive at bounds on the mean recovery time of any channel, of arbitrary order, without having to resort to the time-consuming methods of simulations or quasi-simulations.

In this Section, we have presented the techniques and algorithms developed for determining the operation and performance of the decision-feedback equalizer at all SNR, and the results of applying these methods using the maximal distortion channels as examples were shown and discussed. Much of the discussion centered on the problem of error bursts, and the properties of the recovery time. Our final summaries regarding the operation of the decision-feedback equalizer are included in Sec. VI, where we also compare it with the operation of the conventional equalizer studied in Sec. IV.
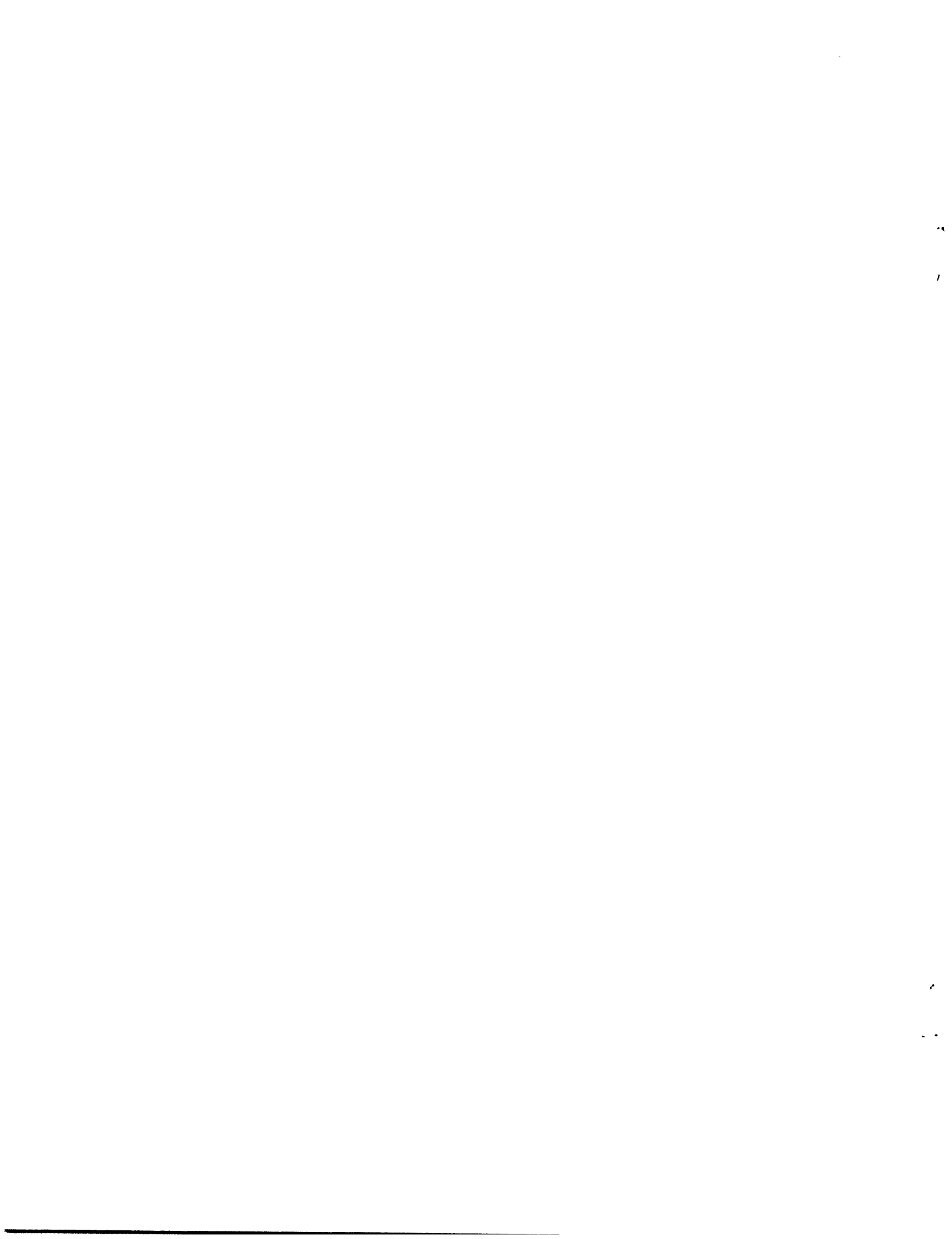
VI. CONCLUSIONS – SUGGESTIONS FOR FURTHER RESEARCH

In this report, we have adopted a decision-theory approach to digital communication over dispersive channels, arriving at the optimal receiver and sub-optimal conventional equalizer in Sec. II, and the sub-optimal decision-feedback equalizer in Sec. III. Further, we determined the parameter settings of these sub-optimal equalizers which minimize their total output distortion. After deriving the class of channels we wished to study (the maximal distortion channels), we developed in Sec. IV an algorithm for evaluating the performance of the conventional equalizer, and in Sec. V an algorithm to enable performance evaluation of the decision-feedback equalizer even at high SNR where simulation methods fail. In Secs. IV and V, we also presented and discussed the performance achieved by the conventional and decision-feedback equalizers when applied to the maximal distortion channels, with additional attention paid to the error-propagation behavior of the decision-feedback equalizer. Now, we briefly compare the operations and performances of the two equalizers. First we note the differences found in their performances, as presented separately in Secs. IV and V, and then we explain these differences in terms of their respective residual noise and intersymbol interference distortions appearing at their outputs. We conclude with some brief discussions of issues which may prove of interest in future research in this area.

Through Figs. 39 and 40, we summarize the typical overall characteristics of the conventional and decision-feedback equalizer performances, respectively, using the N-21 cases as examples. At very low SNR, both equalizer performances approach that of the nondispersive N = 1 channel, since the additive noise dominates the channel dispersion, as explained previously. At intermediate SNR, comparison of Figs. 39 and 40 reveals that the performance of the decision-feedback equalizer can become worse than that of the conventional equalizer. Thus, for example, at a SNR of 8 db the error rate of the decision-feedback equalizer is 0.143 in the 5-21 case, compared with the smaller 0.134 error probability of the conventional equalizer. While this difference is small, it nonetheless demonstrates that at low SNR and high error rates, the additional sidelobes caused by erroneous decision feedback can cause the decision-feedback equalizer to exhibit a poorer performance than the conventional equalizer not employing decision feedback. With increasing SNR, the performance of the decision-feedback equalizer improves more rapidly, however, than that of the conventional equalizer, until at some point they become equal. We refer to this SNR at which the two equalizer performances coincide as the "threshold" SNR. The threshold is in the range from about 8 to 14 db for the maximal distortion channels.

With increasing the SNR above threshold, the decision-feedback equalizer performance improves very rapidly. Thus, from Figs. 39 and 40, we observe that at all error rates of practical importance, the decision-feedback equalizer operates much better than the conventional equalizer. For example, in the 2-21 case at 14 db, we find from Fig. 39 that the conventional equalizer probability of error is 6.28×10^{-3} compared with an error rate of 1.36×10^{-4} achieved by the decision-feedback equalizer of Fig. 40. Moreover, comparison of these figures reveals that this performance advantage of the decision-feedback equalizer becomes greater, the larger the channel distortion and the higher the SNR. Thus, despite the fact that error-propagation effects occur with the decision-feedback equalizer, its performance still is vastly better than that of the conventional equalizer currently finding application in dispersive channel equalization.
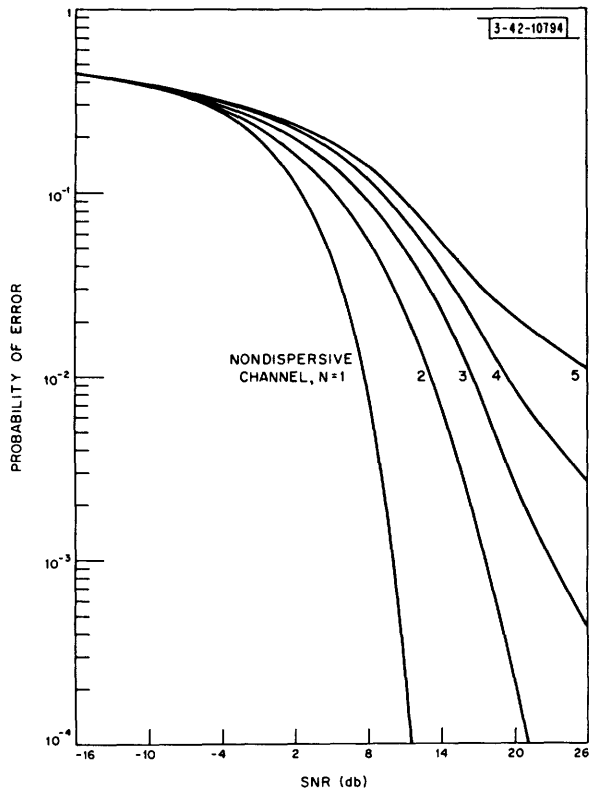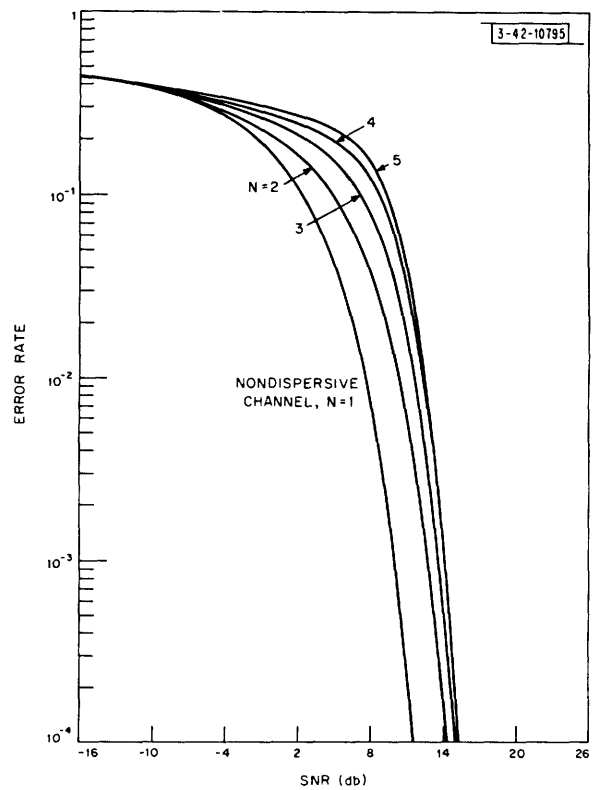
Fig. 39. Performance vs SNR of conventional equalizer having 21 taps, applied to maximal distortion channels.

Fig. 40. Error rate vs SNR of decision-feedback equalizer having 21 taps, applied to maximal distortion channels.

80

We may obtain some feeling as to the degree to which the conventional and decision-feedback equalizers are sub-optimal, through comparing the N = 2 through N = 5 curves of Figs. 39 and 40 with the nondispersive N = 1 curve, since this curve represents an upper bound on the performance of the optimal equalizer derived in Sec. II. We observe that the conventional equalizer N = 2 curve is about 9.5 db poorer than the N = 1 bound at a probability of error of 10^{-4}, with the loss being even greater for the higher-order maximal distortion channels. On the other hand, from Fig. 40 for the decision-feedback equalizer in this N = 2 case, the loss in SNR is only about 2.8 db compared with the N = 1 bound, and moreover the loss increases by less than an additional 2 db for the higher-order maximal distortion channels considered, at this same error rate of 10^{-4}. Thus, we conclude that, although their hardware-implementation requirements were made identical, the conventional equalizer is much more sub-optimal than the decision-feedback equalizer which, in turn, is so close to the upper bound on performance that the maximum improvement in SNR which could possibly be achieved through any alternative sub-optimal equalization scheme is probably not worth the additional complexities it would require.

As mentioned in our concluding discussions of Sec. III, it is in the different treatment given by the decision-feedback equalizer to the intersymbol interference contributions arising from past and future bauds which accounts for the performance advantages it enjoys over the conventional equalizer. The respective sidelobe-suppression behavior of the two equalizers is illustrated in Fig. 41, where we have plotted D_α and D_β vs SNR for the 5-21 case. These curves, typical of those obtained in all other cases studied, explain why the conventional equalizer performances shown in Figs. 21(a) to (d) reach limiting values with increasing SNR, while the corresponding decision-feedback equalizer performances shown in Figs. 27(a) to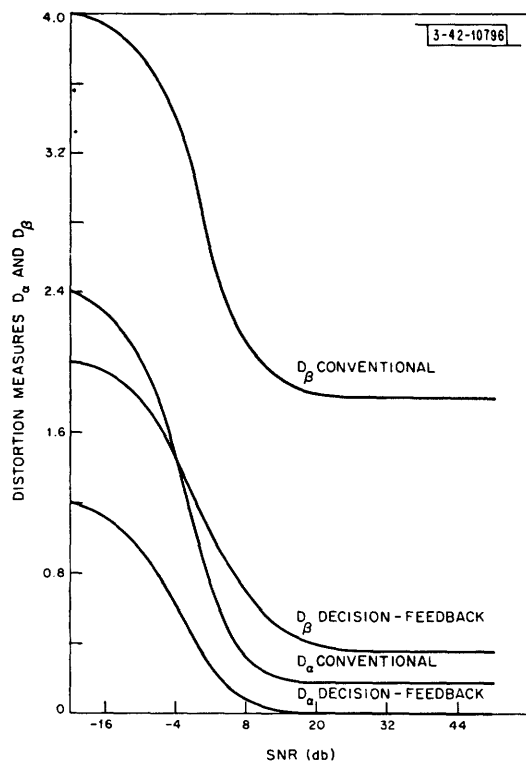 (d) continue to improve with SNR. At high SNR, the limiting D_β for the conventional equalizer is seen to approach a value of approximately 1.81. Thus, if a sufficient number of sidelobes collaborate to oppose a correct decision, the net intersymbol interference distortion can exceed unity, thus leading to a decision error even in the absence of noise. Of course, regardless of D_β, the probability that this will occur will drop off rapidly with the overall number of sidelobes; hence, by using a sufficiently long TDL in the conventional equalizer, we may obtain any desired performance level at high SNR. The SNR levels and TDL lengths involved, however, are much larger than those required using the decision-feedback equalizer to obtain the same performance levels. Of course, this is because generally the decision-feedback equalizer is able to devote many more of its total number of taps to reducing the intersymbol interference arising from future baud transmissions than can the corresponding conventional equalizer with the same number of taps available, as discussed in Sec. III. As a result, we find from Fig. 41 that the D_β obtained with the

Fig. 41. Distortion measures D_α and D_β vs SNR for conventional and decision-feedback equalizers in 5-21 case.

decision-feedback equalizer is less than unity beyond approximately 2 db; thus, above this SNR, the intersymbol interference acting alone cannot cause a decision error, and therefore the performance will continue to improve with SNR, as we observed earlier in Sec. V. To confirm the sidelobe-suppressing advantage of the decision-feedback equalizer still more, we have plotted the limiting value of D_β with increasing SNR vs the TDL length of the conventional equalizer in Fig. 42. Comparison of this figure with Fig. 30 illustrates the higher residual sidelobe distortion levels obtained with the conventional equalizer, and accounts for its much poorer performance than that of the decision-feedback equalizer at the high SNR of practical importance.

A further advantage of the decision-feedback equalizer is in terms of its noise enhancement, which is less than that of the conventional equalizer, as we see in Fig. 43 where their noise enhancements are plotted vs SNR for the 2-3 case. Despite the fact that the noise enhancement is smaller with the decision-feedback than with the conventional equalizer, we found above that it nonetheless accounts for nearly all the degradation in performance encountered with decision-feedback equalizers of long length at high SNR, whereas with the conventional equalizer the residual sidelobes were seen to determine its limiting performance, independent of the additive noise enhancement.

From our recovery-time and guard-space studies of Sec. V, it is clear that at all those error rates and SNR of practical interest, the mean guard space greatly exceeds the mean burst duration, and even the maximum burst durations encountered in our simulations. Such large error-free guard spaces between error bursts are very desirable from the viewpoint of applying coding techniques to further improve the overall performance of the decision-feedback equalizer. In the error-detecting and -correcting scheme of Ref. 20, for example, the guard space need only be three times as long as the longest possible burst duration in order to insure 100-percent error correction. Such a scheme applied here with the decision-feedback equalizer would have
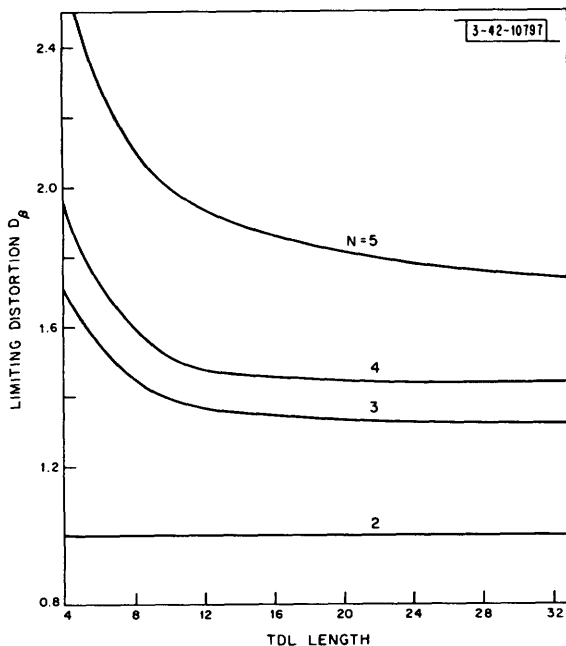

Fig. 42. Limiting distortion D_β vs TDL length of conventional equalizer, applied to maximal distortion channels.
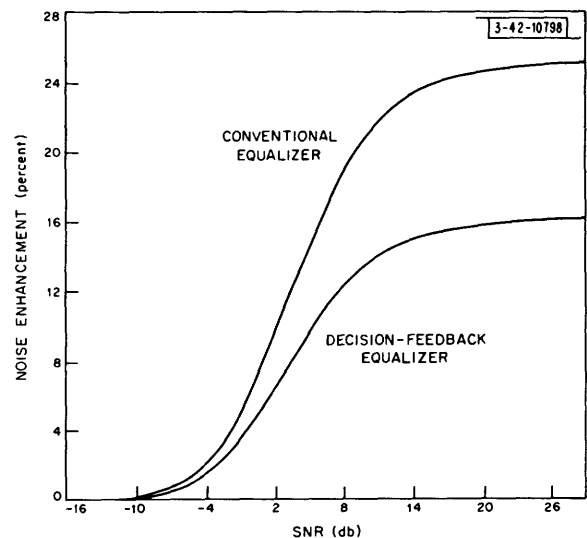
Fig. 43. Example of noise enhancement vs SNR for conventional and decision-feedback equalizers in 2-3 case.

enabled virtually error-free data transmission. Other schemes requiring even smaller guard spaces may be employed as well, for although these permit certain error sequences to remain undetected, such sequences have sufficiently low probability of occurrence that again one attains virtually error-free data transmission. The method of Ref. 20 is being applied in the construction of equipment capable of correcting error bursts of up to 1000 bauds in duration, and with relative simplicity. Thus, we conclude that in view of the error-burst and guard-space data we obtained on the decision-feedback equalizer, its use in conjunction with coding techniques for eliminating its error bursts is both quite feasible and highly desirable.

The present work may easily be extended to include the colored noise case, the only essential difference in structures of the equalizers considered being that the matched filter becomes replaced by a "whitening filter" in cascade with a second filter, the latter being matched to the equivalent channel in cascade with the whitening filter. Also, if the output noise statistics are non-Gaussian but known, then our algorithms for determining the equalizer performances still apply, except now the erfc($\cdot$) function of Eq. (123) must be replaced throughout the calculations, and the noise samples given the appropriate statistical distribution in the simulation studies.

Correlated message sequences are easily handled by redefining the total output distortions of Eqs. (34) and (90) to include the effects of the correlation between the signals upon the inter-symbol interference component of the distortion. This, however, merely modifies the definitions of the elements of the $\underline{X}$ matrices of Eqs. (39) and (82), but otherwise leaves unaltered the tap-gain vector solutions of both the conventional and decision-feedback equalizers.

Another issue for further investigation is the use of multilevel signaling schemes. Four- and eight-level digital communication systems are common, and even more levels are used in some applications. The algorithms used here could be directly extended to such multilevel systems. The error rate of the decision-feedback equalizer at the higher bit rates attained through multilevel signaling would, of course, be somewhat poorer than in the binary signaling scheme considered throughout our studies in this report. This could occur for two reasons. First, a large noise can cause an error regardless of its polarity in a multilevel signaling system, whereas with a binary scheme it will always assist a decision with probability of 1/2. Second, this same effect applies to the large intersymbol interference distortions arising through erroneous decision feedback, hence we would expect that the recovery times might be somewhat longer than with a binary signaling system. The degree to which these factors are important thus should also prove a matter of interest in future research.

The decision-feedback equalizer structure, as derived under our assumptions in Sec. III, involves a nonlinear feedback loop, inasmuch as we may consider the decision-feedback operation to be implemented by our first passing the output samples through a hard limiter, and then taking the limiter output as the feedback-TDL input as shown in Fig. 44(a). Alternative schemes which might prove even more effective readily come to mind. For example, if the output statistic were passed through the "soft-limiter" of Fig. 44(b), an improvement in performance might be realized. Looking into different types of nonlinear feedback such as this is thus another topic of interest.

Finally, and perhaps one of the most important issues remaining to be studied, is the question of the sensitivity of the performances of the conventional and decision-feedback equalizers to channel measurement errors. In all the studies presented here, of course, perfect channel measurement was assumed; as a result, the tap gains of both equalizers were able to
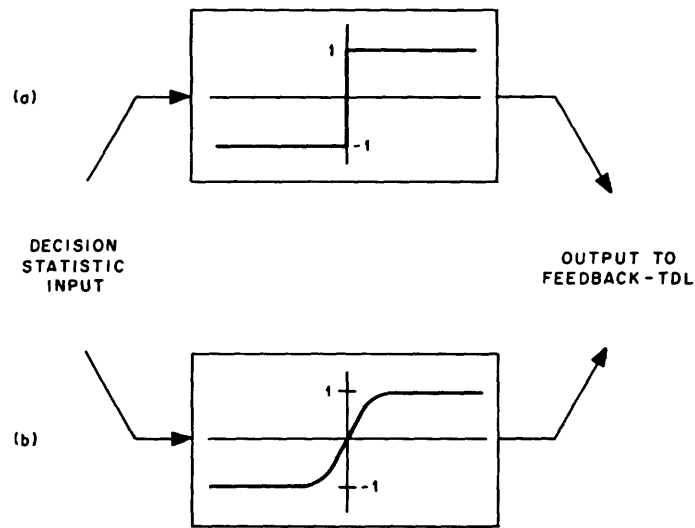
Fig. 44. Decision-feedback via nonlinear transfer functions:
(a) hard-limiting, as effectively considered in this report, and
(b) alternative approach using soft-limiting.

be set optimally under our output distortion measure. With channel measurement errors, how-
ever, the equalizer performances must deteriorate. The question of sensitivity is especially
of interest in the case of the decision-feedback equalizer, which allows large sidelobes to occur
after the mainlobe (recall Fig. 10) with the expectation that they will be canceled out by the
feedback-TDL output. With channel measurement errors, even in the absence of previous
decision errors, such cancellation will be imperfect, leading to poorer performance. Thus,
also requiring investigation is the extent to which such measurement errors affect the high
performance levels achieved by the decision-feedback equalizer in our studies, when compared
with the type of conventional equalizer currently employed.

ACKNOWLEDGMENTS

REFERENCES

1. O. J. Zobel, "Distortion Correction in Electrical Circuits with Constant Resistance Recurrent Networks," Bell System Tech. J. $\underline{7}$, 438 (1928).

2. H. E. Kallmann, "Transversal Filters," Proc. IRE $\underline{28}$, 302 (1940).

3. R. Price and P. E. Green, "A Communication Technique for Multipath Channels," Proc. IRE $\underline{46}$, 555 (1958).

4. M. L. Doelz, E. T. Heald, and D. L. Martin, "Binary Data Transmission Techniques for Linear Systems," Proc. IRE $\underline{45}$, 656 (1957).

5. R. R. Mosier and R. G. Clabaugh, "Kineplex, A Bandwidth-Efficient Binary Transmission System," AIEE Commun. and Electron., No. 34, 723 (January 1958).

6. M. E. Austin, "An Efficient Transversal Equalizer for Two-Path Channels," Quarterly Progress Report No. 81, Research Laboratory of Electronics, M.I.T. (April 1966), p. 161.

7. R. W. Lucky and H. R. Rudin, "Generalized Automatic Equalization for Communication Channels," Proc. IEEE (Letters) $\underline{54}$, 439 (1966).

8. M. J. DiToro, "A New Method of High-Speed Adaptive Serial Communication Through any Time-Variable and Dispersive Transmission Medium," Conference Record, IEEE Communications Convention, Boulder, Colorado, June 1965, p. 763.

9. R. W. Lucky, "Techniques for Adaptive Equalization of Digital Communication Systems," Bell System Tech. J. $\underline{45}$, 255 (1966).

10. _____, "Automatic Equalization for Digital Communication," Bell System Tech. J. $\underline{44}$, 547 (1965).

11. Private discussions with P. R. Drouilhet and C. W. Niessen of M.I.T. Lincoln Laboratory, Lexington, Massachusetts; see also, "Adaptive Equalizer for Pulse Transmission," IEEE International Conference on Communications, Minneapolis, Minnesota, 12 – 14 June 1967.

12. H. L. VanTrees, Optimum Signal Processing (Wiley, New York, 1967).

13. M. R. Aaron and D. W. Tufts, "Intersymbol Interference and Error Probability," IEEE Trans. Inform. Theory IT-12, No. 1, 26 (1966).

14. F. B. Hildebrand, Methods of Applied Mathematics (Prentice-Hall, Englewood Cliffs, New Jersey, 1952).

15. M. Athans and P. L. Falb, Optimal Control (McGraw-Hill, New York, 1966).

16. U. Grenander and G. Szego, Toeplitz Forms and Their Applications (University of California Press, Berkeley and Los Angeles, 1958).

17. D. A. George, "Matched Filters for Interfering Signals," IEEE Trans. Inform. Theory IT-11, No. 1, 153 (1965).

18. D. C. Coll, "A System for the Optimum Utilization of Pulse Communication Channels," Ph. D. Thesis, Carleton University, Ottawa, Ontario, Canada (March 1966).

19. R. A. Howard, Dynamic Programming and Markov Processes (M.I.T. Press, Cambridge, Massachusetts, 1960).

20. J. L. Massey, "Implementation of Burst-Correcting Convolutional Codes," IEEE Trans. Inform. Theory IT-11, No. 3, 416 (1965).
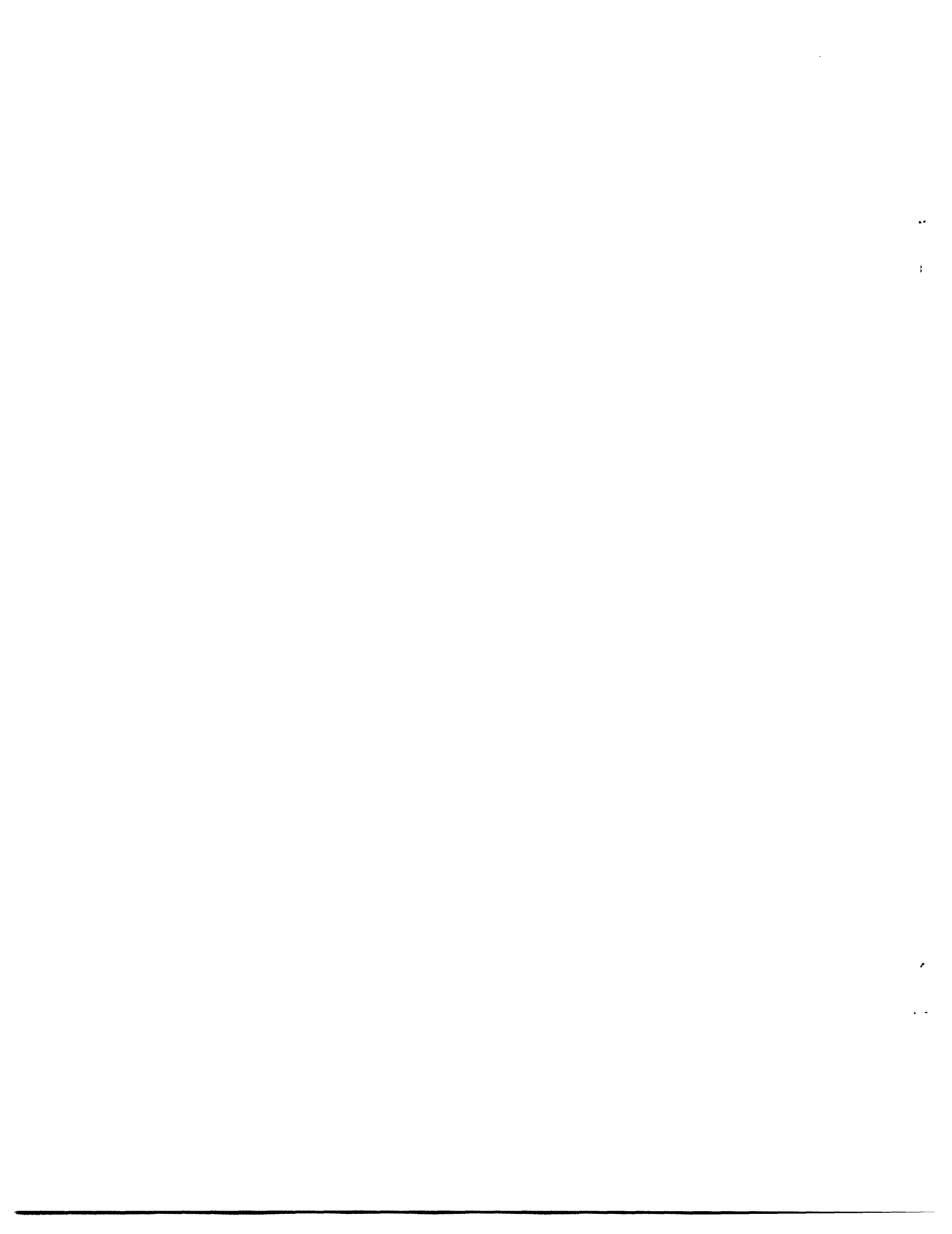
JOINT SERVICES ELECTRONICS PROGRAM
REPORTS DISTRIBUTION LIST

Department of Defense

Dr. A. A. Dougal
Asst Director (Research)
Ofc of Defense Res & Eng
Department of Defense
Washington, D.C. 20301

Office of Deputy Director
(Research and Information Room 3D1037)
Department of Defense
The Pentagon
Washington, D.C. 20301

Director
Advanced Research Projects Agency
Department of Defense
Washington, D.C. 20301

Director for Materials Sciences
Advanced Research Projects Agency
Department of Defense
Washington, D.C. 20301

Headquarters
Defense Communications Agency (333)
The Pentagon
Washington, D.C. 20305

Defense Documentation Center
Attn: TISIA
Cameron Station, Bldg. 5
Alexandria, Virginia 22314

Director
National Security Agency
Attn: Librarian C-332
Fort George G. Meade, Maryland 20755

Weapons Systems Evaluation Group
Attn: Col. Daniel W. McElwee
Department of Defense
Washington, D.C. 20305

Director
National Security Agency
Fort George G. Meade, Maryland 20755
Attn: Mr. James Tippet
    R3/H20

Central Intelligence Agency
Attn: OCR/DD Publications
Washington, D.C. 20505

Department of the Air Force

Colonel Kee
AFRSTE
Hqs. USAF
Room ID-429, The Pentagon
Washington, D.C. 20330

Aerospace Medical Division
AMD (AMRXI)
Brooks Air Force Base, Texas 78235

AUL3T-9663
Maxwell AFB, Alabama 36112

AFFTC (FTBPP-2)
Technical Library
Edwards AFB, Calif. 93523

AF Unit Post Office
Attn: SAMSO(SMSDI-STINFO)
Los Angeles, California 90045

Lt. Col. Charles M. Waespy
Hq USAF (AFRDSD)
Pentagon
Washington, D. C. 20330

SSD(SSTRT/Lt. Starbuck)
AFUPO
Los Angeles, California 90045

Det #6, OAR (LOOAR)
Air Force Unit Post Office
Los Angeles, California 90045

Systems Engineering Group (RTD)
Technical Information Reference Branch
Attn: SEPIR
Directorate of Engineering Standards
and Technical Information
Wright-Patterson Air Force Base,
Ohio 45433

Mr. H. E. Webb (EMIA)
Rome Air Development Center
Griffiss Air Force Base, New York 13442

ARL (ARIY)
Wright-Patterson AFB, Ohio 45433

Dr. H. V. Noble
Air Force Avionics Laboratory
Wright-Patterson AFB, Ohio 45433

Mr. Peter Murray
Air Force Avionics Laboratory
Wright-Patterson AFB, Ohio 45433

AFAL (AVTE/R. D. Larson)
Wright-Patterson AFB, Ohio 45433

Commanding General
Attn: STEWS-WS-VT
White Sands Missile Range
New Mexico 88002

RADC (EMLAL-1)
Griffiss AFB, New York 13442
Attn: Documents Library

Academy Library (DFSLB)
U.S. Air Force Academy
Colorado Springs, Colorado 80912

Lt. Col. Bernard S. Morgan
Frank J. Seiler Research Laboratory
U.S. Air Force Academy
Colorado Springs, Colorado 80912

APGC (PGBPS-12)
Eglin AFB, Florida 32542

AFETR Technical Library
(ETV, MU-135)
Patrick AFB, Florida 32925

AFETR (ETLLG-1)
STINFO Officer (for Library)
Patrick AFB, Florida 32925

Dr. L. M. Hollingsworth
AFCRL (CRN)
L. G. Hanscom Field
Bedford, Massachusetts 01731

AFCRL (CRMXLR)
AFCRL Research Library, Stop 29
L. G. Hanscom Field
Bedford, Massachusetts 01731

Colonel Robert E. Fontana
Department of Electrical Engineering
Air Force Institute of Technology
Wright-Patterson AFB, Ohio 45433

Colonel A. D. Blue
RTD (RTTL)
Bolling Air Force Base, D.C. 20332

Dr. I. R. Mirman
AFSC (SCT)
Andrews Air Force Base, Maryland 20331

AFSC (SCTR)
Andrews Air Force Base, Maryland 20331

Lt. Col. J. L. Reeves
AFSC (SCBB)
Andrews Air Force Base, Maryland 20331

ESD (ESTI)
L. G. Hanscom Field
Bedford, Massachusetts 01731

AEDC (ARO, INC)
Attn: Library/Documents
Arnold AFS, Tennessee 37389

European Office of Aerospace Research
Shell Building
47 Rue Cantersteen
Brussels, Belgium

Lt. Col. Robert B. Kalisch (SREE)
Chief, Electronics Division
Directorate of Engineering Sciences
Air Force Office of Scientific Research
Arlington, Virginia 22209

Department of the Army

U.S. Army Research Office
Attn: Physical Sciences Division
3045 Columbia Pike
Arlington, Virginia 22204

Research Plans Office
U.S. Army Research Office
3045 Columbia Pike
Arlington, Virginia 22204

Commanding General
U.S. Army Materiel Command
Attn: AMCRD-TP
Washington, D.C. 20315

Commanding General
U.S. Army Communications Command
Fort Huachuca, Arizona 85163

Commanding Officer
U.S. Army Materials Research Agency
Watertown Arsenal
Watertown, Massachusetts 02172

Commanding Officer
U.S. Army Ballistics Research Laboratory
Attn: V. W. Richards
Aberdeen Proving Ground
Aberdeen, Maryland 21005

Commandant
U.S. Army Air Defense School
Attn: Missile Sciences Division C&S Dept.
P.O. Box 9390
Fort Bliss, Texas 79916

Commanding General
U.S. Army Missile Command
Attn: Technical Library
Redstone Arsenal, Alabama 35809

Commanding General
Frankford Arsenal
Attn: SMUFA-L6000-64-4 (Dr. Sidney Ross)
Philadelphia, Pennsylvania 19137

U.S. Army Munitions Command
Attn: Technical Information Branch
Picatinney Arsenal
Dover, New Jersey 07801

Commanding Officer
Harry Diamond Laboratories
Attn: Dr. Berthold Altman (AMXDO-TI)
Connecticut Avenue and Van Ness St. N. W.
Washington, D.C. 20438

Commanding Officer
U.S. Army Security Agency
Arlington Hall
Arlington, Virginia 22212

Commanding Officer
U.S. Army Limited War Laboratory
Attn: Technical Director
Aberdeen Proving Ground
Aberdeen, Maryland 21005

Commanding Officer
Human Engineering Laboratories
Aberdeen Proving Ground, Maryland 21005

Director
U.S. Army Engineer
Geodesy, Intelligence and Mapping
Research and Development Agency
Fort Belvoir, Virginia 22060

Commandant
U.S. Army Command and General
    Staff College
Attn: Secretary
Fort Leavenworth, Kansas 66270

Dr. H. Robl, Deputy Chief Scientist
U.S. Army Research Office (Durham)
Box CM, Duke Station
Durham, North Carolina 27706

Commanding Officer
U.S. Army Research Office (Durham)
Attn: CRD-AA-IP (Richard O. Ulsh)
Box CM, Duke Station
Durham, North Carolina 27706

Librarian
U.S. Army Military Academy
West Point, New York 10996

The Walter Reed Institute of Research
Walter Reed Medical Center
Washington, D.C. 20012

Commanding Officer
U.S. Army Engineer R&D Laboratory
Attn: STINFO Branch
Fort Belvoir, Virginia 22060

Commanding Officer
U.S. Army Electronics R&D Activity
White Sands Missile Range,
    New Mexico 88002

Dr. S. Benedict Levin, Director
Institute for Exploratory Research
U.S. Army Electronics Command
Fort Monmouth, New Jersey 07703

Director
Institute for Exploratory Research
U.S. Army Electronics Command
Attn: Mr. Robert O. Parker, Executive
    Secretary, JSTAC (AMSEL-XL-D)
Fort Monmouth, New Jersey 07703

Commanding General
U.S. Army Electronics Command
Fort Monmouth, New Jersey 07703
Attn: AMSEL-SC

RD-D	HL-CT-A
RD-G	NL-D
RD-GF	NL-A
RD-MAT	NL-P
XL-D	NL-R
XL-E	NL-S
XL-C	KL-D
XL-S	KL-E
HL-D	KL-S
HL-CT-R	KL-TM
HL-CT-P	KL-TQ
HL-CT-L	KL-TS
HL-CT-O	VL-D
HL-CT-I	WL-D

JOINT SERVICES REPORTS DISTRIBUTION LIST (continued)

Department of the Navy

Chief of Naval Research
Department of the Navy
Washington, D.C. 20360
Attn: Code 427

Naval Electronics Systems Command
ELEX 03
Falls Church, Virginia 22046

Naval Ship Systems Command
SHIP 031
Washington, D.C. 20360

Naval Ship Systems Command
SHIP 035
Washington, D.C. 20360

Naval Ordnance Systems Command
ORD 32
Washington, D.C. 20360

Naval Air Systems Command
AIR 03
Washington, D.C. 20360

Commanding Officer
Office of Naval Research Branch Office
Box 39, Navy No 100 F.P.O.
New York, New York 09510

Commanding Officer
Office of Naval Research Branch Office
219 South Dearborn Street
Chicago, Illinois 60604

Commanding Officer
Office of Naval Reasearch Branch Office
1030 East Green Street
Pasadena, California 91101

Commanding Officer
Office of Naval Research Branch Office
207 West 24th Street
New York, New York 10011

Commanding Officer
Office of Naval Research Branch Office
495 Summer Street
Boston, Massachusetts 02210

Director, Naval Research Laboratory
Technical Information Officer
Washington, D.C. 20360
Attn: Code 2000

Commander
Naval Air Development and Material Center
Johnsville, Pennsylvania 18974

Librarian
U.S. Naval Electronics Laboratory
San Diego, California 95152

Commanding Officer and Director
U.S. Naval Underwater Sound Laboratory
Fort Trumbull
New London, Connecticut 06840

Librarian
U.S. Navy Post Graduate School
Monterey, California 93940

Commander
U.S. Naval Air Missile Test Center
Point Mugu, California 93041

Director
U.S. Naval Observatory
Washington, D.C. 20390

Chief of Naval Operations
OP-07
Washington, D.C. 20350

Director, U.S. Naval Security Group
Attn: G43
3801 Nebraska Avenue
Washington, D.C. 20390

Commanding Officer
Naval Ordnance Laboratory
White Oak, Maryland 21502

Commanding Officer
Naval Ordnance Laboratory
Corona, California 91720

Commanding Officer
Naval Ordnance Test Station
China Lake, California 93555

Commanding Officer
Naval Avionics Facility
Indianapolis, Indiana 46241

Commanding Officer
Naval Training Device Center
Orlando, Florida 32811

U.S. Naval Weapons Laboratory
Dahlgren, Virginia 22448

U.S. Naval Applied Science Laboratory
Flushing and Washington Avenues
Brooklyn, New York 11251
Attn: Robert Schwartz, Code 926

Head, Ocean Engineering Branch
Code 5352, Box 31
Naval Missile Center
Point Mugu, California 93041

Weapons Systems Test Division
Naval Air Test Center
Patuxtent River, Maryland 20670
Attn: Library

Head, Technical Division
U.S. Naval Counter Intelligence
    Support Center
Fairmont Building
4420 North Fairfax Drive
Arlington, Virginia 22203

Other Government Agencies

Mr. Charles F. Yost
Special Assistant to the Director
    of Research
National Aeronautics and
    Space Administration
Washington, D.C. 20546

Dr. H. Harrison, Code RRE
Chief, Electrophysics Branch
National Aeronautics and
    Space Administration
Washington, D.C. 20546

Goddard Space Flight Center
National Aeronautics and
    Space Administration
Attn: Library C3/TDL
Green Belt, Maryland 20771

NASA Lewis Research Center
Attn: Library
21000 Brookpark Road
Cleveland, Ohio 44135

National Science Foundation
Attn: Dr. John R. Lehmann
Division of Engineering
1800 G Street, N.W.
Washington, D.C. 20550

U.S. Atomic Energy Commission
Division of Technical Information Extension
P.O. Box 62
Oak Ridge, Tennessee 37831

Los Alamos Scientific Laboratory
Attn: Reports Library
P.O. Box 1663
Los Alamos, New Mexico 87544

NASA Scientific & Technical Information
    Facility
Attn: Acquisitions Branch (S/AK/DL)
P.O. Box 33,
College Park, Maryland 20740

NASA, Langley Research Center
Langley Station
Hampton, Virginia 23365
Attn: Mr. R. V. Hess, Mail Stop 160

Non-Government Agencies

Director
Research Laboratory of Electronics
Massachusetts Institute of Technology
Cambridge, Massachusetts 02139

Polytechnic Institute of Brooklyn
55 Johnson Street
Brooklyn, New York 11201
Attn: Mr. Jerome Fox
    Research Coordinator

Director
Columbia Radiation Laboratory
Columbia University
538 West 120th Street
New York, New York 10027

Director
Coordinated Science Laboratory
University of Illinois
Urbana, Illinois 61803

Director
Stanford Electronics Laboratories
Stanford University
Stanford, California 94305

Director
Electronics Research Laboratory
University of California
Berkeley, California 94720

Director
Electronic Sciences Laboratory
University of Southern California
Los Angeles, California 90007

Dr. C. L. Coates, Director
Laboratories for Electronics and
    Related Sciences Research
University of Texas
Austin, Texas 78712

Division of Engineering and
        Applied Physics
210 Pierce Hall
Harvard University
Cambridge, Massachusetts 02138

Aerospace Corporation
P.O. Box 95085
Los Angeles, California 90045
Attn: Library Acquisitions Group

Professor Nicholas George
California Institute of Technology
Pasadena, California 91109

Aeronautics Library
Graduate Aeronautical Laboratories
California Institute of Technology
1201 E. California Blvd.
Pasadena, California 91109

Director, USAF Project RAND
Via: Air Force Liaison Office
The RAND Corporation
1700 Main Street
Santa Monica, California 90406
Attn: Library

The Johns Hopkins University
Applied Physics Laboratory
8621 Georgia Avenue
Silver Spring, Maryland 20910
Attn: Boris W. Kuvshinoff
        Document Librarian

Hunt Library
Carnegie Institute of Technology
Schenley Park
Pittsburgh, Pennsylvania 15213

Dr. Leo Young
Stanford Research Institute
Menlo Park, California 94025

Mr. Henry L. Bachmann
Assistant Chief Engineer
Wheeler Laboratories
122 Cuttermill Road
Great Neck, New York 11021

School of Engineering Sciences
Arizona State University
Tempe, Arizona 85281

Engineering and Mathematical
        Sciences Library
University of California at Los Angeles
405 Hilgrad Avenue
Los Angeles, California 90024

California Institute of Technology
Pasadena, California 91109
Attn: Documents Library

University of California
Santa Barbara, California 93106
Attn: Library

Carnegie Institute of Technology
Electrical Engineering Department
Pittsburgh, Pennsylvania 15213

University of Michigan
Electrical Engineering Department
Ann Arbor, Michigan 48104

New York University
College of Engineering
New York, New York 10019

Syracuse University
Dept. of Electrical Engineering
Syracuse, New York 13210

Yale University
Engineering Department
New Haven, Connecticut 06520

Airborne Instruments Laboratory
Deerpark, New York 11729

Bendix Pacific Division
11600 Sherman Way
North Hollywood, California 91605

General Electric Company
Research Laboratories
Schenectady, New York 12301

Lockheed Aircraft Corporation
P.O. Box 504
Sunnyvale, California 94088

Raytheon Company
Bedford, Massachusetts 01730
Attn: Librarian

Dr. G. J. Murphy
The Technological Institute
Northwestern University
Evanston, Illinois 60201

Dr. John C. Hancock, Director
Electronic Systems Research Laboratory
Purdue University
Lafayette, Indiana 47907

Director
Microwave Laboratory
Stanford University
Stanford, California 94305

Emil Schafer, Head
Electronics Properties Info Center
Hughes Aircraft Company
Culver City, California 90230

Department of Electrical Engineering
Texas Technological College
Lubbock, Texas 79409

DOCUMENT CONTROL DATA - R & D

(Security classification of title, body of abstract and indexing annotation must be entered when the overall report is classified)

1. ORIGINATING ACTIVITY *(Corporate author)*	2a. REPORT SECURITY CLASSIFICATION
Research Laboratory of Electronics Massachusetts Institute of Technology Cambridge, Massachusetts 02139	Unclassified
	2b. GROUP None

3. REPORT TITLE

Decision-Feedback Equalization for Digital Communication over Dispersive Channels

4. DESCRIPTIVE NOTES *(Type of report and inclusive dates)*

Technical Report

5. AUTHOR(S) *(First name, middle initial, last name)*

Michael E. Austin

6. REPORT DATE	7a. TOTAL NO. OF PAGES	7b. NO. OF REFS
August 11, 1967	100	20

8a. CONTRACT OR GRANT NO.	9a. ORIGINATOR'S REPORT NUMBER(S)
(1) Contract DA 28-043-AMC-02536(E)	
b. PROJECT NO. 200-14501-B31F	Technical Report 461
c. (2) Contract N00140-67-C-0201	9b. OTHER REPORT NO(S) *(Any other numbers that may be assigned this report)*
d.	ESD-TR-67-466; Lincoln Laboratory Technical Report 437

10. DISTRIBUTION STATEMENT

This document has been approved for public release and sale; its distribution is unlimited.

11. SUPPLEMENTARY NOTES	12. SPONSORING MILITARY ACTIVITY
	Joint Services Electronics Electronics Program thru USAECOM, Fort Monmouth, N. J. and U.S. Navy Purchasing Office

13. ABSTRACT

In this report, a decision-theory approach to the problem of digital communication over known dispersive channels is adopted to arrive at the structures of the optimal and two sub-optimal receivers: the "conventional" and "decision-feedback" equalizers, both employing matched and transversal filters. The conventional equalizer is similar to some equalization modems finding current application, while the new decision-feedback equalizer (as its name implies) utilizes its previous decisions in making a decision on the present baud.

The parameters of these two equalizers are optimized under a criterion which minimizes the sum of the intersymbol interference and additive noise distortions appearing at their outputs. Algorithms for evaluating the performances of the conventional and decision-feedback equalizers are developed, proving especially useful at high SNR where simulation techniques become ineffective.

To determine the dependence of their performance and sidelobe-suppression properties upon SNR and transversal filter length, the new algorithms were used to study the conventional and decision-feedback equalizers when they are applied in equalization of the class of channels exhibiting the maximum realizable intersymbol interference. In addition, error-propagation effects found to arise in the decision-feedback equalizer operation are studied. High overall error rates (as found at low SNR) lead to a threshold effect as the decision-feedback equalizer performance becomes poorer than that of the conventional equalizer.

Despite such error-propagation behavior, however, the decision-feedback equalizer is found to be considerably better than the conventional equalizer at all SNR and error rates of practical importance, due to its sidelobe-suppression behavior; moreover, its advantages become more pronounced, the higher the SNR and the greater the channel dispersion.

DD FORM 1473 (PAGE 1)
I NOV 65

S/N 0101-807-6811

14. KEY WORDS	LINK A		LINK B		LINK C	
	ROLE	WT	ROLE	WT	ROLE	WT
decision-feedback						
digital communication						
dispersive channels						
equalization filters						
threshold effects						

DD FORM 1 NOV 65 **1473** (BACK)